

Ecole doctorale Science Pour l'Ingénieur

Design and Control of an Integrated Haptic Interface for Touch Screen Applications

THÈSE

présentée et soutenue publiquement pour l'obtention du

Doctorat de l'Université des Sciences et Technologies de Lille
(spécialité Génie Électrique)

par

Yi YANG

Le 1^{er} Novembre 2013

Composition du jury

<i>Président</i>	Pr. Vincent Hayward, Université Pierre et Marie Curie
<i>Directeurs de thèse</i>	Pr. Betty Lemaire-Semail, Université Lille1 Pr. Yuru Zhang, Université Beihang China
<i>Rapporteurs:</i>	Pr. Aiguo Song Southeast University China Pr. Vincent Hayward, Université Pierre et Marie Curie
<i>Examineurs:</i>	Pr. Hong Z. Tan, Université Purdue, US

Abstract

The lack of haptic feedback is a significant problem of current touch screens. Without haptic feedback, users have to rely almost entirely on visual feedback to operate on a touch screen. As a result, users' performance is deteriorated and users' visual workload is increased. Adding tactile feedback to touch screens has shown to be a promising solution to address this problem. However, the force feedback in interactions with virtual objects on touch screens is not provided.

This thesis presents the design and evaluation of an integrated haptic device for enhancing interactions on touch screens. The device consists of a cable-driven force feedback device and a squeeze film based tactile device. The cable-driven force feedback device uses four cables to provide force feedback to one finger or dual fingers through controlling the cable tensions. It can provide force feedback when the user clicks a button, grasps an object and interacts with other objects. The tactile device is based on the squeeze film effect to reduce the friction coefficient on the touch surface. We propose an accurate model to analyze the power consumption of the device and use the model to develop a large area (198 mm × 138mm) tactile device with very few piezoelectric actuators and low power consumption. Each of these two component devices can be used individually and the integrated device is able to provide simultaneous force feedback and tactile f on a touch surface. The coupled haptic feedback has been evaluated through simulating a boundary. As compared with using a single type of haptic feedback (e.g. force feedback), the coupled haptic feedback enhances the simulation by making the boundary stiffer and crisper.

Keywords: Haptic, touch screen, force feedback, tactile feedback, cable-driven, friction, piezoelectricity.

Acknowledgements

I am very grateful to the support from the L2EP¹ in Lille 1² and the Human-Machine Interaction lab³ in Beihang University⁴ in my PhD thesis. The fundings from INRIA⁵ and Beihang University enable me to implement the PhD thesis.

First of all, I would like to thank Betty Semail, my thesis supervisor, who offers me the opportunity to study in L2EP. Her expertise, foresight, and patience helped me to pursue my PhD in Lille 1. Meanwhile, I am also grateful to Michel Amberg and Frédéric Giraud who assisted me to develop the tactile device and discussed every problem I met in the process.

As a co-supervised PhD student, I am also very grateful to my co-supervisor, Yuru Zhang, in Beihang University. She inspired me to design the force feedback device and offered me invaluable suggestions on how to do research as a PhD candidate. Without her support during the years, I cannot finish this thesis.

I appreciate the feedback from Prof. Vincent Hayward and Prof. Aiguo Song, as reporters of this thesis, and other jury members. Their comments significantly improved the thesis.

I also appreciate comments and discussions with Ludovic Potier and Ibrahim Yapici in evaluating the large STIMTAC. Thanks go to Hong Tan who provided helpful discussions and comments during my PhD. Her insights into problems saved a lot of my time and corrected me when I tended to go towards a wrong way in research. I am also grateful to Mark Buck, my English teacher and friend, who proofread all papers that I have published.

Other members of L2EP and HMI lab also helped me a lot in my pursuit of

¹<http://l2ep.univ-lille1.fr/index2.php>

² <http://www.univ-lille1.fr/>

³ http://haptic.buaa.edu.cn/EN/home_en.html

⁴ <http://ev.buaa.edu.cn/>

⁵ <http://www.inria.fr/en/centre/lille>

PhD, including Tao Zeng, Nguyen Thanh Hung, Razvan Chitic, DangXiao Wang, XiaoWei Dai, Ge Yu, LingZhi Liu, ZhongYuan Chen, and Zhu Hou.

Finally, I am grateful to the support from my parents and my families. Their company enabled me to get through all difficulties in my studies.

Contents

Chapter 1 Introduction.....	1
Chapter 2 Haptic Feedback in Touch Interaction	6
2.1. Human Haptic System	7
2.2. Haptic Interfaces for Indirect Interaction	9
2.2.1. Adding force feedback to indirect interactions.....	9
2.2.2. Adding tactile feedback to indirect interactions	13
2.2.3. Adding coupled tactile and force feedback to indirect interactions	15
2.3. Tactile Displays for Direct Touch Interaction	16
2.3.1. Vibrotactile feedback	16
2.3.2. Surface shape	31
2.3.3. Friction	33
2.3.4. Hardness	40
2.3.5. Non-contact tactile feedback	40
2.3.6. Electrotactile feedback	42
2.4. Summary.....	43
Chapter 3 Design of the force feedback device.....	46
3.1. Introduction	47
3.2. Related work.....	48
3.3. Configuration and Kinematic Design	51
3.3.1. Configuration.....	51
3.3.2. Kinematics	53
3.4. Cable tension control.....	55

3.4.1.	Feasibility of Exerting 4-DOF Force Feedback with Four Cables	55
3.4.2.	Cable Tension Calculation	57
3.4.3.	Maintain Positive Cable Tension	60
3.5.	Implementation	62
3.5.1.	Mechanical Design.....	62
3.5.2.	Control System Configuration	64
3.5.3.	Application Demonstration	65
3.6.	Evaluation	69
3.6.1.	Simulating a button-click	69
3.6.2.	Knob manipulation.....	75
3.7.	Conclusion	80
Chapter 4 Design of the Tactile Feedback Device.....		83

4.1.	Introduction.....	84
4.1.1.	Squeeze Air Film Effect.....	84
4.1.2.	Motivation and difficulties of designing a large area tactile device	87
4.2.	Power consumption measurements.....	89
4.2.1.	Measurement Setup.....	90
4.2.2.	Dielectric Power Losses.....	90
4.2.3.	Mechanical Power Losses From the Resonator	92
4.2.4.	Power Losses in Electromechanical Conversion Stage	93
4.2.5.	Summary	95
4.3.	Power consumption modeling.....	96
4.3.1.	General Assumption.....	96
4.3.2.	Plate Deflection.....	96
4.3.3.	Power Calculation	99
4.3.4.	Variation Of The Piezoelectric Loss Tangent.....	104
4.3.5.	Effect Of The Actuator Layout	105
4.3.6.	Summary	105
4.4.	Design of a large tactile device	106

4.4.1.	Design Guidelines	106
4.4.2.	Implementation.....	107
4.4.3.	Modal analysis.....	108
4.4.4.	Experimental measurements.....	109
4.5.	Psychophysics evaluation of the tactile plate	113
4.5.1.	Motivation	113
4.5.2.	Method.....	115
4.5.3.	Results	120
4.5.4.	Discussion.....	121
4.6.	Conclusion.....	123
Chapter 5 Evaluation of the Coupled Haptic Device		125
<hr/>		
5.1.	Introduction	126
5.2.	Apparatus.....	130
5.3.	Experiment 1: Perception of a boundary simulated by a step function of force feedback.....	132
5.3.1.	Task and stimuli.....	132
5.3.2.	Design.....	133
5.3.3.	Participants	134
5.3.4.	Results and discussion.....	135
5.4.	Experiment 2: Perception of a boundary simulated by a coupled haptic feedback.	137
5.4.1.	Experiment details	137
5.4.2.	Results and discussion	139
5.4.3.	Limitations of the current research.....	144
5.5.	Conclusion.....	146
Conclusion		147
Glossary		152
Reference		154

List of Tables

Table 2.1 Haptic feedback terminology (adapted from [27, 28]).....	7
Table 2.2 Characteristics of the four types of mechanoreceptor in the human skin (summarized from [28, 30, 31]).	8
Table 4.2 Measurement results according to the length of the resonator.	93
Table 4.3 Measurements of the 1-column and 2-column tactile plates.....	94
Table 4.4 Material parameters of the big tactile plate.....	108
Table 5.1 Experiment 1 comparison stimuli for force levels.	134
Table 5.2 Average JNDs for the three standard force levels.	136
Table 5.3 Experiment 2 comparison stimuli for force levels.	138
Table 5.4 Perceived force increment and maximum friction increment in the second experiment. Data are averaged across standard stimuli levels.....	143

List of Figures

Figure 1.1 Influence of tactile and kinesthetic systems on different tasks (adapted from [5]).	2
Figure 1.2 Lack of haptic feedback on touch surfaces (adapted from [6-8]).	2
Figure 2.1 The PHANToM force feedback device from SensAble Technology (adapted from [36]).	10
Figure 2.2 FEELit Mouse, Immersion Co. (adapted from [39]).	11
Figure 2.3 The HapticMaster force feedback device in the experiment (adapted from [44]).	12
Figure 2.4 Haptic Trackpoint and the bump points in the tunnel (adapted from [45]).	13
Figure 2.5 The Logitech iFeel mouse (adapted from [46]).	13
Figure 2.6 The tactile transducer used in a handheld device to provide lateral traction on the surface of the finger skin (adapted from [47]).	14
Figure 2.7 The haptic mouse with a solenoid driven pin (adapted from [48]).	15
Figure 2.8 SemFeel used five vibration motors on the backside of a mobile touch-screen device to generate vibrotactile patterns (adapted from [18]).	18
Figure 2.9 The Ubi-pen prototype and its application on a touch screen (adapted from [53]).	19
Figure 2.10 The stylus and the vibration motor (adapted from [54]).	19
Figure 2.11 Actuator is mounted on the surface of the touch panel for creating button click feeling (adapted from [9]).	20
Figure 2.12 Putting three vibrators on the forearm to encode information (adapted from [59]).	21
Figure 2.13 The multi-actuator PDA used to indicate downloads progress (adapted from [60]).	22

Figure 2.18 An example of solenoid actuator. The solenoid generates electromagnetic force to attract or repel the vibrator (adapted from [61]).	23
Figure 2.19 Both a piezoactuator and a solenoid actuator were utilized for the tactile feedback (adapted from [62]).	23
Figure 2.20 Haptic Pen – a tactile feedback stylus with solenoid actuator mounted at the end (adapted from [63]).	24
Figure 2.21 Indirect and direct input with a Haptic Pen (adapted from [13]).	24
Figure 2.14 The TouchEngine tactile actuator and its application to touch screen devices (adapted from [10], [67] and [66]).	25
Figure 2.15 Piezoelectric actuators raised the touch surface in the Nokia 7710 (adapted from [65]).	27
Figure 2.16 The “Snap-Crackle-Pop” tactile mobile device (adapted from [64]).	29
Figure 2.17 Gluing piezoelectric actuator at the back of a handheld device to simulate button-click feedback; force sensors were used to detect finger contact on the device (adapted from [16]).	29
Figure 2.22 The operation of the impact motor and its application in a pen-like input interface (adapted from [72]).	30
Figure 2.23 Neutral, negative and positive appearance of the pneumatic buttons (adapted from [74]).	32
Figure 2.24 The Tactus button (adapted from [75]).	32
Figure 2.25 Displaying text and pictures using pins (adapted from [76]).	33
Figure 2.26 The Large Area Tactile Pattern Display (LATPaD, adapted from [79]).	34
Figure 2.27 The STIMTAC haptic device (adapted from [80]).	35
Figure 2.28 Activating two piezoelectric actuators at two different frequencies produced more expressive tactile feedback (adapted from [81]).	35
Figure 2.29 The SAW tactile interface (adapted from [82]).	36
Figure 2.30 The principle and an example of the TeslaTouch (adapted from [83]).	36
Figure 2.31 The magnetic coil attracts the ball and causes higher friction (adapted from [85]).	38
Figure 2.32 The principle of the ShiverPad (adapted from [78]).	38

Figure 2.33 The LateralPad (adapted from [86]).	39
Figure 2.34 The two actuators produced lateral movement of the mobile phone (adapted from [87]).	39
Figure 2.35 MudPad is a system that provides localized haptic feedback independently at multiple points (adapted from [88]).	40
Figure 2.36 The user holds the mobile TV and feels haptic feedback at the back of the device. The ultrasonic acoustic pressure moved tapes when various regions of transducers are triggered (adapted from [89]).	41
Figure 2.37 The FingerFlux interactive surface (adapted from [90]).	42
Figure 2.38 Touch screen with electrotactile feedback (adapted from [91]).	43
Figure 3.1 The SPIDAR force feedback devices (adapted from [98], [99] [92] and [100] respectively).	49
Figure 3.2 The 2-DOF force feedback device used to simulate bumps on a touch screen (adapted from [103]).	50
Figure 3.3 Configuration and kinematic diagram of the FingViewer force feedback devices.	52
Figure 3.4 Static diagram of the FingViewer-II(S).	57
Figure 3.5 Static diagram demonstrating the spring force and the grasp force.	57
Figure 3.6 The FingViewer force feedback devices.	62
Figure 3.7 System architecture of the FingViewer device.	64
Figure 3.8 The three stages of the virtual grasp task.	65
Figure 3.9 Force and cable tensions in the virtual grasp task.	66
Figure 3.10 Force feedback capability of the FingViewer-II. The user can use his/her fingers to grasp and manipulate virtual objects and obtain 4-DOF force feedback.	68
Figure 3.11 Acceleration measurement during a keystroke on a physical keyboard and on a haptic enhanced touch screen button. The acceleration along the y-axis was collected and plotted (the gravity effect was eliminated from the data).	70
Figure 3.12 Maximum acceleration on the fingertip as a function of applied force feedback. A saturation effect can be noticed when force is greater than 2 N.	71
Figure 3.13 Reciprocal tapping task.	72

Figure 3.14 Force feedback in the experiment.....	73
Figure 3.15 Mean task completion time and error rate in the tapping task, by feedback conditions. Error bars indicate 95% confidential interval.....	74
Figure 3.13 Diagram of the virtual knob-control experiment.....	76
Figure 3.14 Aggregate results from 12 subjects demonstrating the effect of force feedback on their performance. The means and error bars with 95% confidence interval are plotted.	78
Figure 4.1 Schematic of epidermal ridges and the vibrating plate (adapted from [25])... 85	85
Figure 4.2 Power changes in the three tactile plates. Piezoceramics were glued on the resonator to excite the resonance vibration.....	91
Figure 4.3 Two tactile plates with piezoceramics glued at the edges.	94
Figure 4.4 A half-wavelength section of the bended plate. h_i and h_p are thickness of the resonator layer and piezoceramics layer respectively.	97
Figure 4.5 Aluminum resonators with different piezoceramics layouts. The amplification factor (Q) has been measured in each condition, as explained further.	103
Figure 4.6 Piezoelectric loss tangent in different tactile plates as a function of applied voltage.....	104
Figure 4.7 The layout of the eight piezoceramics on the big tactile plate.....	107
Figure 4.8 Modal analysis of the big tactile plate by ANSYS Workbench: deformed shape at (21, 0) mode.	109
Figure 4.9 Cartography of the big tactile plate.	110
Figure 4.10 Vibration amplitude as a function of applied voltage.....	111
Figure 4.11 Measured and estimated power as a function of the square of voltage. The measured and estimated amplification factor and piezoelectric loss tangent are also listed (The estimated values are obtained according to the measurement results on the small samples).	111
Figure 4.12 Measurement result of a 4 piezoelectric actuators tactile plate. The mean error between the measured power and estimated power is 6.3%.	113
Figure 4.13 Measurement result of a 16 piezoelectric actuators tactile plate. The mean error between the measured power and estimated power is 5.96%.	113

Figure 4.15 The large STIMTAC and its controller.....	116
Figure 4.16. Stimuli in the experiments. The x-axis represents the workspace while the y-axis represents the vibration amplitude. The test and reference stimuli were presented to the participants in a random order.	117
Figure 4.14. Transverse and standard standing wave mode shapes. The labels in the pictures indicating the variation of amplitude along the width direction of the tactile plate.	123
Figure 5.1 The Contact Location Display and its assembly with a PHANToM device (adapted from [22]).....	128
Figure 5.2 The coupled haptic device. In the experiment, the device was used to simulate a boundary located at the center. The gray patch indicates where haptic feedback was exerted.	129
Figure 5.3 Control architecture of the integrated haptic device.	130
Figure 5.4 Experiment setup for both experiments. In the training session of the second experiment, a slider was shown on the computer monitor to represent the normal force. Participants were instructed to maintain the normal force in the green area which indicated the gauge output of 1-1.5 N. The slider was hidden when the experiment started.	132
Figure 5.5 Typical response of a participant at the level of 0.8N.....	135
Figure 5.6 Average Weber's fraction for the three standard force levels. Error bars represent 95% confidence interval.	136
Figure 5.7 Haptic feedback in simulation of a boundary.....	138
Figure 5.8 The PSEs at the three standard stimuli levels. Error bars represent 95% confidence interval. The force feedback magnitudes in the standard stimuli are also plotted as a reference to indicate the increment of perceived force due to the addition of tactile feedback.	141
Figure 5.9 The perceived force increment and the maximum increment of friction in the second experiment.	142

Chapter 1.

Introduction

Touch screens are prevalent user interfaces in our daily life nowadays. They have been widely applied to smart phones, tablet PCs, electric readers, public kiosks, ticket machines and Automatic Teller Machines (ATMs). The economic success of touch screens can be attributed to the directness and intuitiveness of touch interaction. The modality of acquiring digital objects by touching them directly on touch surfaces follows human's natural cognitive pattern for acquiring physical objects. Therefore, touch interaction has been entitled as "Natural" interaction.

Unlike conventional input devices (e.g., keyboard, mouse, touch pad, etc), touch screens serve as both input and output interfaces. Direct interaction, rich input-gesture vocabulary, reconfigurable user interface and large display estate make touch screen increasingly replace conventional mechanical interfaces [1, 2]. Although the replacement of buttons and knobs expands the display estate, it also deprives the inherent haptic feedback on physical controllers. As a result, a user can see a graphic interface (e.g. a button), but he cannot identify it from the background through touching on a touch screen. Without haptic feedback, users have to rely mainly on visual feedback to operate on touch screens. Consequently, user's visual work load is aggravated and more errors are made as compared with using physical counterparts [3, 4].

In general, human haptic system consists of two major subsystems: tactile and kinesthetic subsystems (more details can be found in Section 2.1). Depending on the task we perform, the tactile and kinesthetic systems play roles of varying

influence [5], as shown in Figure 1.1.

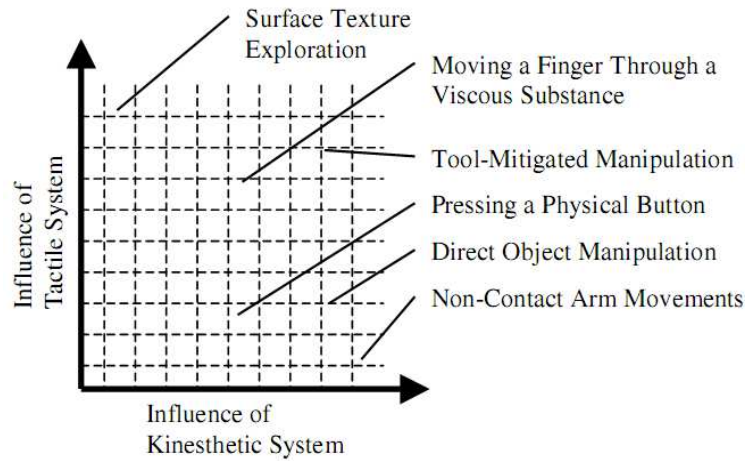


Figure 1.1 Influence of tactile and kinesthetic systems on different tasks (adapted from [5]).

When operating on a touch surface, a user loses two types of haptic feedback that deteriorates his performance [2]. The first one is tactile feedback. A typical example is the raised bump on home keys. On a physical keyboard, users can place their fingers easily on the home row keys by explore the raised bumps on the F and J keys through touch. On the contrary, when the bumps dissipate on touch screens, users have to find their ways to the keys by looking at the screens, as shown in Figure 1.2 (a). The second is force feedback. Without force feedback, a user cannot obtain the concrete feeling of handling a solid object that his fingers used to when he manipulates a virtual object, such as when rotating a picture or grasping virtual objects, as presented in Figure 1.2 (b).

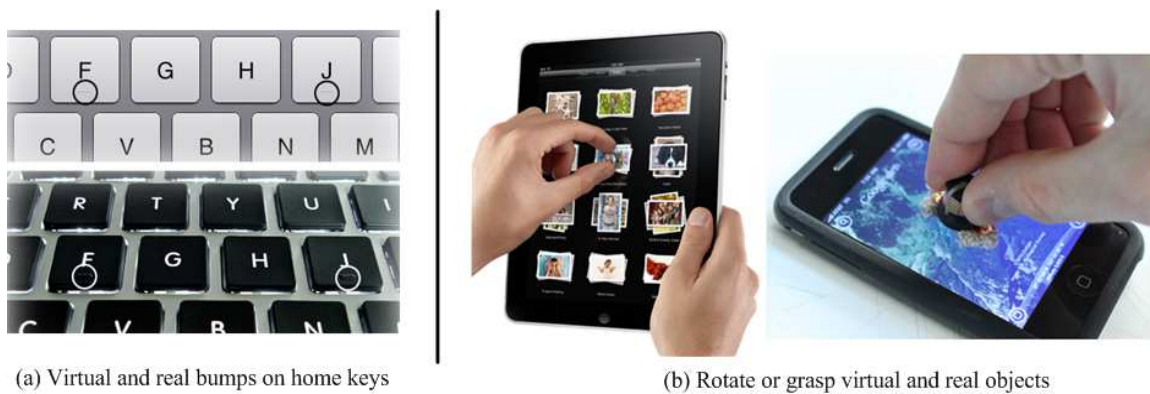


Figure 1.2 Lack of haptic feedback on touch surfaces (adapted from [6-8]).

An effective and direct method to solve the problem of lacking haptic feedback is to apply haptic interfaces to touch interaction to enhance physicality. Previous research has shown that haptic enhanced touch interaction has increased task speed [9-13], reduced errors [10, 14] and workload [14], and gained users' preferences [11, 12, 15]. Although these studies are promising, a majority of them only add tactile feedback to help user perceive the context of interaction, such as completing a task [11], crossing item boundaries [10], clicking inside or outside a button [16, 17], and the spatial location of the touch point [18]. The force feedback obtained when the user interacts with physical worlds, such as when grasping and rotating a mechanical knob, pushing a slider, and exploring the shape of an object, cannot be simulated by tactile displays. Consequently, the fidelity of interacting with virtual objects on touch screens is deteriorated [2].

Since the human haptic system includes both force feedback and tactile feedback, the aim of the thesis is to design an integrated haptic device which provides not only tactile feedback but also force feedback when users interact with touch screens. Although there are some literatures about integrating force feedback devices and tactile devices, they mainly focus on improving certain properties of virtual objects, such as textures [19, 20], stiffness [21], friction [22] and shape [23]. In the L2EP, we have also developed a coupled device for displaying shape and texture [24]. However, these devices were not designed for enhancing touch interaction on touch screens.

This research is based on the cooperation between the Human-Machine Interaction Lab of Beihang University in China and the L2EP (Laboratoire d'Electrotechnique et d'Electronique de Puissance) of Lille 1 in France. We take advantage of the priority of technology of each lab to design and develop this integrated device. The design principle is to design the force feedback device and tactile device as individual modules so that each of them can be used independently; and, after assembled, they can work as an integrated device.

In the following parts of the thesis, we first review some aspects about adding

haptic feedback to touch interaction in Chapter 2. The physiology of human touch sensation is summarized at first, including how touch sensation is categorized and perceived. Then, previous research about adding haptic interfaces to indirect interactions with Graphic User Interfaces (GUIs) is introduced. Finally, literatures on adding tactile feedback to direct touch interactions are reviewed. The features, applications and effects of each haptic interface are summarized.

In Chapter 3, the design of the cable-driven force feedback device is presented. The device is used to provide force feedback to user's fingers. We first introduce the design of a reconfigurable mechanism so that the device could provide force feedback to either a single finger or two fingers. In this case, we can add force feedback to single-touch or multi-touch interactions. Then, the kinematics and cable tension control of the device are presented to illustrate how the device works. Finally, two experiments to evaluate the force feedback device are proposed. The first experiment evaluates the single-touch interaction with a button. A button-click feedback is simulated and compared with a physical button. Then, in the second experiment, we evaluate the multi-touch force feedback in a knob control experiment.

In Chapter 4, we demonstrate the design of the large area tactile feedback device which is based on the STIMTAC device developed by our laboratory (L2EP) [25]. This device is based on the squeeze air film effect which reduces the friction coefficient of the touch surface. The objective of this research is to enlarge the workspace of the STIMTAC device, while reducing the number of piezoelectric actuators and power consumption. To achieve this goal, we first present a series of measurements that have been carried out to investigate the source of the power consumption of the STIMTAC device. We then develop an analytical model to estimate the power. We find that, when the vibration amplitude is constant, the power consumption is not related to the number of piezoelectric actuators but related to their layouts. With this result, we design a large area tactile plate with very few piezoelectric actuators and very little power consumption. Finally, we evaluate the device with a psychophysics experiment. The experiment validates

the tactile feedback capability of the device.

In Chapter 5, the evaluation of the integration of the force feedback and tactile device is presented. In particular, we investigate the merit of applying simultaneous force feedback and tactile feedback to the simulation of a crisp and stiff boundary. We use the Method of Constant stimuli to quantify the amount of perceived force increment caused by adding tactile feedback to force feedback. Experimental result shows that using a small amount of force feedback plus a tactile feedback can simulate a boundary which feels as stiff as that simulated by a large force feedback. This result confirms the benefit of integrating force feedback and tactile feedback devices in touch interaction.

At the end of the thesis, we draw conclusion of this work and discuss on potential improvements of the integrated device.

Chapter 2.

Haptic Feedback in Touch Interaction

Summary

2.1.	Human Haptic System	7
2.2.	Haptic Interfaces for Indirect Interaction.....	9
2.2.1.	Adding force feedback to indirect interactions	9
2.2.2.	Adding tactile feedback to indirect interactions	13
2.2.3.	Adding coupled tactile and force feedback to indirect interactions.....	15
2.3.	Tactile Displays for Direct Touch Interaction.....	16
2.3.1.	Vibrotactile feedback	16
2.3.2.	Surface shape	31
2.3.3.	Friction.....	33
2.3.4.	Hardness.....	40
2.3.5.	Non-contact tactile feedback.....	40
2.3.6.	Electrotactile feedback.....	42
2.4.	Summary	43

The objective of this research is to add holistic haptic feedback to touch interaction. This chapter provides an overview of related research including physiology of human touch sensation, previous research on adding haptic feedback to indirect interaction with GUIs, and adding tactile feedback in direct touch interactions.

We first introduce what haptics is and how human being perceives haptic

feedback. We then review literatures about adding haptic interfaces for indirect interaction with GUIs. Finally, we review research on adding tactile feedback to direct touch interactions. The features, applications and effects of each haptic interface are summarized. According to the survey, we draw conclusion that although tactile feedback is useful to touch interaction, its expressiveness is still limited. A holistic haptic feedback is needed to further enhance interactions on touch screens.

2.1. Human Haptic System

The human sense of touch is a primary channel to perceive the surrounding world. The adjective “haptic” is a more formal synonym for the term “touch-based.” It stems from the Greek word *haptikos*, which means “able to touch or grasp,” a descendant of the Greek verb *haptain* or “fasten” [26]. According to ISO: Ergonomics of human-computer interaction—Part 910: Framework for tactile and haptic interaction, the term haptic means “sensory and/or motor activity based in the skin, muscles, joints and tendons” [27]. With this definition, the haptic sensation includes several sub-categories as shown in Table **Erreur ! Utilisez l'onglet Accueil pour appliquer 标题 1 au texte que vous souhaitez faire apparaître ici..1**.

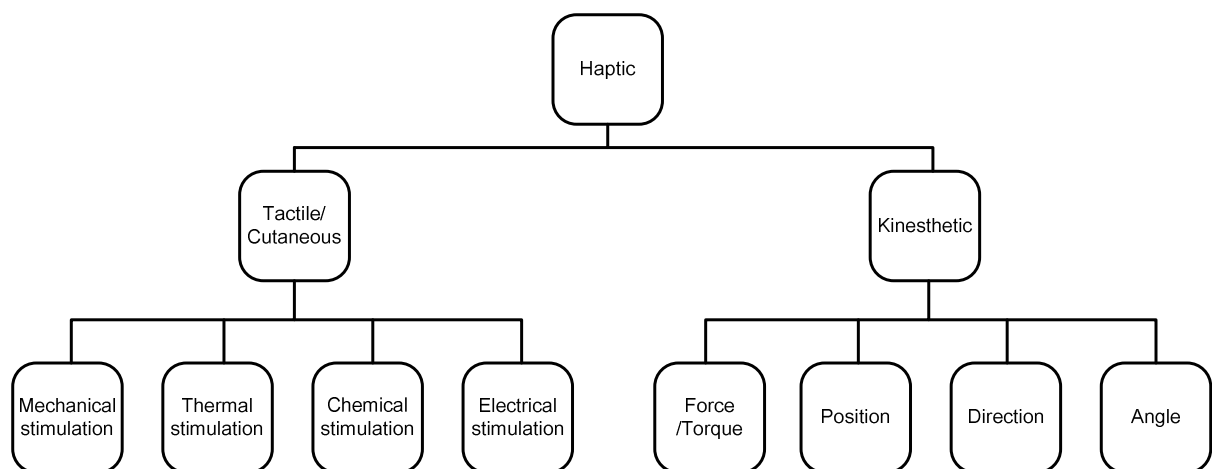


Table **Erreur ! Utilisez l'onglet Accueil pour appliquer 标题 1 au texte que vous souhaitez faire apparaître ici..1** Haptic feedback terminology (adapted from [27, 28])

The kinesthetic/proprioceptive subsystem enables the nervous system to decode the limb position and movement [29], along with the associated forces, and to receive information from sensory receptors in the skin around the joints, joint capsules, tendons, and muscles, as well as from motor-command signals. The tactile/cutaneous subsystem, on the other hand, receives information by the response of mechanoreceptors in the skin [5].

	Merkel discs	Ruffini endings	Meissner corpuscles	Pacinian corpuscles
Property	SA Type I	SA Type II	RA Type I	RA Type II
Adaption	Slow	Slow	Rapid	Very Rapid
Area (cm²)	70	9	140	21
Distribution	Superficial skin	Deeper tissue	Superficial skin	Deeper tissue
Frequency (most sensitive at)	0.4 to 100 Hz (7 Hz)	15 to 400	10 to 100 Hz (200–300 Hz)	40 to 800 Hz (200–300 Hz)
Sensation	Pressure, texture	Stretch	Tap, flutter	Vibration

Table **Erreur ! Utilisez l'onglet Accueil pour appliquer 标题 1 au texte que vous souhaitez faire apparaître ici..**2 Characteristics of the four types of mechanoreceptor in the human skin (summarized from [28, 30, 31]).

In glabrous skin, there are four types of mechanoreceptors: Merkel discs (SA I), Ruffini ending (SA II), Meissner corpuscle (RA I), and Pacinian corpuscle (RA II) [32]. Table **Erreur ! Utilisez l'onglet Accueil pour appliquer 标题 1 au texte que vous souhaitez faire apparaître ici..**2 shows a list of specific characteristics for each fiber. They are categorized by their rate of adaption and sensory modalities. When a mechanoreceptor receives a stimulus, it causes impulses in the nerve system. However, the receptor will adapt to a static stimulus, and impulses in the nerve system will become weaker. This is called adaption. Two of the four

mechanoreceptors are known to demonstrate a rapid adaptation rate (impulses in the nerve system become weak quickly after the initial stimulus is provided). These Rapidly-Adapting (RA) mechanoreceptors contribute to the sense of rapidly changing simulation, such as texture or vibration [31]. Mechanoreceptors are further differentiated by whether they have a small receptive field with well defined borders (Type I) or a large receptive field with diffuse borders (Type II).

The four types of mechanoreceptors have been documented extensively via microneurography. The frequency range in which each mechanoreceptor type is most sensitive is also listed (adapt from [28] and [30]), though it should be noted that these sensitivity bands depend somewhat on the magnitude of the input. Following their distinct response characteristics, each mechanoreceptor has been found to respond most intensely to a certain type of stimulus. For example, the Pacinian corpuscles (RA II) respond best to the high-frequency vibrations that stem from contact between hard objects. Meissner corpuscles and Merkel discs respond to deflection of the skin, and Ruffini endings respond best to rapid indentation of the skin [33].

2.2. Haptic Interfaces for Indirect Interaction

Before the popularity of touch screens, users used other input devices (e.g. mouse, joystick) to interact with GUIs in an indirect mode. The term *indirect* means the display surface is different from the input surface [34]. Interacting with GUIs in an indirect mode also has the problem of lacking haptic feedback. When a user moves a cursor to an icon, he cannot feel any haptic feedback. Instead, he has to rely on visual feedback to implement the task. To facilitate users' interaction with GUIs in indirect mode, researchers have proposed several methods to add haptic feedback in the interaction process.

2.2.1. Adding force feedback to indirect interactions

Rosenberg and Brave used a force feedback joystick to enhance the

interaction with GUIs [35]. They compared three feedback conditions: no forces, passive forces and active forces. In the passive force condition, force feedback was applied only when the user deviated from a given target as a barrier. While in the active force condition, force feedback attracted the joystick to the center of the target. Experimental results showed that, both force feedback conditions increased the task completion and active force feedback further enhanced this benefit. However, no details of the experiment were presented to evaluate the results completely.

Oakley et al. [36] used a PHANToM force feedback device (Figure 2.1) to haptically augment buttons and scrollbars. In the first experiment, four haptic enhanced buttons (textures, friction, recess and gravity well) were compared in a pointing task. In the second experiment, two haptic effects (recess and gravity well) were added to scroll bars to help users keep their eyes on the scrollable text. They found that although haptic effects did not lead to improved task completion times, participants made significantly fewer errors when haptic feedback was enabled and perceived many aspects of workload to be significantly lighter. After decreasing the magnitude of force feedback according to the movement speed, they investigated haptic effect on multi-target interaction (Menus, tool bars and icons) [37, 38]. The adjusted force feedback improved interaction speed, decreased errors and workloads while the normal force feedback reduced speed and increased workload.



Figure 2.1 The PHANToM force feedback device from SensAble Technology (adapted from [36]).

Dennerlein, Martin, and Hasser [39] examined the benefits of force-feedback for the desktop computer human interface. They applied a force feedback mouse

(FEELit Mouse, Immersion Corporation, San Jose, CA, as shown in Figure 2.2) in steering experiments crossing a tunnel. The mouse produced force that pulled the cursor to the center of the tunnel. Experimental results showed that force feedback assisted subjects to complete the task and reduced the task completion time by 52 % and 25 % in the pure steering task and combined steering and pointing task respectively as compared to a conventional mouse.



Figure 2.2 FEELit Mouse, Immersion Co. (adapted from [39]).

In a Fitt's pointing task, Dennerlein and Yang investigated the effect of attractive force field on users' performance and musculoskeletal loading [40]. When the attractive force field was added to the desired target, the force feedback improved 25% of task completion compared with no force feedback condition. Moreover, the force feedback also reduced discomfort and pain that users perceived in the task. However, when distracters were added, the force feedback added became distractive to users. As a result, the benefit of reducing musculoskeletal loading and improving task completion decreased while the number of distracters increased.

Smyth and Kirkpatrick [41] presented a new approach to haptically enhance the GUI, called Pokespace. Users hold the stylus of a PHANToM force-feedback device with their non-dominant hand to interact with GUIs. Users could push or pull the stylus to pop in or out of a virtual wall to change the values of tool parameters. Two studies conducted with Pokespace showed no performance improvement over a traditional interface, but showed that participants learnt to use the interface presciently after about 10 minutes, and could do so without visual attention.

Boeck, Vanacken, and Coninx investigated the effect of shape (amplitude over

time), duration and magnitude [42] of force on users' targeting performance [43]. They used the definite integral (Force Integral, FI) to compare different combination of the shape, duration and magnitude of the force feedback. In a Fitts' targeting task, they placed a force rendered bump at the half-way path to the target as a distracter. They found that the FI had a significant effect on task completion speed. Above a certain force magnitude, the user's performance significantly deteriorated. In this case, designers could rely on the FI to predict users' performance.

Jay and Hubbard studied the effect of delaying haptic, and/or visual feedback on users' performance and experience in Fitts' tapping task [44]. They used the HapticMaster force feedback device (Figure 2.3) to highlight the target so that it felt like a solid plane. They compared 5 levels of delay in 3 feedback conditions. Experimental results showed that delaying visual feedback seriously degrades performance while delaying haptic feedback has a small effect on performance only when the delay was considerable.



Figure 2.3 The HapticMaster force feedback device in the experiment (adapted from [44]).

Summary

Generally speaking, force feedback showed to be useful in assisting users' movement towards a target and stop users' movement when they reached the target. However, the force feedback needed to be carefully designed since undesirable feedback would deteriorate users' performance and increase workload especially in multi-target tasks [37, 38, 40].

2.2.2. Adding tactile feedback to indirect interactions

Campbell et al. studied the effect of collocation of visual and tactile feedback on users' interaction with GUIs [45]. They added vibrotactile feedback to the isometric trackpoint on a laptop (Figure 2.4). The vibrotactile feedback was used to simulate bump points on the screen. The researchers compared user's performance when visual bumps appeared in concert with tactile bumps (at the same location) and when the two feedbacks were not in concert. They found that the tactile bumps could reduce errors and increase task speed but only when it was presented coincidentally with visual feedback.

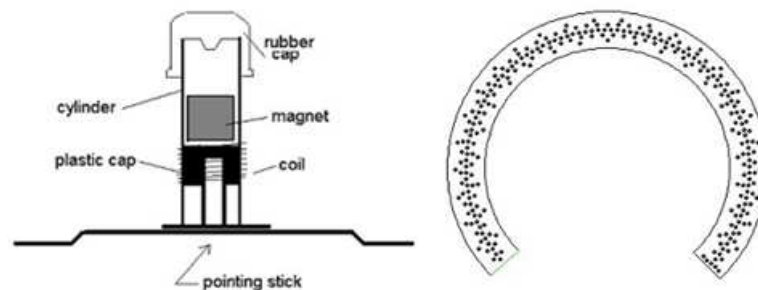


Figure 2.4 Haptic Trackpoint and the bump points in the tunnel (adapted from [45]).



Figure 2.5 The Logitech iFeel mouse (adapted from [46]).

Cockburn and Brewster [46] investigated how multimodal feedback helps small-target acquisition in graphical user interfaces. They compared three feedback modes and their combinations in two target acquisition tasks. The three feedback types were: non-speech audio; tactile; and pseudo-haptic 'sticky' feedback. They used the Logitech iFeel tactile mouse (Figure 2.5) to provide vibrotactile

feedback (200 Hz). Tactile feedback continued until the user moved off the target or made a selection. Experimental results showed that, all feedback modes reduce targeting times, with stickiness providing substantial improvements when the targets were located discretely. However, in a cascade menu selection task, additional feedback slowed down the targeting performance and made users more hesitant once the cursor was over the target. This result revealed that excessive feedback could damage interaction when distracters were distributed around the target.

Pasquero and Heyward introduced a handheld device with tactile feedback [47]. Tactile feedbacks are created by using an array of piezoelectric benders that were able to cause distributed lateral deformation in the skin, as shown in Figure 2.6. Short and long wave tactile feedback was applied to indicate items in a long list. Experimental results from a long list selection test showed that, although tactile feedback did not improve the task completion speed, it decreased 28% of reliance on vision.



Figure 2.6 The tactile transducer used in a handheld device to provide lateral traction on the surface of the finger skin (adapted from [47]).

Akamatsu, Mackenzie and Hasbroucq compared users' performance under five different sensory feedback conditions (normal, auditory, color, tactile, and combined) in a target selection task [48]. Tactile feedback was added via a solenoid-driven pin projecting through a hole in the left mouse button (Figure 2.7). Each feedback condition was activated when the cursor was in the target. Although there was no difference in overall movement times, error rates or

bandwidths, significant differences were found in the final positioning times. The tactile feedback reduced the positioning time as compared with normal condition.

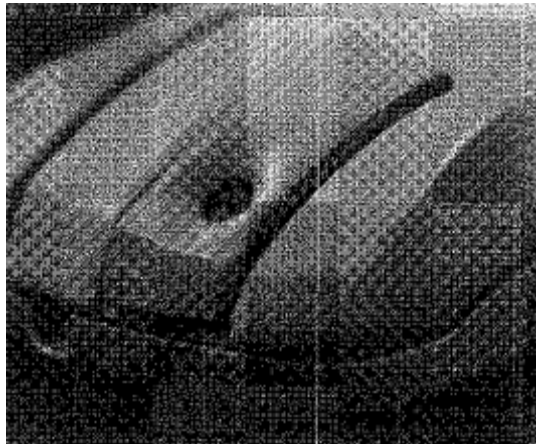


Figure 2.7 The haptic mouse with a solenoid driven pin (adapted from [48]).

Summary

The above literatures are characteristic research that applying tactile feedback to indirect interactions in the Human-Computer Interaction (HCI) domain. Tactile feedback in the examples performed mainly as a context reminder to the user, such as in condition the user moved across a boundary or out of the targeting routine. This helps users to respond faster as compared with providing visual feedback alone.

2.2.3. Adding coupled tactile and force feedback to indirect interactions

Akamatsu and Mackenzie investigated how different feedback modalities affected the dynamics of movements in a target acquisition task with a haptic mouse [49] (also shown in Figure 2.7). They compared four feedback conditions: normal, tactile feedback, force feedback and tactile + force feedback. When the cursor was inside the target boundary, the tactile feedback was realized by emerging a solenoid driven pin to stimulate the index finger resting on the mouse button. The force feedback was realized by activating the electromagnet in the mouse chassis to create drag between the mouse and an iron mouse pad. Haptic feedback only affected after the cursor entered the target. Experimental results

showed that, tactile feedback significantly reduced the overall movement time and the time to stop the cursor after entering the target, especially for small targets. However, tactile feedback also caused the highest error rate. This effect was explained as a reflexive muscle response. Force feedback, by contrast, had more effect on reducing errors but resulted in the longest task completion. Combining tactile feedback with force feedback resulted in the top task completion speed but also a high error rate.

In this study, although the projecting pin reminded the user that he entered the target, it caused reflexive muscle response which disturbed user's manipulation of the mouse. Therefore, when we couple force feedback and tactile feedback, we should preclude interferences of the two feedbacks that may interfere users' operation.

2.3. Tactile Displays for Direct Touch Interaction

Various tactile feedback devices have been applied to direct touch interactions to broaden feedback modality, enhance physicality and user experience. Each of them produced a specific tactile respond. Base on their operating principles, we demonstrate these technologies in the following categories: vibrotactile feedback, surface shape, friction, hardness, non-contact tactile feedback and electrotactile feedback.

2.3.1. Vibrotactile feedback

Vibrotactile feedback is widely applied to touch screen devices to encode data. A typical example is the phone alarm vibration generated by a vibration motor in mobile phones. To deliver vibrotactile feedback, an actuator can be placed beneath the touch surface, attached to the body of a handheld device or mounted inside the input interface (for pen computing). Accordingly, the user can perceive vibrotactile feedback when he touches the touch surface, holds the device or uses the input interface.

Inertia actuator

Inertia actuators are widely used to provide vibration among consumer electronics for their features of simple structure, small weight and ease of control. There are two types of inertia actuators: eccentric rotating-mass (ERM) actuator and linear resonant actuator (LRA). The ERM actuator works at a given rotation speed to obtain the maximum amplitude. ERM actuator is easy to generate vibration to alert or notice the user. However, it responds slowly and thus it is not suitable to generate sharp and crispy vibrotactile feedback [50], unless very accurate control is applied, such as the Immersion's VibTonz system [51].

An alternative way to use the ERM to produce rich tactile feedback is to modulate other parameters and take advantage of their combinations. For example, Pakkanen et al. [52] used the built-in ERM vibrator in a Nokia 5800 mobile phone to compare three haptic representation models with two representation rates to facilitate distinguishing the numbers used in the phone number keypad when visual feedback is not available. Haptic representations for the three types of numbers were generated by modulating the vibration amplitude, length, motor rotation direction and pause between vibrations. Experimental results showed that the three models had no effect on the input speed nor the error rate, but subjective experiences were affected. The Arabic numbers with slower speed were most preferred.

Besides, Yatani and Truong [18] presented the SemFeel, a tactile feedback system which was able to inform the presence of an object and offer additional semantic information about that item when a user touched it on the screen. They attached five vibration motors on the backside of a mobile touch-screen device (as shown in Figure 2.8). By controlling the vibration sequence, they were able to realize three types of patterns: positional, linear, and circular patterns. The patterns could help users to distinguish different buttons on a touch screen without looking at the screen. Experiment results showed that users could distinguish ten different patterns, including linear patterns and a circular pattern,

at approximately 90% of accuracy. In a number entering experiment, subjects entered more accurately but less quickly without looking at the screen as compared with simple tactile feedback or without tactile feedback.

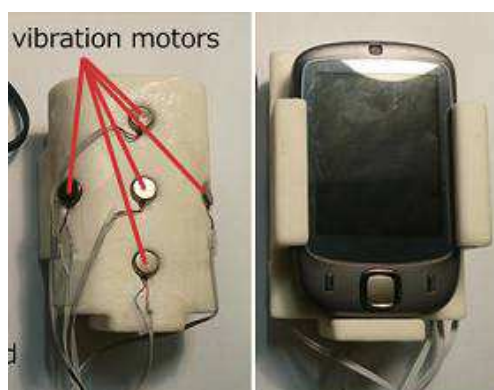


Figure 2.8 SemFeel used five vibration motors on the backside of a mobile touch-screen device to generate vibrotactile patterns (adapted from [18]).

Due to its compact size, the ERM actuator can be mounted inside pen-like input devices. Kyung, Lee and Park [53] presented the Ubi-Pen, a pen-like haptic interface providing texture and vibration stimuli. Texture patterns were simulated by a 3×3 pin-array tactile display which was stimulated by ultrasonic linear actuators. In addition, a pancake-type vibration motor was embedded at the tip of the pen to provide a sense of clicking (Figure 2.9). Experimental results showed that the clicking feedback of the Ubi-Pen decreased the time to enter calculations. With a similar idea, Sun, Ren and Cao mounted a vibration motor at the top of an input stylus (Figure 2.10) to investigate the relationship between “error feedback” (when tracking or trajectory errors are made) and users’ performance in steering tasks [54]. They compared audible, visual and tactile feedback and their combinations in a round tunnel steering task. Experimental results showed that, feedback conditions did not affect the movement time but significantly reduced error. Users performed most accurately with tactile feedback.

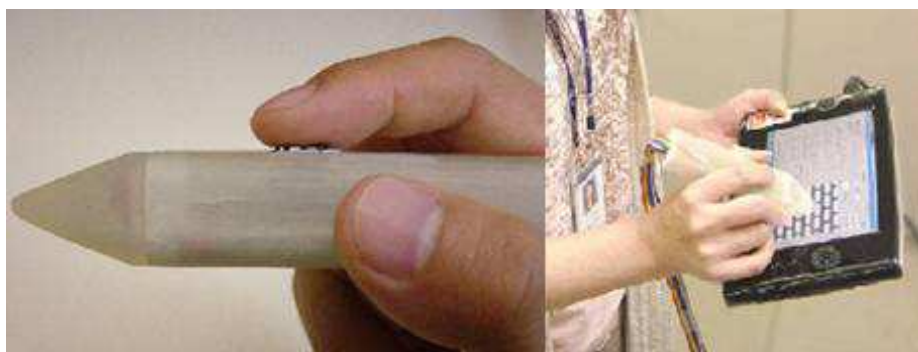


Figure 2.9 The Ubi-pen prototype and its application on a touch screen (adapted from [53]).



Figure 2.10 The stylus and the vibration motor (adapted from [54]).

However, a significant limitation of the ERM actuator is due to its low respond speed and great latency. It is not applicable to provide complex tactile patterns in interactive applications where small latency is crucial [10]. ERM motors rotate eccentrically weighted shafts that vibrate at low frequency (e.g. 130Hz [10]). By contrast, Liner Resonance Actuator (LRA) can generate higher frequency vibration (e.g. 175 Hz [1] which is close to the most sensitive frequency of finger skin as shown in Table **Erreur ! Utilisez l'onglet Accueil pour appliquer 标题 1 au texte que vous souhaitez faire apparaître ici..2**). The LRA has the advantage of fast respond speed and therefore can be used to generate crispy and instantaneous vibrotactile feedback [14]. Nevertheless, the limitation of the LRA is from its low frequency bandwidth — it can only work at resonance frequency. As a result, it is difficult to modulate its frequency to generate tactile patterns.

The LG Electronics company⁶ developed an advanced LRA — the dual-mode actuator (DMA). This motor had two spring-mass systems thus could work in two different frequencies. By modulating the two frequencies, researchers could

⁶ <http://patents.justia.com/patent/8461969>

design rich tactile feedback [55]. Park et al. compared tactile button click feedback produced by the LRA and DMA respectively. They designed and compared 72 vibrotactile stimuli by varying signal amplitude, duration, carrier signal, enveloped modulation method, and actuator. With users' subjective feedbacks, they established the relations between the vibration design parameters of button click tactile stimuli and subjective usability measures [55]. The LRA simulated button was more realistic and more preferable than the DMA due to shorter rising time. Therefore, using actuators which have short rising time is a key point when designing realistic button-click feedback.

Voice coil motor

Voice coil motors have smaller latency as compared with ERM actuators. They are applied to simulate tactile feedback that requires fast response. For example, single or continuous pulse signals generated by the voice coil motors are used to simulate button-click feedback [9, 56]. Fukumoto and Sugimura [9] were perhaps the first researchers to embed a voice coil actuator in a mobile touch-screen device. Button-click feedback was expressed by adding a single pulse or a short burst signal on the user's clicking finger or on the holding palm (as shown in Figure 2.11). This Active Click improved the input speed in a touch panel number input task especially in noisy situations.

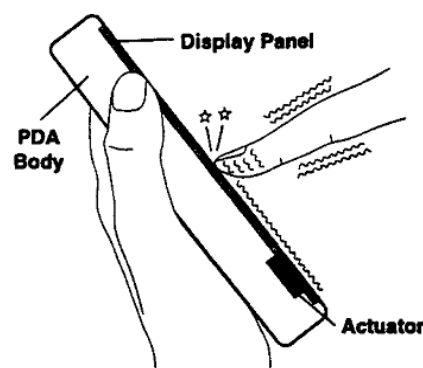


Figure 2.11 Actuator is mounted on the surface of the touch panel for creating button click feeling (adapted from [9]).

Brewster and his research team conducted a series of research about using

voice coil vibrators to add vibrotactile feedback on touch screens. Brewster and Brown [57] invented the Tactons, or tactile icons: they were structured, and by that way, abstract tactile messages that could be used for non-visual communication. A range of different parameters can be used to represent different meaning including: frequency, amplitude and duration of a tactile pulse, plus other parameters such as rhythm and location. Roughness feeling created by vibrotactile feedback could also be used as a parameter for constructing Tactons. Experimental results showed that the Tactons achieved an overall recognition rate of 71%, with a particular recognition rate of 93% for rhythm and 80% for roughness in the investigation of effectiveness [58]. The distribution of voice coil vibrators can also be applied to communicate complex information. Brown, Brewster and Purchase enhanced a calendar with vibrotactile feedback by associating rhythm, roughness, and spatial location of the vibrations with the type, priority and urgency of an event, respectively. Three voice coil vibrators located equidistantly on the user's forearm to indicate information about the time remaining before the appointment, as shown in Figure 2.12. The results showed that identification rate for three-parameter Tactons was only 48%, but could be increased to 81% by reducing the number of a parameter (roughness) [59].



Figure 2.12 Putting three vibrators on the forearm to encode information (adapted from [59]).

Compared with using single vibrator on touch screen devices, multiple actuators embedded in mobile devices were proved to produce a richer set of vibration patterns. Hoggan, Anwar and Brewster [60] investigated the perception and application of multi-actuator situated on a mobile device. In the research, actuators were placed in four different positions on the PDA corresponding to the

locations on the hand, as shown in Figure 2.13. A circular motion was presented to the participant across the actuators. The speed of the motion indicated the rate of the download. Results indicated that the participants responded faster to the completion of downloads when tactile feedback was added.



Figure 2.13 The multi-actuator PDA used to indicate downloads progress (adapted from [60]).

Brewster, Chohan and Brown [3] applied the concept of Tactons to investigate the use of vibrotactile feedback for touch-screen keyboards on PDAs. They added a C2 actuator (voice coil type) at the back of the PDA to vibrate at 250 Hz but at different amplitudes so that the user could distinguish successful button press and errors. They conducted stylus-based text entry experiments to compare standard buttons to ones with tactile feedback added in both laboratory and underground. Results showed that with tactile feedback users entered significantly more text, made fewer errors and corrected more of the errors they made. Strong subjective feedback in favor of the tactile display was also found. Hoggan, Brewster and Johnston [14] carried on the study of finger-based text entry for mobile devices with touch screens. They compared mobile devices with a physical keyboard, a standard touch screen and a touch screen with embedded resonant actuator. Results showed that the addition of vibrotactile feedback to the touchscreen significantly improved finger-based text entry, bringing it close to the performance of a real physical keyboard. Higher specification vibrators could improve performance though not significantly.

Solenoid actuator

Similar to the voice coil actuator, solenoid actuators also use magnetic forces to actuate vibration. The difference is that, in voice coils, the vibrating part is the coil while in solenoid the vibrating part is the permanent magnet [61], as shown in Figure 2.14. Unlike inertia actuators, solenoid actuators can be controlled by modulating frequency and amplitude respectively. Moreover, solenoid actuators have small latency, thus suitable to simulate crispy and fast tactile feedback.

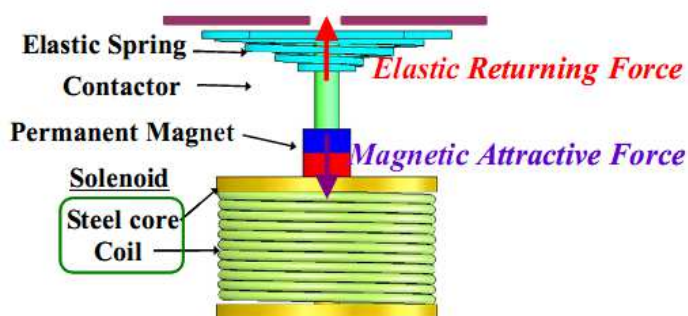


Figure 2.14 An example of solenoid actuator. The solenoid generates electromagnetic force to attract or repel the vibrator (adapted from [61]).

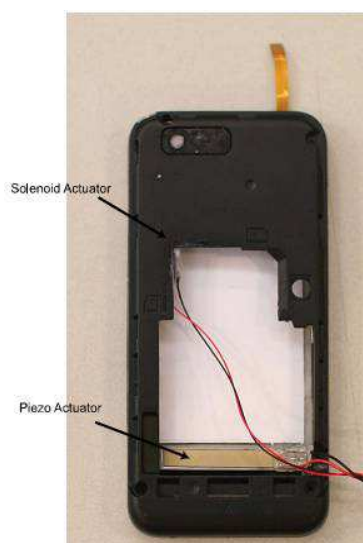


Figure 2.15 Both a piezoactuator and a solenoid actuator were utilized for the tactile feedback (adapted from [62]).

Kim et al. applied a piezo-actuator and a solenoid actuator to generate tactile impulses or vibrations on a touch screen, as shown in Figure 2.15. A user could distinguish tactile impulses through the proposed actuators in a manner that differs from existing vibration motors. The piezo-actuator was proved to be

suitable for simulating crisp tactile feedback while the solenoid actuator was suitable for creating smooth feeling. Psychophysical experiments also revealed that low-frequency vibrations or impulses could be used to create roughness on a smooth and nearly frictionless touch surface [62].

Lee et al. [63] presented a system for providing tactile feedback to stylus-based touch-screen displays. A pressure-sensitive stylus was combined with a small solenoid actuator at the end of a touch-stylus to generate a wide range of tactile sensations, as shown in Figure 2.16. Eight click-feelings were simulated.

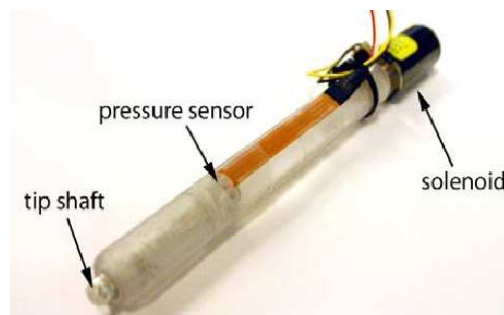


Figure 2.16 Haptic Pen – a tactile feedback stylus with solenoid actuator mounted at the end (adapted from [63]).



Figure 2.17 Indirect and direct input with a Haptic Pen (adapted from [13]).

Forlines and Balakrishnan [13] investigate users' performance with pointing and crossing interfaces controlled via both direct and indirect pen-input device. They used an improved Haptic Pen [63] to provide vibrotactile feedback when the user pointed or cross a target, as shown in Figure 2.17. Results show that tactile feedback was beneficial for both pointing and crossing selection, most noticeably

in crossing tasks when using direct input where visual feedback is often occluded by a hand or stylus.

Piezoelectric actuator

Piezoelectric actuator is a commonly used hardware for generating vibrotactile feedback. Piezoelectric actuators have several potential benefits: thin form factor, fast response time, and high bandwidth. These features make it suitable to be used in thinner devices with relatively large screens [1]. Piezoelectric actuators generate vibration based on the inverse piezoelectric effect: voltage applied to the electrodes causes a deformation. By placing the actuators beneath the touch surface or inside the handheld device, the actuators generate tactile feedback by either moving the touch surface [64-67] or vibrating the entire device [10, 62].

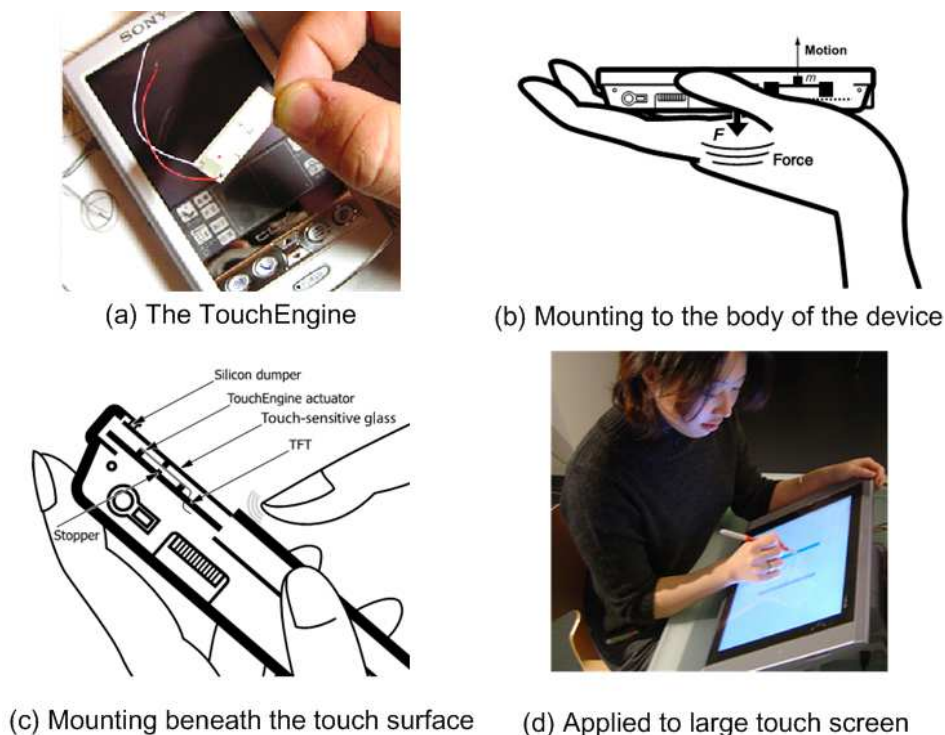


Figure 2.18 The TouchEngine tactile actuator and its application to touch screen devices (adapted from [10], [67] and [66]).

Poupyrev, Maruyama and Rekimoto [10] developed a tactile actuator, the TouchEngine, which was a universal tactile display that could produce a variety of

tactile feelings from simple clicks to complex vibrotactile patterns. The TouchEngine actuator was constructed as a sandwich of thin ($\sim 0.28\mu\text{m}$) piezoceramic films with printed adhesive electrodes in between, forming an extremely thin (less than 0.5mm) beam. When a signal was applied, the entire structure bent. They embedded a TouchEngine tactile display into a Sony Clie PEG-N700C Palm OS based PDA, as shown in Figure 2.18 (a) and (b). By controlling the amplitude and the frequency of vibrations at the same time, it was feasible to create a variety of tactile waveforms. User studies demonstrated a 22% faster task completion when they enhanced handheld tilting interfaces with tactile feedback in a text selection task. In this prototype, the tactile actuator was placed inside the body of the PDA. Device vibration was delivered to the user's hand that held the device instead of the touching finger. This would partially mask vibrations perceived by a touching finger, significantly reducing the perceived strength of tactile feedback from the touch screen. In order to solve this problem, Poupyrev and Maruyama [67] embedded four TouchEngine actuators at the corners of the touch screen between the display and the touch-sensitive glass plate (Figure 2.18 (c)) so that only the glass plate vibrated instead of the whole PDA. In this case, users could feel tactile feedback through their fingers when touching the screen. Five interaction gestures (i.e., touchdown, hold, drag, lift off in the element, lift off outside the element) were augmented with different tactile feedback effects when the user touched buttons, scroll bars and menus. An informal usability study with 10 colleagues proved that the haptic feedback was well received, and was most effective when the GUI elements needed to be held down or dragged across the screen. A larger reproduction of this design was then applied to a 15 inch LCD monitor with larger size ($30 \times 5 \text{ mm}$) TouchEngine. Four TouchEngine actuators were placed in the corners of a display in between the LCD and the thin protective glass panel on the top, as shown in Figure 2.18 (d). When the piezoelectric actuators bent in response to a signal, they pushed the glass outwards and the user could feel vibration through the pen which was

touching the screen. In Fitts' tapping task, tactile feedback did not improve the user performance. However, tactile feedback improved user performance in the drawing (dragging) task by a statistically significant amount. User preferences to the combination of active gesture with tactile feedback were also found.

Another example is given by the Nokia 7710 internet tablet, a commercial smart phone which embedded a piezoelectric actuator to raise and release the touch surface by bending the layers of the actuator [65], as shown in Figure 2.19. The displacement amplitude ranged from a few micrometers to a few hundred's of micrometers. Various forms of single pulses were created with frequencies up to 1 KHz.

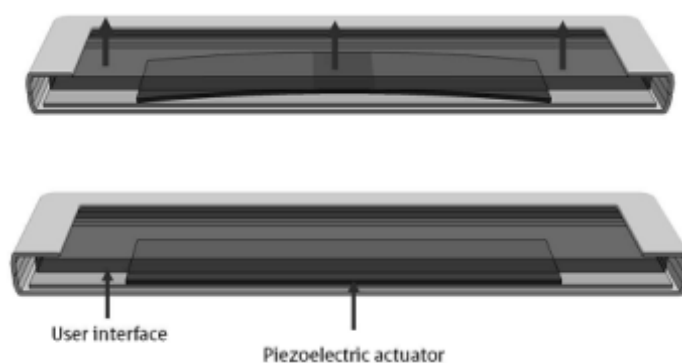


Figure 2.19 Piezoelectric actuators raised the touch surface in the Nokia 7710 (adapted from [65]).

Researchers implemented several studies with this mobile phone. Leung, MacLean, Bertelsen and Saubhasik [12] evaluated the haptic augmentations of touch screen GUI buttons, progress bars, and scroll bars under varying cognitive loads. Experiment results demonstrated that haptically augmented progress bars and scroll bars led to significantly faster task completion, and favorable subjective reactions. Moreover, they were more useful when the user is under cognitive load than under no cognitive load. Pakkanen et al. [68] compared three alternative designs for creating haptic edges for buttons. They found that clear and sharp stimuli were needed to simulate a more realistic button and a bit crisp but fast stimulus was a good choice when simulating button edges. Rantala et al. compared three interaction methods to present Braille characters on mobile touch

screen devices [69]. The tactile feedback for raised dots was set to be a vibration of 30 μm amplitude and 19 ms duration. All the three methods were able to convey information as the blind participants could accurately (91-97%) recognize individual characters. At last, Hoggan et al. investigated methods to congruently simulate a virtual button so that the button's appearance was congruent with its audio/tactile feedback. The result offered guidelines on how to select the most appropriate audio and tactile feedback to a certain visual button style [70].

Similar to the principle of Nokia 7710's tactile feedback, Kaaresoja, Brown and Linjama [64] demonstrated a mobile device with tactile feedback — the Snap-Crackle-Pop, as shown in Figure 2.20. They placed off-the-shelf piezo-actuators under a resistive touch screen to provide tactile feedback to a stylus or finger using the device and to the holding hand. Tactile feedbacks were added to four different applications: numerical keypad, text selection, scrolling, drag and drop. In the following research, Koskinen, Kaaresoja and Laitinen [71] investigated which type of tactile button on a touch screen was the most pleasant to use with a finger. They compared two actuator solutions in a small mobile touch screen: piezo actuator and a standard vibration motor. They found that tactile feedback was superior to a non-tactile condition when virtual buttons were used with the finger, regardless of the technology to generate the tactile feedback. In a phone number input test, users perceived the feedback generated by piezo actuators slightly more pleasant than the vibration motor based feedback, although not statistically significant.



Figure 2.20 The “Snap-Crackle-Pop” tactile mobile device (adapted from [64]).

Chen et al. affixed a single layer of piezoelectric actuator to a stainless steel plate that served as the cover of a handheld device to provide button-click feedback (Figure 2.21). By modulating amplitude, frequency, and number of cycles of raised cosine waveforms used to drive the piezo-actuator, they successfully created up to 5 to 6 identifiable button-click feedback [16].

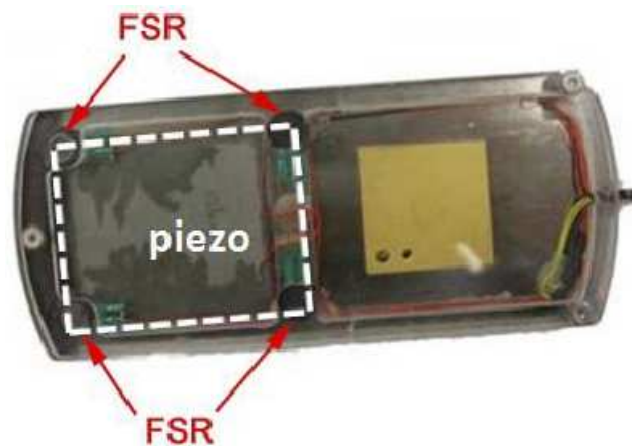


Figure 2.21 Gluing piezoelectric actuator at the back of a handheld device to simulate button-click feedback; force sensors were used to detect finger contact on the device (adapted from [16]).

Impact motor

The impact motor is a kind of linear vibration motor. It works by driving a mass move along a longitudinal axis of the case through electromagnetic force induced by electric signals [72], as shown in Figure 2.22 (a). The impact motor has

short setting time and is suitable to simulate button-click feedback.

Kyung, Lee and Srinivasan [72] designed a haptic stylus which embedded vibration, impact and sound feedback. They applied this stylus to interact with touch screen GUIs. Several haptic feedbacks were designed for events like clicking, drag and drop, moving, scrolling, highlighting, and other things. Experimental results showed that haptic feedback improved certain tasks including equation inputting, icon selection and dragging, and text handling, as shown in Figure 2.22 (b). Subjective feedback from users also indicated that haptic feedback improved users' comfort and manipulation. Authors also noted that impact motors had better controllability than vibration motors due to shorter settling time.

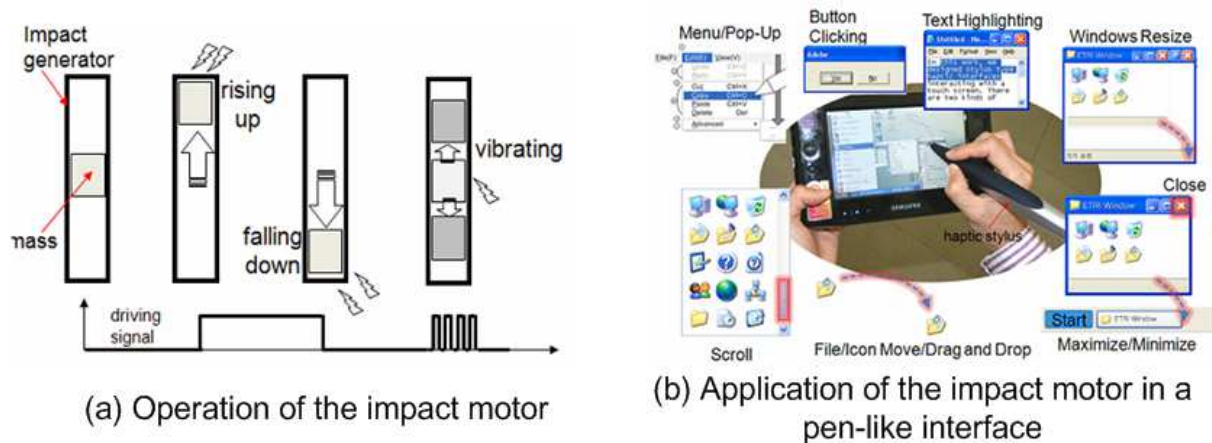


Figure 2.22 The operation of the impact motor and its application in a pen-like input interface (adapted from [72]).

Electro-active polymer (EAP)

EAP has the advantages of high deformation rate, low driving voltage, low weight, and thin thickness [73]. It was commonly used to control artificial muscles and recently be implemented to enhance mobile interactions.

Shin et al. evaluated the application of electro-active polymer (EAP) to simulation of button-click feedback [73]. The EAP simulated button-click feedback was more favorable to users, as compared with a traditional LRA vibrator. A significant reason was that the EAP had a short response time (within 5 ms) and

falling time. Researchers also pointed out that short and clear pulse pattern were important to simulate a favorable button-click feedback. This finding also confirmed Park et al.'s research [55] in which they found that a short rising time was important to simulate button-click feedback.

Summary

Applying vibrotactile feedback in touch interaction is most widely used. New technologies are proposed to further enhance its fidelity. According to the review, the trend of the vibrotactile feedback application emerges: apply small latency, fast response, frequency and amplitude decoupled actuators to provide rich tactile patterns. This trend offers guideline for us to select a good actuator when vibrotactile feedback is needed in touch interaction.

2.3.2. Surface shape

While vibrotactile feedback can encode information on the touch surface, surface shape changing tactile devices change the shape of the touching surface.

Harrison and Hudson presented a technique for creating dynamic physical buttons using pneumatic actuation [74]. Physical form and appearance of buttons could be dynamically controlled by providing positive or negative air pressure, as shown in Figure 2.23. If no pressure was applied, the display was simply flat. The curvature of the pneumatic buttons provided an extra clue for users to identify them. In a user study, subjects were able to locate the target pneumatic buttons faster than flat touch screen buttons. Moreover, the performance of the pneumatic button was much like physical buttons.

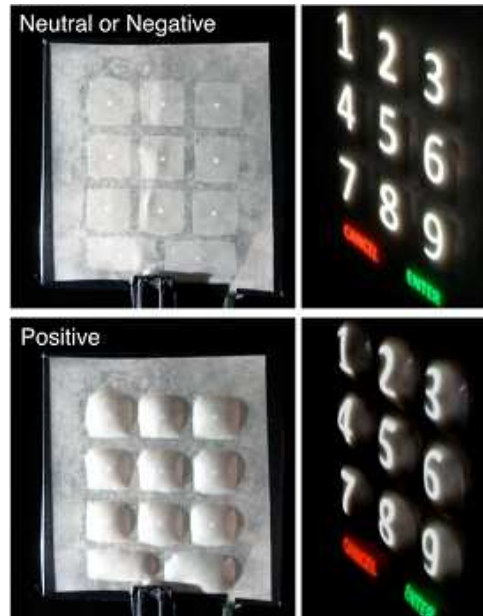


Figure 2.23 Neutral, negative and positive appearance of the pneumatic buttons (adapted from [74]).

The Tactus Technology[©] developed a similar technology but using fluid [75]. The designers placed a multi-layer panel over a touch screen. A number of micro-holes connected the top layers of the panel to a series of micro-channels that run through the underlying substrate. The micro channels were filled with a fluid whose optical index of refraction matches that of the surrounding material to make it fully transparent. A rise of the fluid pressure made the fluid push up through the holes and against the top polymer layer, making it expand in pre-defined locations, as shown in Figure 2.24. This enabled an array of physical and completely transparent buttons to rise out of the surface.

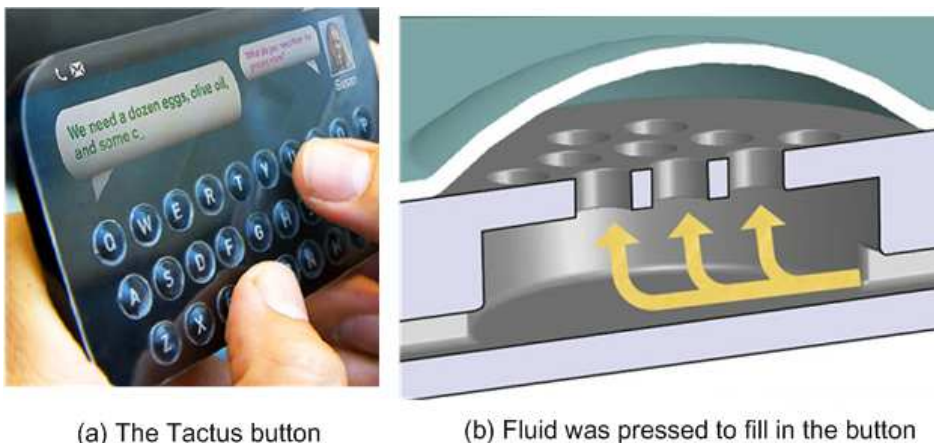


Figure 2.24 The Tactus button (adapted from [75]).

Although these technologies well simulated the shape of buttons on touch screens, the contour and layout of the buttons were afore-customized and could not be changed according to applications. An alternative method was to create the shape of a touch element with distributed pins. Kim et al. developed a dynamically re-formable input device to operate vehicular telematics systems [76]. The device included a 1536 pins (48×32) display matrix to display pictures and texts, as shown in Figure 2.25. Experimental results showed the tactile input device helped increase the input speed compared with a touch monitor.



Figure 2.25 Displaying text and pictures using pins (adapted from [76]).

Summary

The method to reproduce the shape of a virtual button enhances the physicality of the touch surface, brings it close to a physical keyboard. However, the patterns that this technology can produce are limited (mainly for keyboards). Or, plenty distributed actuators are needed to control the surface shape. In that case, its application is limited due to the size and mass of the actuators.

2.3.3. Friction

Dragging the finger on the touch surface is a typical gesture in touch interaction. By dragging, users can move a file, scroll a menu, or draw a picture. Changing the friction of the touch surface helps users identify the current interactions (e.g., contacting an icon or not) and enhances the physicality of touch interaction. Generally, there are three types of interfaces that can change friction

condition of the touch surface: by reducing friction coefficient, by increasing normal force, and by producing lateral force on the finger.

Reducing friction coefficient

This type of tactile interfaces is mainly based on the squeeze air film to reduce friction coefficient of the touch surface [25, 77, 78]. Lévesque et al. investigated the design possibilities and outcomes when touch interactions were enhanced with variable surface friction with a Large Area Tactile Pattern Display (LATPaD) [79], as shown in Figure 2.26. The device reduced friction coefficient of a glass surface from ~ 1.0 to ~ 0.15 by producing a squeeze film of air through 26 kHz piezo-actuated vibrations. The examination of programmable friction showed significant performance advantages for drag-based selections and no adverse effects when distracter targets were present. In addition, variable friction could have a positive impact on the enjoyment, engagement and sense of realism experienced by users of touch interfaces.

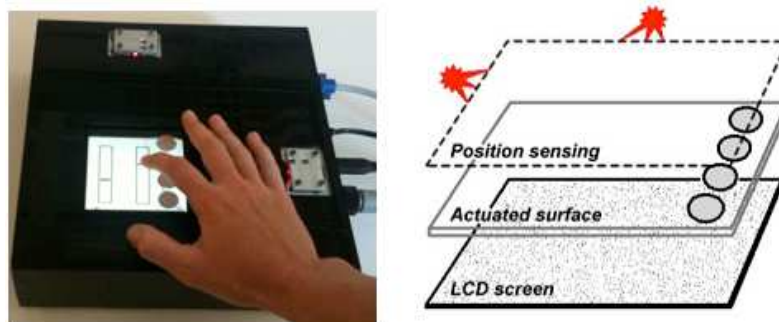


Figure 2.26 The Large Area Tactile Pattern Display (LATPaD, adapted from [79]).

Casiez et al. [80] presented the Surfpad pointing technique which was also based on the squeeze film effect generated by the STIMTAC device (Figure 2.27) to alter a touchpad's friction coefficient. Surfpad led to a performance improvement close to 9% compared to unassisted pointing at small targets without distracters. It was also robust to high distracter densities, keeping an average performance improvement of nearly 10%. Experimental results also suggested that the performance improvement was caused by tactile information

feedback rather than mechanical causes, and that the feedback was more effective when friction was increased on targets using a simple step function.

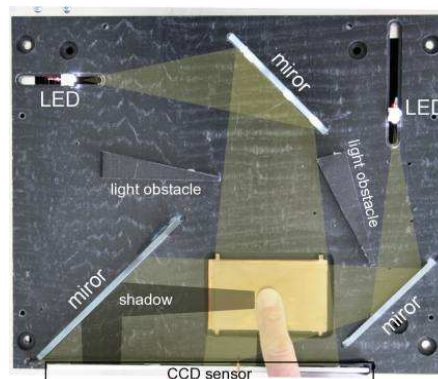


Figure 2.27 The STIMTAC haptic device (adapted from [80]).

While the squeeze film based tactile interfaces always work at the resonance frequency of the device, Ji et al. activated two identical piezoelectric actuators that were placed diagonally on a glass plate (as shown in Figure 2.28) at different frequencies to produce more expressive tactile feedback. By this method, the new device was able to produce three groups of tactile feedback including friction reduction, vibration and tangential forces [81].

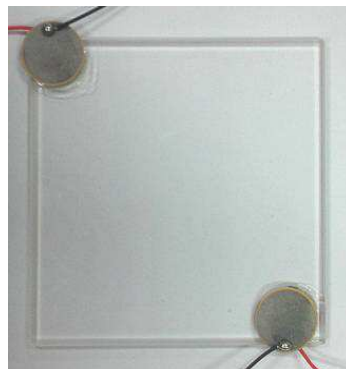


Figure 2.28 Activating two piezoelectric actuators at two different frequencies produced more expressive tactile feedback (adapted from [81]).

Kotani, Takasaki and Mizuno developed a tactile display which used ultrasonic Surface Acoustic Wave (SAW) to reduce friction coefficient [82]. They placed piezoelectric actuators at the edges of a glass to generate 5 MHz SAW (Figure 2.29). By changing the constant contact of the finger to periodic contact

with the touch surface, the device reduced the perceived friction on the touch surface. However, this device needed the user to press on an aluminum pad above the glass to feel the tactile feedback, thus limited its applications.

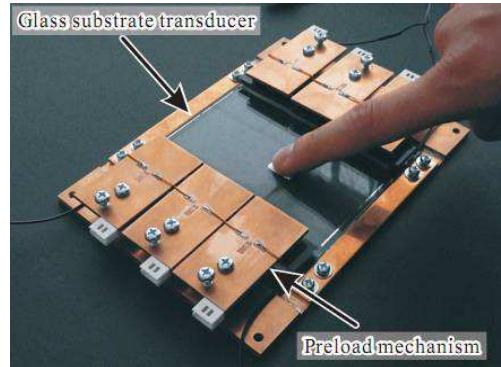


Figure 2.29 The SAW tactile interface (adapted from [82]).

Although friction reduction devices can generate uniform tactile feedback across the touch surface, the workspace of the displays is limited as compared with consumers' requirement of large screen devices. Therefore, large workspace tactile devices are needed to improve users' experience on large touch screens.

Increasing normal force

On the opposite of the previous devices, there are also possibilities to change the friction coefficient of a surface by increasing the normal attractive force between the touch surface and the finger in order to increase the perceived friction of the touch surface.

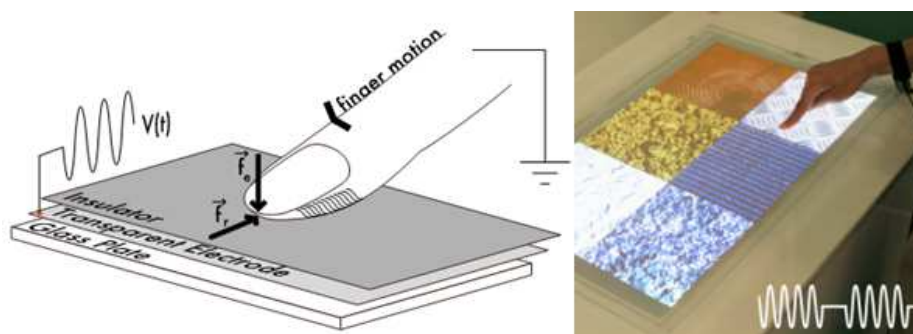


Figure 2.30 The principle and an example of the TeslaTouch (adapted from [83]).

Within this idea, Bau et al. [83] developed the TeslaTouch which was based on

electrostatic effect. This effect can be explained as follows: the insulating layer of users' dry outer finger skin formed the dielectric layer of a capacitor, in which conductive surface of the device and fluids in the finger's tissue were the two opposing plates. When an alternating voltage was applied to the conductive surface, an intermittent attraction force developed between the finger and conductive surface. By changing the amplitude and frequency of the activating voltage signal, the friction between the moving finger and the touch surface can be modulated to simulate different texture patterns, as shown in Figure 2.30. Low frequency stimuli were perceived as rougher compared with high frequency ones. The increase of amplitude could enhance the feeling of roughness. The most attractive advantage of the TeslaTouch was that the device didn't have any moving part. It was highly scalable and could be used on touch surfaces of any size, shape and configuration. Compared with mechanical actuated vibration, the TeslaTouch could generate spatially uniform tactile feedback and avoid attenuation of tactile sensations across frequencies. Although this technology was highly scalable and uniform, it needed high voltage to be applied to the user, or the user needed to be connected to the ground. Moreover, the electrostatic effect is also affected by skin conditions, e.g., excessive sweating [84].

Wintergerst et al.[85] introduced a haptic enhanced stylus for touch screen applications. A rolling ball at the tip of the pen was magnetically attracted by an embedded electromagnetic coil so that the friction between the pen-tip and the touch surface was increased, as presented in Figure 2.31. However, the increase of friction relied on the size and weight of the ball and caused human acceptance problem.

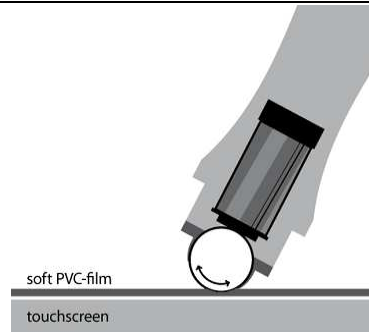


Figure 2.31 The magnetic coil attracts the ball and causes higher friction (adapted from [85]).

Producing lateral force

Lateral force on a finger is usually produced by moving the touch surface laterally. When the finger presses on the touch surface, the lateral movement of the touch surface makes the user feel an increase of friction.

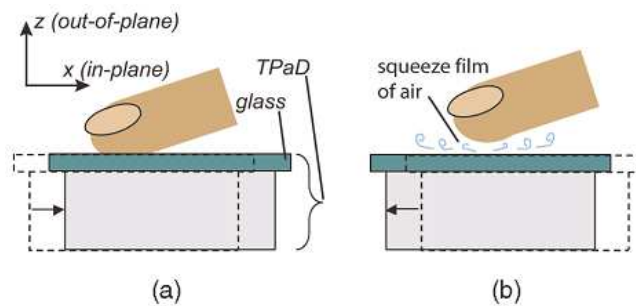


Figure 2.32 The principle of the ShiverPad (adapted from [78]).

The ShiverPad used voice coil actuator to oscillate a TPad [78] which was alternated between high friction and low friction. When the TPad was not working (high friction), the forward movement of the TPad produced lateral force to the finger pad, as presented in Figure 2.32 (a). In contrast, when the TPad was activated (low friction), the backward movement of the TPad only reduced friction coefficient of the touch surface, as presented in Figure 2.32 (b). This oscillation was driven at 854 Hz by the voice coil actuator and could not be distinguished by the user. The ShiverPad had the potential of displaying edge-like features. A human subject study is conducted to demonstrate that users could easily trace virtual edges displayed on the surface of the ShiverPaD.

In the same Lab, Dai, Colgate and Peshkin developed the LateralPad (Figure 2.33) which generated lateral (shear) force on a bare finger through vibrating the touch surface simultaneously in both out-of-plane (normal) and in-plane (lateral) directions. The normal and lateral resonances were both activated at the same ultrasonic frequency (~ 22.3 KHz). As a result, the resultant movement of the touch surface produced lateral force to the finger pad which pressed on the touch surface. By modulating the relative phase of the two resonances, the produced force on the finger could be controlled. However, the maximum lateral force is around 70 mN which is not very easy to be perceived [86].

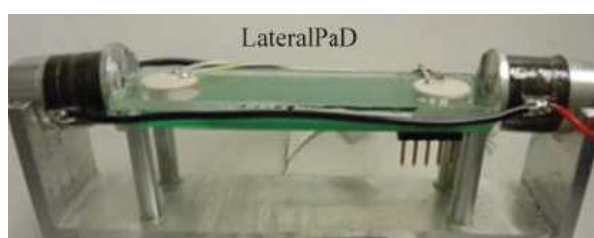


Figure 2.33 The LateralPad (adapted from [86]).

Kaye demonstrated a touch screen prototype which was driven by a pair of powered speakers controlled by a sawtooth wave [87]. The actuators were placed orthogonally at two sides of a mobile phone, as shown in Figure 2.34. By modulating the two actuators at frequency about 140 and 280 Hz, the device could move the mobile phone laterally in the touch surface, providing a lateral force feedback.



Figure 2.34 The two actuators produced lateral movement of the mobile phone (adapted from [87]).

Although lateral force feedback has the advantage of providing directional

friction, the amount of force delivered to the finger needs to be increased.

2.3.4. Hardness

Jansen, Karrer and Borchers [88] developed the MudPad, a system that was able to localize haptic feedback on multi-touch surfaces. They used an array of electromagnets which locally actuates a tablet-sized overlay containing magnetorheological (MR) fluid to change the hardness when a user touched the touch surface, as shown in Figure 2.35. Since the haptic feedback was generated with distributed actuators, this device could realize localized haptic feedback. However, there was no user evaluation about the localized haptic feedback. Moreover, the system was rather bulky making it difficult to be applied to mobile touch screen devices.



Figure 2.35 MudPad is a system that provides localized haptic feedback independently at multiple points (adapted from [88]).

2.3.5. Non-contact tactile feedback

Alexander, Marshall and Subramanian [89] introduced adding a mid-air, ultrasonic haptic feedback to the back of a mobile TV in order to enhance the mobile TV experience. They used a 10×10 array of ultrasonic transmitters to generate acoustic radiation pressure field, as show in Figure 2.36. In this way, the user could feel the haptic feedback even without touch the surface. By modulating frequency, pulse and length parameters, authors produced various vibrotactile textures. In a preliminary experiment, subjects could identify multiple specific

feedback points with 87% accuracy.



Figure 2.36 The user holds the mobile TV and feels haptic feedback at the back of the device. The ultrasonic acoustic pressure moved tapes when various regions of transducers are triggered (adapted from [89]).

Weiss et al. [90] presented the FingerFlux, an output technique to generate near-surface haptic feedback on interactive tabletops. The FingerFlux used electromagnetic field to create haptic feedback. When operating the device, the user attached permanent magnets to his index finger and moved that finger over an interactive surface with electromagnet arrays beneath the surface, as presented in Figure 2.37. Attraction, repulsion, vibration, and directional haptic feedback on and near the surface could be generated by changing the electromagnetic field even before the user touched the surface. Experimental results showed that users were able to perceive vibration patterns up to 35 mm above our table, and that FingerFlux could reduce drifting when operating on-screen buttons without looking.



Figure 2.37 The FingerFlux interactive surface (adapted from [90]).

Summary

Although these new technologies provide possibilities to introduce tactile feedback even before the user touches on the screen, researchers need to simplify their system to make them possible to use in mobile interactions. Moreover, electromagnetic compatibility is also a problem to be solved.

2.3.6. Electrotactile feedback

Altinsoy and Merchel present an electrotactile device for touch screen handheld devices [91]. Small currents are transmitted to users' fingers through a transparent electrode above the display screen (Figure 2.38). The currents excite the coetaneous nerve fibers, thus generate electrotactile feedback. By increasing current or impulse frequency, they can increase the perceived roughness. However, in compassion with real surfaces, subjects tend to match the rough surface with high current magnitude and a low pulse frequency. A limitation of this method was that continuous electrotactile feedback caused sensory adaption. Therefore, long term application should be carefully designed.

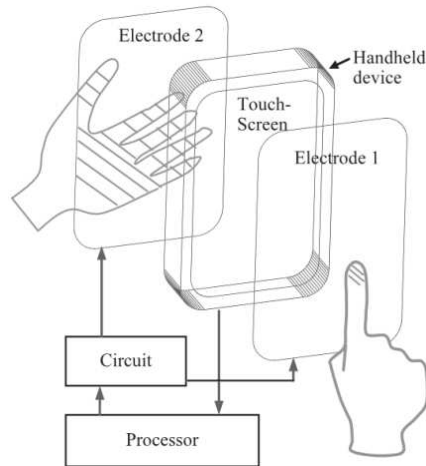


Figure 2.38 Touch screen with electro-tactile feedback (adapted from [91]).

2.4. Summary

This chapter conveys aspects of haptic feedback in touch interaction. The sense of touch and the physiology of human haptic system are introduced firstly. According to the survey, we know that human touch sense includes both kinesthetic and cutaneous sensations. The human haptic sensation is perceived through mechanoreceptors. The function and features of the mechanoreceptors are also reviewed so as to design haptic interfaces accordingly.

An important domain of haptic application is in HCI. In the early age of HCI, haptic technologies were applied to input interfaces to interact indirectly with GUIs. The haptic technologies used in indirect interaction with GUIs were summarized in section 2.2. Force feedback devices as the input device are introduced, as well as adding tactile feedback to input interfaces and applying both force and tactile feedbacks to a modified mouse. In general, force feedback was applied to assist users' movement towards a target and stop users' movement when they reached the target. This effect was useful and improved user's performance. However, the force feedback needed to be carefully designed since undesirable feedback would deteriorate users' performance and increase workload. Tactile feedback, on the other hand, mainly performed as a context reminder to the user, such as in condition the user moved across a boundary or out of the

targeting routine. This helps users to respond faster as compared with providing visual feedback alone. Finally, an example of coupling both force feedback and tactile feedback in a mouse pointing task shows that this feedback causes top task completion speed but also a high error rate. Therefore, when we couple force feedback and tactile feedback, we should preclude interferences of the two feedbacks that may interfere users' operation.

In section 2.3, we reviewed the state of the art of adding tactile feedback in direct touch interaction which related most closely with the present research. By the principle of the tactile interfaces, we categorized them in six types: vibrotactile, surface shape, friction, hardness, non-contact tactile feedback and electro-tactile feedback. The vibrotactile interfaces took a major part of the applications. They were used to encode information on the touch surface, alert users about the current interaction context, and enhance physicality on the touch screen (e.g. by providing button-click feedback). The hardware that provided vibrotactile feedback was summarized. The character and application of each type of actuators were presented. According to the review, we also found the trend of the vibrotactile feedback application – applying small latency, fast response, frequency and amplitude decoupled actuators to provide rich tactile patterns. In this case, the piezoelectric actuator is a good candidate.

An alternative way to provide tactile feedback to touch interaction is to change the shape of the touch surface. This method enhances the physicality of the touch surface, brings it close to a physical keyboard. However, the patterns that this technology can produce are limited. Or, plenty distributed actuators are needed to control the surface shape and in that case, it limits its application.

Another method to enhance touch screen physicality is to change the friction when interacting on the touch surface. This method was realized by reducing friction coefficient by means of the squeeze film effect, increasing normal press on the touch surface or producing lateral force on the finger pad through the touch surface. As compared with vibrotactile feedback, variable friction feedback is

uniform across the touch surface and does not attenuate with the distance from the actuating resource. On the other hand, applying lateral force directly to the finger is promising. However, the amount of force delivered to the finger is limited. As for electrostatic effect, it can increase the friction and is highly scalable, but it needs high voltage to drive the device. Moreover, the effect is also affected by skin conditions. In comparison with electrostatic effect, squeeze film effect which reduces friction coefficient of the touch surface shows potential in touch interactions. However, the workspace of the displays is limited. That is why we intended to apply squeeze film effect based technology in our design of a tactile device but also proposed method to increase its workspace in Chapter 4.

Other modalities of tactile feedback are also added to touch interaction, such as changing surface hardness, producing non-contact tactile feedback, and electrotactile feedback. As compared with aforementioned technologies, these new technologies are either too bulky to be applied to touch screen devices or at the preliminary level of research.

Although many technologies are available to add tactile feedback to touch surfaces, the holistic touch sensation is not fully presented. Little is known about how force feedback affects users' performance and experience in *direct* touch interaction. Moreover, the interaction between force feedback and tactile feedback needs to be learnt before providing both of them to the user. Therefore, we intend to develop an integrated haptic interface for touch interaction. With the device, we can investigate how coupled haptic feedback affects users' interaction on touch screens. The device we propose includes a cable-driven force feedback device and a squeeze film effect based tactile display. In the following chapters, the design of the force feedback device and the tactile device are presented respectively. Finally, an evaluation of the coupled device is conducted to investigate the merit of providing coupled haptic feedback.

Chapter 3.

Design of the force feedback device

Summary

3.1.	Introduction	47
3.2.	Related work	48
3.3.	Configuration and Kinematic Design	51
3.3.1.	Configuration	51
3.3.2.	Kinematics	53
3.4.	Cable tension control	55
3.4.1.	Feasibility of Exerting 4-DOF Force Feedback with Four Cables	55
3.4.2.	Cable Tension Calculation	57
3.4.3.	Maintain Positive Cable Tension	60
3.5.	Implementation	62
3.5.1.	Mechanical Design.....	62
3.5.2.	Control System Configuration	64
3.5.3.	Application Demonstration	65
3.6.	Evaluation	69
3.6.1.	Simulating a button-click	69
3.6.2.	Knob manipulation.....	75
3.7.	Conclusion	80

3.1. Introduction

Although some actuation technologies are available to add tactile feedback to touch screens (as review in Chapter 2), little research about adding force feedback to touch screens has been undertaken. Moreover, high-fidelity force feedback has been shown to produce a more authentic response and a more satisfactory user experience [2]. Therefore adding force feedback to touch screens is both promising and challenging. A significant difficulty of applying force feedback to a touch screen is that the workspace must be transparent. Users want to see their fingers as well as obtain force feedback when they touch virtual objects. However, the transmission of force requires media. Opaque media are not applicable to touch screens. For example, conventional link-driven force feedback devices (e.g. PHANToM [92]) are able to display authentic force information when users operate the devices to interact with a virtual environment. But this type of device is opaque. The links obstruct the user's view on a touch screen when they are placed in front of it. Moreover, their workspace is limited. It cannot satisfy the requirements of ever larger screens such as touch screen walls and tabletops. By contrast, cable-driven haptic devices have the advantages of fast reaction speed, simple structure, and smooth manipulation. Most importantly, they have scalable and transparent workspace [93]. These advantages make cable-driven haptic devices suitable for touch screen applications. In addition, the multi-touch technology has triggered lots of interesting applications on touch screens, such as rotating an image, drawing with multi-finger, and operating bi-manually. Applying multi-finger force feedback to touch screens will not only retain these applications but also make it possible to enable users to perform tasks like grasping, manipulation, and multi-point exploration of virtual objects.

In this chapter, the design and evaluation of a new force feedback interface, The FingViewer, is presented. The FingViewer is designed to realize force feedback on touch screens. This new device is driven by only four cables and realizes either 3-DOF force feedback on one finger or 4-DOF force feedback on

dual fingers. The minimized complexity of this design makes it possible to be easily mounted on an ordinary touch surface without any modification.

In the following sections, we first review research on cable-driven haptic interfaces. Then we describe the configuration and principle of the device in Section 3.3.1 and explain how the device obtains the user's finger positions in Section 3.3.2. After that, we present the force feedback capability of the FingViewer. Section 3.4 explains how the cable tension is calculated to exert the required force feedback. In Section 3.5, we present the implementation of the device and the result of the force feedback in a few applications. Finally, we evaluate the device in a button-click and knob-control experiment respectively. The process and results of this experiment are presented in Section 3.6. The conclusion of this chapter is presented in Section 3.7.

3.2. Related work

Cable-driven haptic interfaces have been widely studied due to their advantages of fast reaction speed, simple structure, smooth manipulation, and scalable and transparent workspace [93]. Cable-driven haptic devices with different DOFs have been developed for various applications, such as a 2-DOF haptic mouse to interact indirectly with a Graphic User Interface [94], a 2-DOF wearable interface to explore bas-relief virtual surfaces [95], a planar 3-DOF haptic interface for locomotion [96], a 5-DOF haptic pen for desktop haptic display [97] and a 6-DOF joystick for a telerobotic system [98].

A typical cable-driven haptic interface named SPIDAR was developed by Sato and his research team. The SPIDAR [99] haptic device used 4 cables and yielded 3-DOF force feedback in the 3D space. The four cables from the four corners of a cubic frame were fixed on a ring, as shown in Figure 3.1 (a). A user wore the ring to interact with virtual objects. Force feedback was applied to the finger that wore the ring. This single-point haptic interface was not efficient in realizing 3D manipulation like picking and placing an object as we do in the real world. In

order to solve this problem, the SPIDAR-II [100] haptic device was developed by

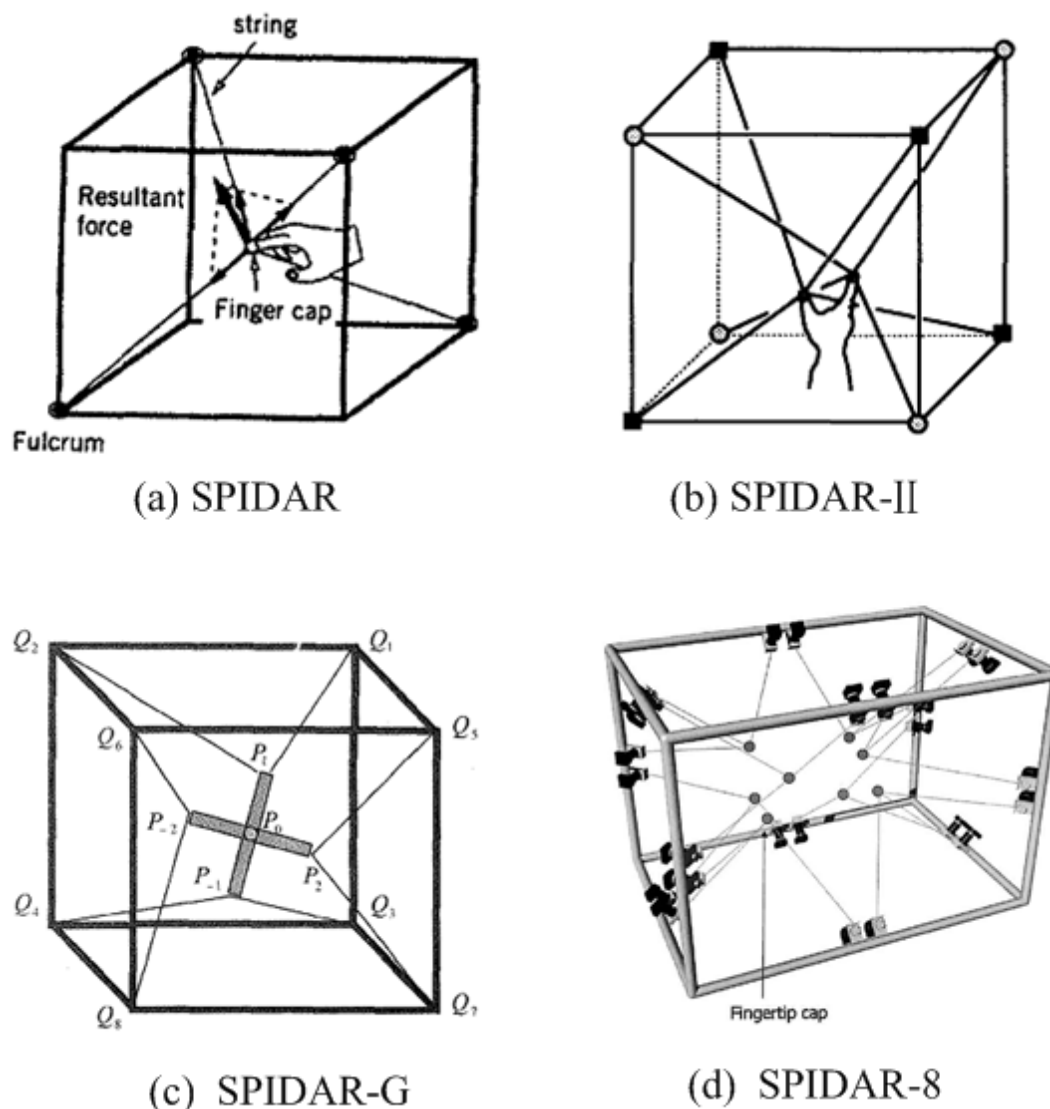


Figure 3.1 The SPIDAR force feedback devices (adapted from [99], [100] [93] and [101] respectively).

combining two SPIDARs, as shown in Figure 3.1 (b). Each SPIDAR haptic device provided 3-DOF force feedback on a finger. As a result, the user was able to experience force feedback when gripping a virtual object in 3D space, although it is possible for an interference of the cables to occur due to an excessive adduction or abduction of the hand. The SPIDAR-G [93, 102] haptic device enabled a cross-type grip which was a 1-DOF grasp related to the centre of the cross. Each tip of the cross was tensed by two cables, as shown in Figure 3.1 (c). The SPIDAR-G realized 1-DOF grasp and 6-DOF manipulation force feedback by 8

cables. Although the SPIDAR-G allowed the user to grasp virtual objects by hand, it was unable to provide force feedback to individual fingertips. Walairacht et al.[101] developed the SPIDAR-8 haptic device which realized force feedback on all fingers of both hands except the little fingers. The force feedback at each fingertip was generated by three cables, as presented in Figure 3.1 (d). The resultant of the tensions was limited within the pyramid enclosed by the three cables. The purpose of this research was to create a mixed reality environment so that users were able to perceive grasp force feedback at their fingertips and see a virtual world with a live image of their hands manipulating virtual objects. Therefore manipulation force, such as the collision force between the grasped object and other virtual objects, was not introduced. An alternative method of realizing both multi-finger grasping and 6-DOF manipulation force feedback in a large space was to integrate a multi-finger force feedback glove to the end effector of a 6-DOF cable-driven force feedback device. This method was applied to develop the SPIDAR-HAND [103] which could generate 6-DOF manipulation force feedback and 5-DOF grasp. The grasp force feedback at each finger was activated by a micro motor on the glove. The glove was mounted at the end effector of the cable-driven haptic device and thus increased system inertia.

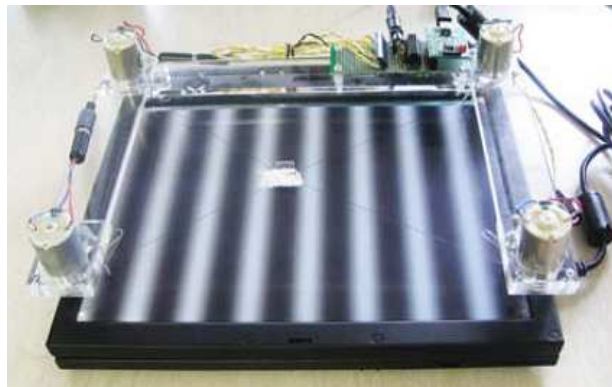


Figure 3.2 The 2-DOF force feedback device used to simulate bumps on a touch screen (adapted from [104]).

Compared with sophisticated multi-DOF and multi-finger cable-driven haptic interfaces which were developed to realize force feedback in space, planar multi-DOF and multi-finger cable-driven haptic interfaces have not been widely

studied. In particular, little research has been undertaken to design and develop a force feedback device to realize force feedback for touch screen applications. Saga and Deguchi applied the SPIDAR-mouse force feedback device [94] to simulate bumps on the touch surface [104]. By providing lateral force according to the haptic illusion effect [105], they simulated several sinusoidal-shape objects with different amplitude and wavelength. However, their device could only provide 2-DOF force feedback through a pad-based interface, as shown in Figure 3.2. Users could not touch directly on the touch surface.

3.3. Configuration and Kinematic Design

3.3.1. Configuration

The configuration of the one finger cable-driven force feedback device (FingViewer-I) is presented in Figure 3.3 (a). The circle centered at O_c represents the ring that the user wears. Treat the ring as a rigid body, it has 3-DOF in a plane (two translational and one rotational). The ring can be fully controlled by the four cables connected to it. This function can also be realized by another configuration as described in [106]. However, we choose the current configuration due to its simple structure and singularity-free workspace [107]. It should be noted that, for a single touch interaction, we only need to track the two translational movements of the finger. In this case, a 2-DOF device (e.g., [104]) is sufficient. However, considering that we need the user to touch the touch surface with their bare fingers⁷, a ring is used as the interface. The selected configuration is suitable to control the ring-type interface and the redundant rotation can be used to expand the expressiveness of input, such as the orientation of the finger.

⁷ There are two reasons for this. The one, touching directly on the touch screen is users' habit when they use conventional touch screen. The second, we intend to provide not only force feedback but also tactile feedback to the user. So, they need to touch on the tactile device we developed in Chapter 4 to perceive the tactile feedback.

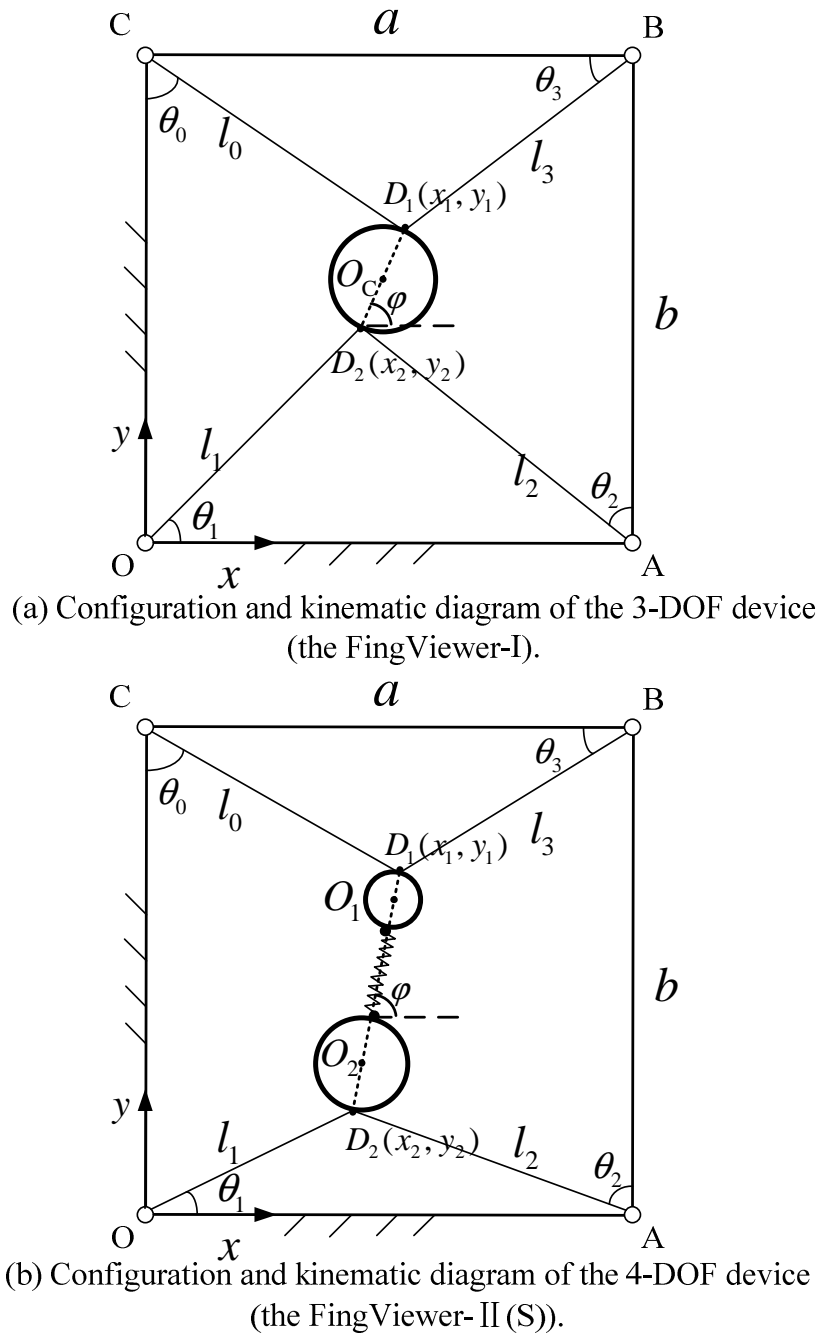


Figure 3.3 Configuration and kinematic diagram of the FingViewer force feedback devices.

The distance between D_1 and D_2 (where the ring is connected with the cables) is constant (equals to the diameter of the ring) in the 3-DOF mechanism. As a result, the FingViewer-I only has 3-DOF. Imagine if the distance between D_1 and D_2 is flexible. The mechanism will have an extra DOF. The mechanism in Figure 3.3 (b) is designed to realize this idea. Each ring is connected by a pair of cables in

D_1 and D_2 respectively. Moreover, the two rings are connected by a draught spring. Since cables cannot exert stress but only tensions, cable tensions should maintain positive all the time. Therefore, there will always be resultant force of cable tensions exerted on the fingers when the user operates the device at D_1 and D_2 . The spring is used to balance the resultant force of cable tensions in free space. Thus when moving the two fingers in free space, the user will not feel any restriction. It should be noted that, the spring is only used to balance the minimum cable tensions rather than exert force feedback. It is useful when the resultant of minimum cable tensions is too much for the user. Otherwise, the spring can be removed. In that case, the resultant force is balanced by the user's hand.

It should be noted that the spring used in the configuration is a draught spring. When it is compressed, it cannot provide any force (just like a rubber band). In that case, the user will feel a resistance caused by the resultant of minimum cable tensions.

3.3.2. Kinematics

Finger positions are the basis of touch screen applications. The FingViewer realizes the track of finger positions through the forward kinematics of the mechanisms presented in Figure 3.3.

In Figure 3.3, D_1 and D_2 are the positions where the cables are attached to the rings. O_C , O_1 and O_2 are the centers of the rings in the FingViewer-I and FingViewer-II(S) respectively. The positions of $D_1(x_1, y_1)$ and $D_2(x_2, y_2)$ are deduced from the inverse kinematics. The inverse kinematics is presented as follows: assuming $D_1(x_1, y_1)$ and $D_2(x_2, y_2)$ are given, we calculate the cable lengths l_0, l_1, l_2, l_3 .

The squares of the cable lengths are presented as follows

$$l_0^2 = x_1^2 + (b - y_1)^2 \quad (3.1)$$

$$l_1^2 = x_2^2 + y_2^2 \quad (3.2)$$

$$l_2^2 = (a - x_2)^2 + y_2^2 \quad (3.3)$$

$$l_3^2 = (a - x_1)^2 + (b - y_1)^2 \quad (3.4)$$

where a and b are the side lengths of the base. The cable lengths can be obtained by extracting the roots.

Subtracting (3.4) from (3.1), we obtain

$$x_1 = \frac{l_0^2 - l_3^2 + a^2}{2a} \quad (3.5)$$

Substituting (3.1) with (3.5), and considering the rings are inside the frame of the device, we then obtain

$$y_1 = b - \frac{\sqrt{4a^2l_0^2 - (l_0^2 - l_3^2 + a^2)^2}}{2a} \quad (3.6)$$

Similarly, we can calculate the coordinate of $D_2(x_2, y_2)$ with (3.2) and (3.3)

$$\begin{aligned} x_2 &= \frac{l_1^2 - l_2^2 + a^2}{2a} \\ y_2 &= \frac{\sqrt{4a^2l_1^2 - (l_1^2 - l_2^2 + a^2)^2}}{2a} \end{aligned} \quad (3.7)$$

The orientation angle φ can be calculated as follows

$$\varphi = \arctan \frac{y_1 - y_2}{x_1 - x_2} \quad (3.8)$$

In the case of the FingViewer-I, the coordinate of the ring center, O_c , is deduced as

$$x_o = \frac{x_1 + x_2}{2}, y_o = \frac{y_1 + y_2}{2} \quad (3.9)$$

In the case of the FingViewer-II(S), the distance between $D_1(x_1, y_1)$ and $D_2(x_2, y_2)$ is calculated in order to calculate the spring force

$$d = \sqrt{(x_1 - x_2)^2 + (y_1 - y_2)^2} \quad (3.10)$$

The gripping of the thumb and index finger is assumed to be a 1-DOF movement. Therefore the movement of O_1 and O_2 is along the center line of the spring. The coordinate of O_1 and O_2 are calculated as

$$\begin{aligned}x_{O_1} &= x_1 - r_{O_1} \cos \varphi \\y_{O_1} &= y_1 - r_{O_1} \sin \varphi\end{aligned}\tag{3.11}$$

$$\begin{aligned}x_{O_2} &= x_2 + r_{O_2} \cos \varphi \\y_{O_2} &= y_2 + r_{O_2} \sin \varphi\end{aligned}\tag{3.12}$$

where r_{O_1} and r_{O_2} are the radii of the rings for the index finger and the thumb respectively. The contours of the fingers are assumed to be two circles with O_1 and O_2 as centers.

3.4. Cable tension control

Cable-driven haptic devices use controlled cable tension to exert force feedback. Cable tension control is the fundamental and core problem of cable-driven force feedback devices. As the cable tension control method for the 3-DOF mechanism is relatively more mature [96, 106, 107] as compared with the new 4-DOF device, we focus on the cable tension control of the FingViewer-II(S). In this section, we first explain why it is possible to exert 4-DOF force feedback with only four cables and one spring. Then we demonstrate how cable tension is calculated. Finally, we explain how cable tension is kept positive during the user's manipulation.

3.4.1. Feasibility of Exerting 4-DOF Force Feedback with Four Cables

The FingViewer-II(S) is designed to simulate 1-DOF grasping force feedback and 3-DOF manipulation force feedback. In this case, the user can obtain the concrete feeling of grasping an object and interacting with other virtual objects. It has been proved that n -DOF cable driven mechanisms need at least $n+1$ cables [108]. However, this conclusion was deduced by analyzing a rigid end

effector. In fact, it would be more accurate to say that n -dimensional force feedback requires $n+1$ cables because a flexible end effector can have extra DOFs (for example, a spring can shrink and extend, but a rigid bar cannot).

Figure 3.4 presents the statics diagram of the FingViewer-II(S) device. We analyze the statics of the end effector (treat the spring and two rings as a whole). Figure 3.4(a) shows the origin statics indicating the forces applied to the end effector. In Figure 3.4(b), we decompose user's forces applied by the index finger (\mathbf{F}_{index}) and the thumb (\mathbf{F}_{thumb}) to grasp forces and manipulation forces. According to the static equilibrium, the force and torque exerted by the user should be balanced by the resultant force and torque of the cables. The statics equations are

$$\sum_{i=0}^3 \mathbf{t}_i = -(\mathbf{F}_W + \mathbf{F}_{G1} + \mathbf{F}_{G2}), \quad \sum_{i=0}^3 \mathbf{R}_i \times \mathbf{t}_i = -\mathbf{T} \quad (3.13)$$

where \mathbf{t}_i is the tension vector on the i^{th} cable, \mathbf{F}_W and \mathbf{T} are the manipulation force and torque transmitted to the center of the spring respectively, \mathbf{F}_{G1} and \mathbf{F}_{G2} are the grasp force transmitted at D_1 and D_2 respectively, and \mathbf{R}_i is the position vector. Equation (3.13) can be written in matrix form as

$$\mathbf{A} \begin{pmatrix} t_0 \\ t_1 \\ t_2 \\ t_3 \end{pmatrix} = \begin{pmatrix} F_{Wx} + F_{Gx} \\ F_{Wy} + F_{Gy} \\ T \end{pmatrix} \quad (3.14)$$

where \mathbf{A} is the 3×4 static Jacobian matrix (in Appendix), F_{Wx} and F_{Wy} are the components of F_W along the x and y axis respectively, and F_{Gx} and F_{Gy} are the components of resultant grasp force F_G along the x and y axis respectively. As we can infer from (3.14), the 4-DOF force feedback becomes 3-dimensional resultant force/torque. Therefore the four cable tensions are sufficient to exert this 3-dimensional force feedback.

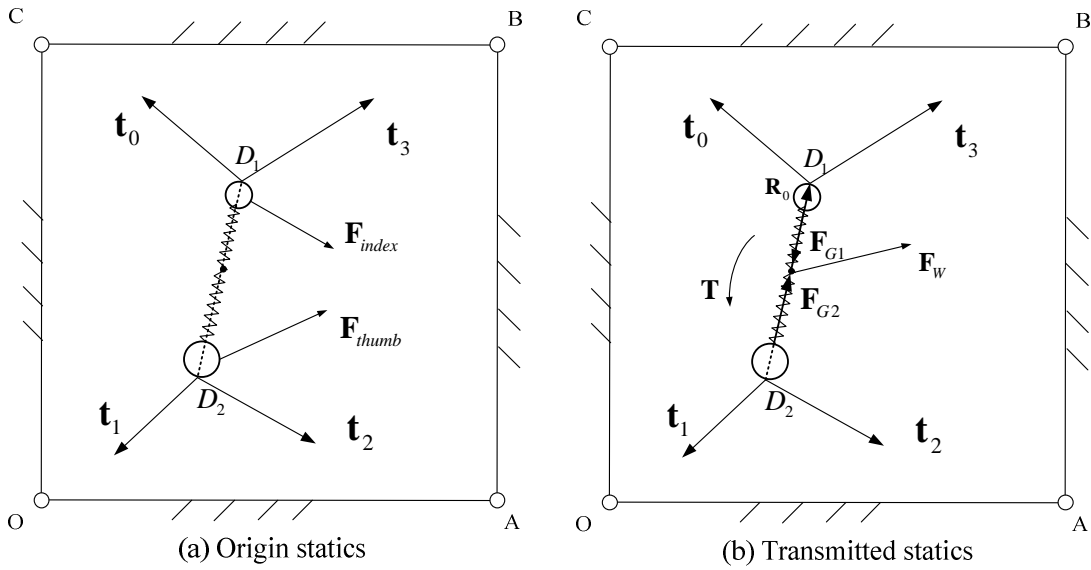


Figure 3.4 Static diagram of the FingViewer-II(S).

3.4.2. Cable Tension Calculation

Although the four cable tensions can exert 4-DOF force feedback, we cannot calculate how great the tension is from (3.14) because the solution of that linear equation is not unique. We need to find a reasonable way of controlling the cable tension. In fact, different force feedbacks are exerted by the cable tension separately at different stages.

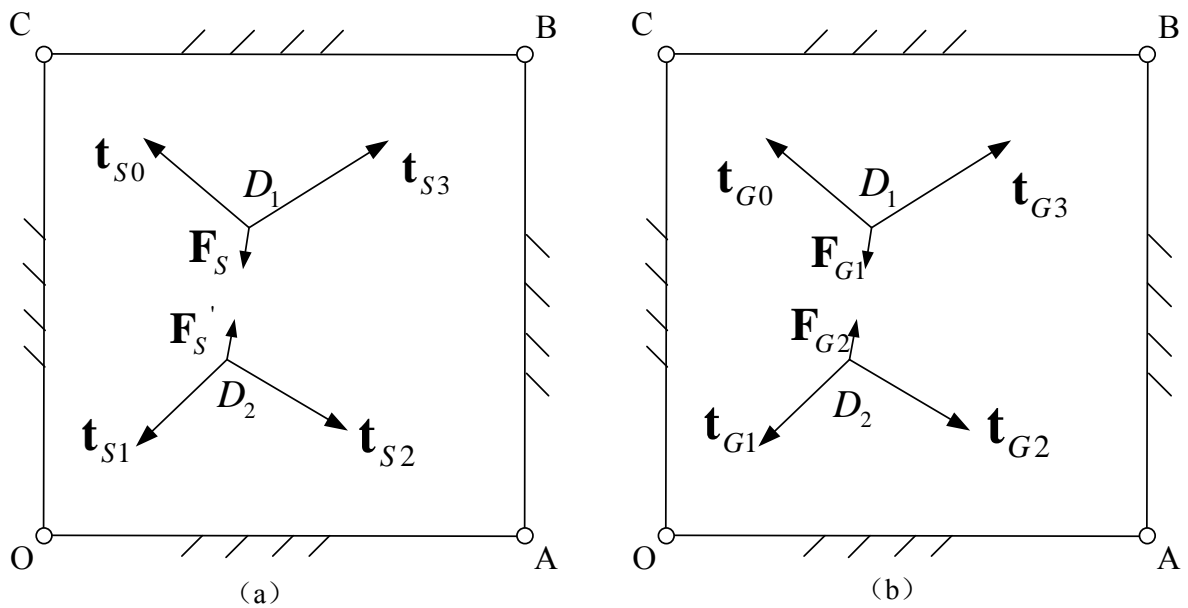


Figure 3.5 Static diagram demonstrating the spring force and the grasp force.

First, in free space, when the fingers do not collide with virtual objects, they should be able to move freely without feeling any restriction. The spring exerts tension when it is stretched. The magnitude of spring tension is calculated by Hook's Law:

$$F_s = \begin{cases} k_s(d_s - d_0), & d_s > d_0 \\ 0, & 0 \leq d_s \leq d_0 \end{cases} \quad (3.15)$$

where F_s is the magnitude of the spring tension, k_s is the spring constant, d_0 is the original length of the spring, and d_s is the length of the spring ($d_s = d - 2r_{o1} - 2r_{o2}$, where d is calculated by (3.10)). The spring force is balanced by cable tension to enable the user to move freely in the free space. The static equilibrium equations are set up at D_1 and D_2 respectively, as shown in Figure 3.5 (a).

$$\mathbf{t}_{s0} + \mathbf{t}_{s3} = \mathbf{F}_s, \mathbf{t}_{s1} + \mathbf{t}_{s2} = \mathbf{F}_s' = -\mathbf{F}_s \quad (3.16)$$

where \mathbf{t}_{s_i} ($i=0,1,2,3$) is the cable tension to balance the spring tension, \mathbf{F}_s and \mathbf{F}_s' are the spring tensions transmitted at D_1 and D_2 respectively, and $\|\mathbf{F}_s\| = \|\mathbf{F}_s'\| = F_s$. The solution of (3.16) is positive and unique. The resultant force of the spring at this stage is zero. Therefore the solution of (3.16) also obeys the following equation

$$\mathbf{A} \begin{pmatrix} t_{s0} \\ t_{s1} \\ t_{s2} \\ t_{s3} \end{pmatrix} = \begin{pmatrix} 0 \\ 0 \\ 0 \\ 0 \end{pmatrix} \quad (3.17)$$

Similarly, when the user grasps a virtual object, the grasp force is balanced by the cable tension. The static equilibrium equations are set up at D_1 and D_2 respectively, as shown in Figure 3.5 (b)

$$\mathbf{t}_{g0} + \mathbf{t}_{g3} = \mathbf{F}_{G1}, \mathbf{t}_{g1} + \mathbf{t}_{g2} = \mathbf{F}_{G2} \quad (3.18)$$

where \mathbf{t}_{g_i} ($i=0,1,2,3$) is the cable tension to balance the grasp force, and \mathbf{F}_{G1} and

\mathbf{F}_{G_2} are the grasp forces transmitted at D_1 and D_2 respectively. The solution of Equation (3.18) is positive and unique. The grasp forces are equal to each other when the grasp is stable. Nevertheless, when only one finger is in contact with the virtual object (as in the case of contour following), the contact force can also be simulated by calculating the cable tension through Equation(3.18). However, the limitation of this system is that the direction of the force exerted at each finger is limited to the angle formed by the two corresponding cables ($\angle CD_1B$ and $\angle OD_2A$ in Figure 3.3 (b)). As a result, the device cannot exert force beyond this range, for example, a lateral force along the x axis.

The grasp force is along the central axis of the spring. As a result, no torque is yielded by the grasp force. The solution of (3.18) satisfies

$$\mathbf{A} \begin{pmatrix} t_{G0} \\ t_{G1} \\ t_{G2} \\ t_{G3} \end{pmatrix} = \begin{pmatrix} F_{Gx} \\ F_{Gy} \\ 0 \end{pmatrix} \quad (3.19)$$

To simulate solely the manipulation force, the grasped object and the two fingers are considered as a whole. The resultant force of the cable tension will balance the wrench of the manipulation

$$\mathbf{A} \begin{pmatrix} t_{w0} \\ t_{w1} \\ t_{w2} \\ t_{w3} \end{pmatrix} = \begin{pmatrix} F_{wx} \\ F_{wy} \\ T \end{pmatrix} \quad (3.20)$$

where $\mathbf{\$}^w = [F_{wx} \ F_{wy} \ T]^T$ is the wrench of the grasped object and $\mathbf{t}_w = [t_{w0} \ t_{w1} \ t_{w2} \ t_{w3}]^T$ is the cable tension vector to balance the wrench. The solution of (3.20) contains two parts

$$\mathbf{t}_{wi} = \mathbf{A}^+ \mathbf{\$}^w + (\mathbf{I} - \mathbf{A}^+ \mathbf{A}) \mathbf{z} \quad (3.21)$$

where \mathbf{A}^+ is the Moore-Penrose pseudo inverse of \mathbf{A} , \mathbf{z} is an arbitrary vector, \mathbf{I} is the 4×4 identity matrix, $\mathbf{A}^+ \mathbf{\w is the particular solution of (3.20), and $(\mathbf{I} - \mathbf{A}^+ \mathbf{A}) \mathbf{z}$ is the homogeneous solution that projects \mathbf{z} into the null space of \mathbf{A} . Equation (3.21) can also be written as

$$\mathbf{t}_w = \begin{Bmatrix} t_{wp0} \\ t_{wp1} \\ t_{wp2} \\ t_{wp3} \end{Bmatrix} + k_0 \begin{Bmatrix} n_0 \\ n_1 \\ n_2 \\ n_3 \end{Bmatrix} \geq 0 \quad (3.22)$$

where $[t_{wp0} \ t_{wp1} \ t_{wp2} \ t_{wp3}]^T$ is the minimum norm solution of Equation (3.20), k_0 is an arbitrary scalar, and $\mathbf{n} = [n_0 \ n_1 \ n_2 \ n_3]^T$ is the null space basis of \mathbf{A} . The value of k_0 is calculated from

$$k_{0i} = \frac{-t_{wpi}}{n_i}, (i = 0, 1, 2, 3) \quad (3.23)$$

If all n_i are negative, then k_0 is selected as the negative k_{0i} whose magnitude is largest; if all n_i are positive, then k_0 is selected as the positive k_{0i} whose magnitude is the largest [109].

The total cable tension of each cable is the sum of the three components that balance the different forces

$$\mathbf{t}_i = \mathbf{t}_{Si} + \mathbf{t}_{Gi} + \mathbf{t}_{wi}, i = 0, 1, 2, 3 \quad (3.24)$$

where \mathbf{t}_i is the total cable tension. The components of \mathbf{t}_i are calculated from (3.16), (3.18) and (3.22). If we add (3.17), (3.19) and (3.20), we obtain

$$\mathbf{A} \begin{pmatrix} t_{S0} + t_{G0} + t_{W0} \\ t_{S1} + t_{G1} + t_{W1} \\ t_{S2} + t_{G2} + t_{W2} \\ t_{S3} + t_{G3} + t_{W3} \end{pmatrix} = \begin{pmatrix} F_{Wx} + F_{Gx} \\ F_{Wy} + F_{Gy} \\ T \end{pmatrix} \quad (3.25)$$

This result is identical to (3.14). It also proves that the cable tension can be calculated as the sum of separate components.

3.4.3. Maintain Positive Cable Tension

In cable-driven force feedback devices, cables are wound on pulleys that are connected with motors. The torque of the motor is converted to the tension of the cable. One important feature of the cable-driven mechanism is that the cables cannot exert stress but only tension. Negative tension will cause unwinding of the

cables and finally make the device uncontrollable [110]. Therefore we need to keep each component of the cable tension positive and the sum of these components greater than the minimum cable tension so that

$$\mathbf{t} = \mathbf{t}_S + \mathbf{t}_G + \mathbf{t}_W \geq \mathbf{t}_{\min} \quad (3.26)$$

where $\mathbf{t}_{\min} = [t_{\min} \ t_{\min} \ t_{\min} \ t_{\min}]^T$, and t_{\min} is the magnitude of the minimum cable tension. As we have shown in the previous section, the tension to balance the spring force, \mathbf{t}_S , and the tension to balance the grasp force, \mathbf{t}_G , are positive and unique; and the tension to balance the manipulation wrench, \mathbf{t}_W , is positive and is calculated by (3.22) and (3.23). Although the sum of the tensions to balance different forces is positive (as presented in (3.24)), in certain circumstances the cable tension does not rise above the minimum. For example, in free space, the tension to balance the grasp force and the manipulation wrench is zero. If the user fails to extend the spring far enough to enable the cable tension to reach the minimum cable tension, the cables will become loose. For this reason, we need to add extra cable tension to meet the criterion of minimum cable tension

$$\mathbf{t} = \mathbf{t}_S + \mathbf{t}_G + \mathbf{t}_W + k_m \mathbf{n} \geq \mathbf{t}_{\min} \quad (3.27)$$

The value of k_m is calculated from

$$k_{mi} = \frac{t_{\min} - t_{Si} - t_{Gi} - t_{Wi}}{n_i}, (i = 0, 1, 2, 3) \quad (3.28)$$

If all n_i are negative, then k_m is selected as the negative k_{mi} whose magnitude is largest; if all n_i are positive, then k_m is selected as the positive k_{mi} whose magnitude is the largest. If the inequality (3.26) is met, we don't need to add extra cable tension. In this case, $k_m = 0$.

After the cable tension is calculated, the magnitude of \mathbf{t}_i is used to control the motor current.

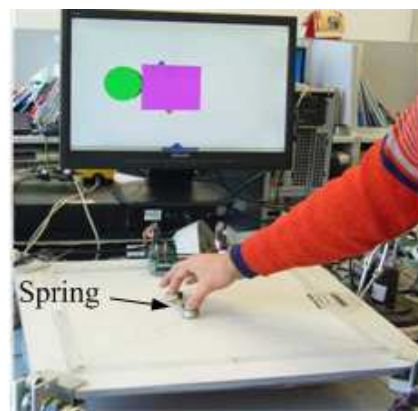
3.5. Implementation

Three prototypes have been implemented for different applications: a FingViewer-I (Figure 3.6 (a)), a FingViewer-II(S) (Figure 3.6 (b)) with spring and a FingViewer-II without spring (Figure 3.6 (c)). The FingViewer-I and FingViewer-II are implemented for touch screen applications, while the FingViewer-II(S) is used for indirect interactions.

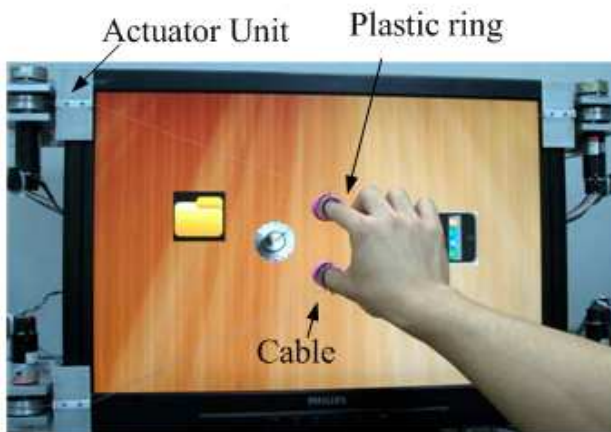
3.5.1. Mechanical Design



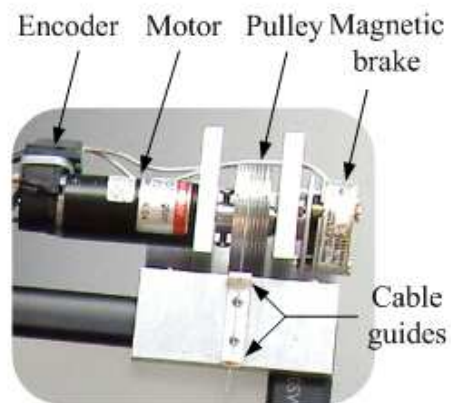
(a) The FingViewer-I.



(b) The FingViewer- II (S).



(c) The FingViewer- II .



(d) The actuator unit

Figure 3.6 The FingViewer force feedback devices.

The mechanical part of the FingViewer devices all consist of four identical actuator units. They can be fitted easily on the frames of touch screens or a support frame with screws. Each actuator unit includes a grooved pulley, a DC

motor and an optical encoder, as shown in Figure 3.6 (d). The 10 Watt Maxon RE 25 motor is used⁸. The motor can exert 28.9 Nmm maximum continuous torque and 133 Nmm stall torque. The attached encoder generates 100 pulses per turn.

The pulley and the encoder are fixed to the shaft of the motor. The diameter of the pulley is 42 mm. One end of the cable is wound on the pulley. The other end of the cable is connected with a ring. The ring for the thumb is bigger than the ring for the index finger. The rotation of the pulley is tracked by the encoder in order to calculate changes in the length of the cable. Then the positions of the rings (i.e. the fingers' positions) are obtained through calculating the lengths of the cables, i.e. the forward kinematics of the mechanism (Section 3.3.2).

It should be noted that we use rings instead of “caps” as the user interface because rings allow users to touch the screen in the same way they operate on a normal touch screen. Moreover, after a tactile feedback device has been integrated with the present design, this design will make it possible for users to obtain not only kinesthetic sensation but also tactile feedback when operating on the haptic touch screen. We also embed a rubber ring into the plastic ring for users whose fingers are too thin to wear the plastic ring tightly. The rubber rings are tight and their soft edges make them comfortable to wear.

There are two reasons to remove the spring in the FingViewer-II(S) when it is applied to touch screen applications (FingViewer-II). The first is that, as the spring is opaque, it would more or less occlude the user's view of the screen. Secondly, removing the spring would lower the limit on the size of the virtual objects that can be grasped without colliding with the spring. Since the spring is removed, the user has to feel the resultant force of cable tension in free space, although this force is very weak. It should be noted that, the only function of the spring is to balance the resultant force of the minimum cable tension. Removing the spring does not affect the generation of force feedback. Consequently, the spring stiffness is calculated as zero to control cable tensions.

⁸ In the actuator units of the FingViewer-II(S) prototype, a gear box ($k=4.8$) was added to the motor to generate greater cable tension.

status when the FingViewer is applied for touch screen applications (such as in the first experiment in section 3.6.1). The system architecture is illustrated in Figure 3.7.

3.5.3. Application Demonstration

In this section, we present some test results of the force feedback and the potential applications of the FingViewer-II(S) and FingViewer-II devices⁹. The purpose is to show the basic capability of the device. A formal user evaluation of the FingViewer-I and FingViewer-II devices on touch screen applications are presented in Section 3.6. Generally, the force feedback is realized by a simplified impedance control method ($F = k\Delta x$), the purpose of which is to demonstrate how the force feedback is realized in different situations. The stiffness of the virtual objects is set as 2 N/mm. The force feedback was updated at a frequency of 1 KHz.

(a) Demonstration of the FingViewer-II(S)

This example is provided in order to simulate the virtual grasp task. Figure 3.8 presents the three stages of the virtual grasp task. The movement of the two balls corresponds with the two fingers. The user moves the fingers to grasp the rectangular box (Stage 1), then he grasps the box and moves it (Stage 2), finally he manipulates the box to collide with the cylinder (Stage 3).

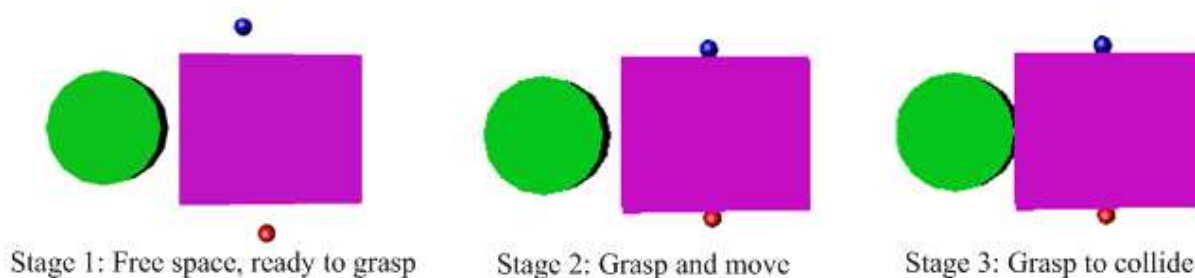
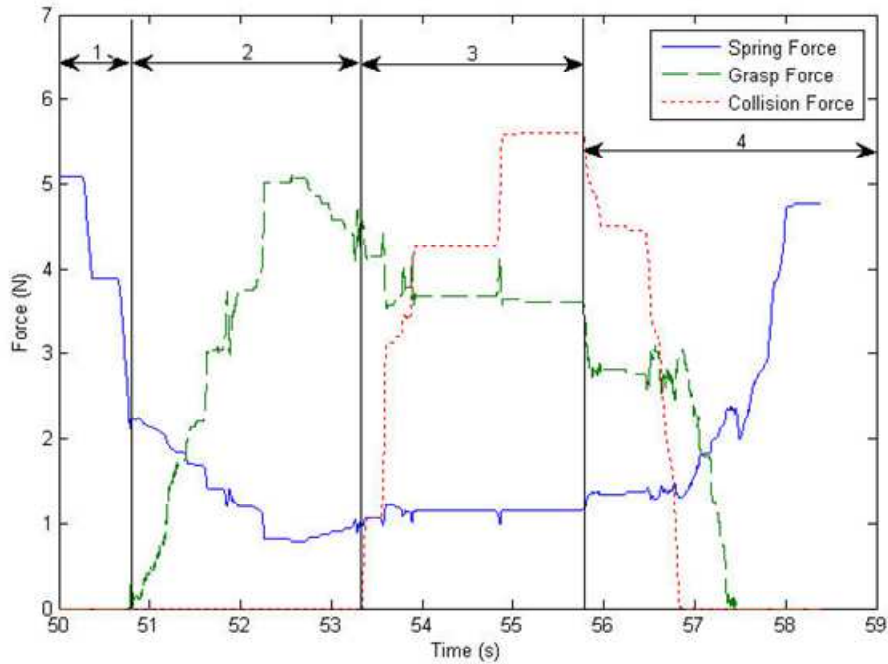
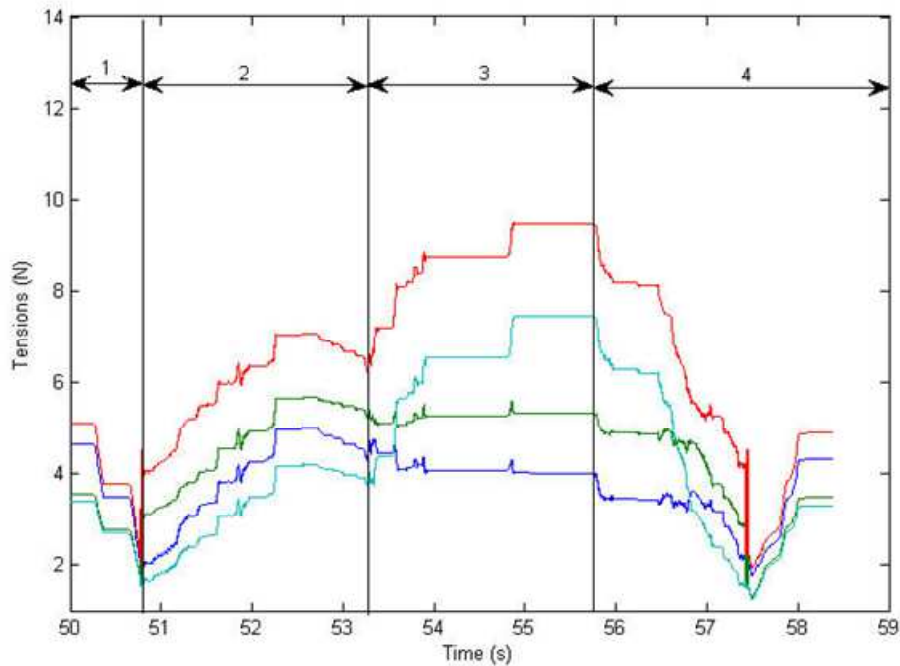


Figure 3.8 The three stages of the virtual grasp task.

⁹ Demos of these devices can be downloaded from our laboratory website at: http://haptic.buaa.edu.cn/video/English_Video.htm.



(a) Force feedback in the interaction.



(b) Cable tensions in the interaction

Figure 3.9 Force and cable tensions in the virtual grasp task.

Figure 3.9(a) presents the force exerted in the virtual grasp experiment. In Stage 1, the user attempts to grasp the box. The distance between his fingers is shortened. Therefore the spring force decreases. In Stage 2 and Stage 3, the user

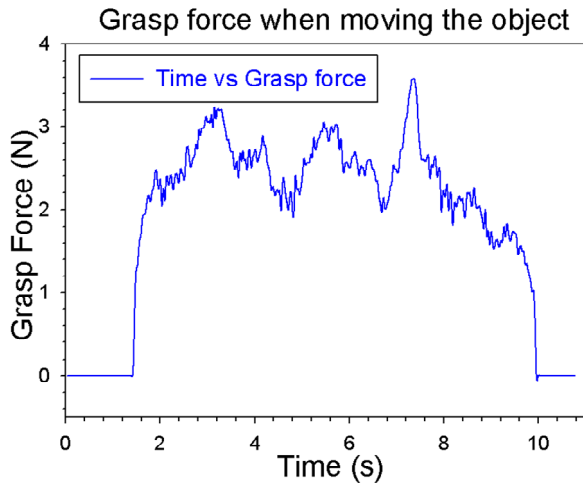
grasps the box. He experiences the grasp force clearly with a maximum force of about 5.1 N . In Stage 3, the user moves the box to collide with the cylinder. He feels the collision force, with a maximum value of about 5.6 N . Stage 4 in Figure 3.9(a) presents the reverse procedure. In this stage, the user releases the box and moves the fingers in free space.

During the process of the virtual grasp task, all cable tensions remain positive, as presented in Figure 3.8(b). The user is able to feel the grasp force and the collision force clearly when he manipulates the grasped object. In free space, the resultant force of cable tensions is balanced by the spring force. The user can move his fingers freely.

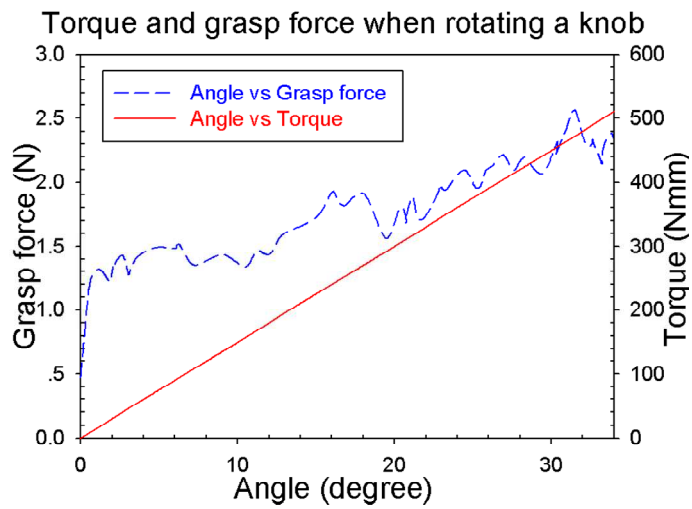
(b) Demonstration of the FingViewer-II

The scenario to demonstrate the FingViewer-II on a touch screen is similar to that of the FingViewer-II (S)'s — grasping and moving an object to interact with the other. In addition, we add torque feedback in this demo to show the force feedback capability. In the application, the user can rotate knobs/handles on a virtual device (like a radio or a music player) or in an immersive video game. The user is able to feel the contour of the knob, as shown in Figure 3.10(b). When he grasps and rotates the knob, he feels a resistant torque as if rotating a coil spring (the stiffness is set to be 15 $Nmm/degree$). The torque feedback can also be set to simulate detent, jog shuttle, hard stops and other types of effect. After grasping a virtual object, the user can move it and interact with other objects. In Figure 3.10 (c), the user moves the cell phone and collides with the knob. He can feel not only the colliding force but also the torque as if he is prying the knob. This scene demonstrates the 4-DOF force feedback of the FingViewer-II.

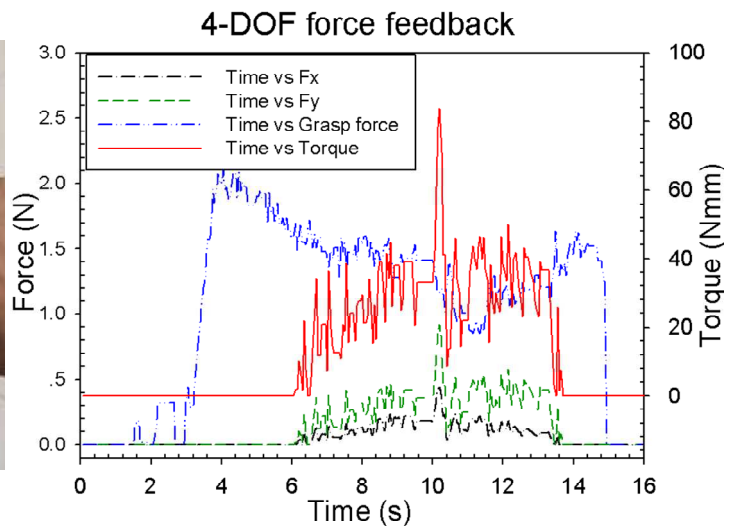
Erreur ! Utilisez l'onglet Accueil pour appliquer 标题 1 au texte que vous souhaitez faire apparaître ici.. Design of the force feedback device



(a) To grasp and move



(b) To rotate a knob



(c) To interact with other objects

Figure 3.10 Force feedback capability of the FingViewer-II. The user can use his/her fingers to grasp and manipulate virtual objects and obtain 4-DOF force feedback.

3.6. Evaluation

This section presents the evaluation of the FingViewer-I and FingViewer-II device through two typical touch screen applications—simulating a button-click feedback and rotating a knob, respectively.

3.6.1. Simulating a button-click

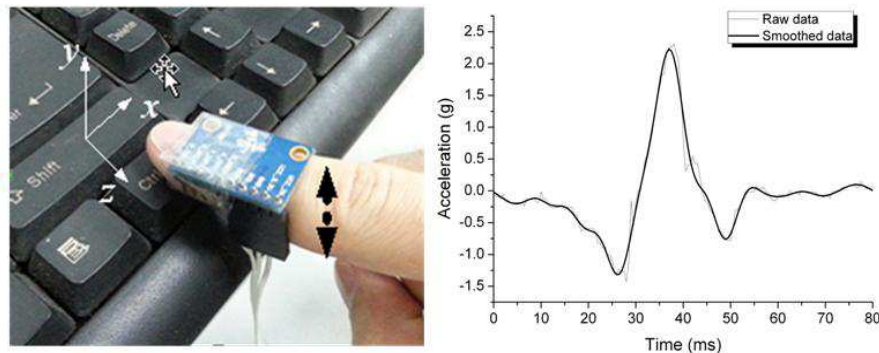
Comparing with a physical button

The force feedback produced by the FingViewer-I device can be applied to the finger to simulate a button-click effect. The method takes advantage of haptic illusion by providing a lateral acceleration when the user taps on a touch screen button to substitute the normal acceleration when pressing on a physical key. This method has been shown to be an effective way to simulate key-click feedback on touch screens [51, 111]. In our case, the lateral acceleration on the finger is yielded by the force feedback device. To compare haptic click feedback with physical click, we measure the acceleration of these two operation modes as a standard to judge the fidelity of the simulation.

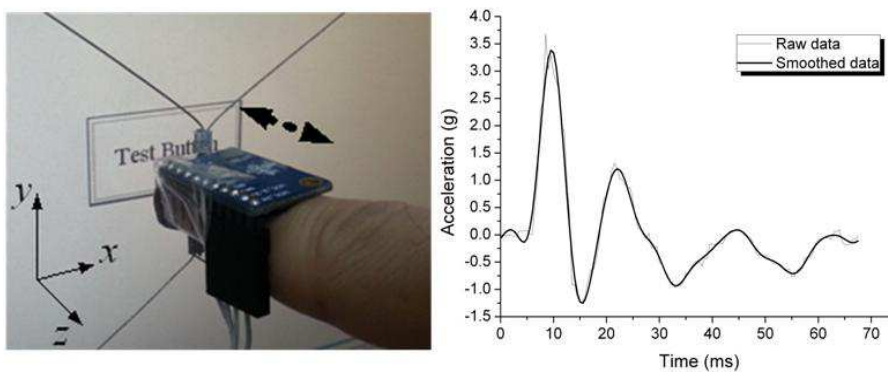
We used a digital accelerometer ADXL345 which was connected to a MCU (Micro Controller Unit) via I²C bus to measure the click acceleration, and transferred the data through a COM port from MCU to a computer. In the experiment, the accelerometer was fixed on the operator's index-finger with a plastic tape. The sampling rate was 2 KHz. The acceleration value was restored in the MCU and transferred to the computer after the data collection finished. The FingViewer-I was fixed on an off-the-shelf resistance touch screen to provide force feedback and track the finger position. The touch screen was only used to detect finger contact on the touch screen.

The acceleration signal was collected first in the click process on the Ctrl key on a physical keyboard. Figure 3.11 (a) shows the test condition and the result. The acceleration data show features in a typical keystroke process. The plot contains three clear pulses followed by several “ringing” pulses with diminishing

amplitudes. The first pulse represents the buckling process in keystroke. In this process, the user presses down the button to the bottom. The second pulse represents the restitution process when the button was released and user's finger rose up from the key bottom. The third pulse was due to the "braking" effect that the user tended to stop his finger on the key.



(a) Acceleration measurement during a physical keystroke. Both the user's finger and the key moved along the y-axis.



(b) Acceleration measurement during clicking on a haptic enhanced touch screen button. Finger movement was along the z-axis while a pulse of force was applied in the +y direction once the finger touches on the virtual button.

Figure 3.11 Acceleration measurement during a keystroke on a physical keyboard and on a haptic enhanced touch screen button. The acceleration along the y-axis was collected and plotted (the gravity effect was eliminated from the data).

On touch screens, the buckling process on a virtual button is eliminated since the touch surface cannot deform. The buckling force is replaced by the contact force when the user taps on the screen. Therefore, the button-click feedback is added only to represent the restitution force. A pulse of force (1 N) was applied to the finger in the +y direction once the user taps on the virtual button. Figure 3.11 (b) presents the acceleration curve collected from the click process on the touch

screen enhanced by force feedback. The acceleration profile indicates that the acceleration curve is consistent with the restitution process of the physical keystroke and the acceleration profile obtained using tactile feedback to simulate button-click [16], but the magnitudes of the peak acceleration are different. This is due to the fact that we set a great force feedback at the fingertip. Figure 3.12 shows the maximum acceleration on the fingertip when different forces were applied to the finger. With the data obtained from clicking the physical key, we can further adjust the force value to obtain a similar acceleration as a physical keystroke. According to Figure 3.12, the force feedback of 0.6 N would cause a similar button-click feedback as that on a physical key.

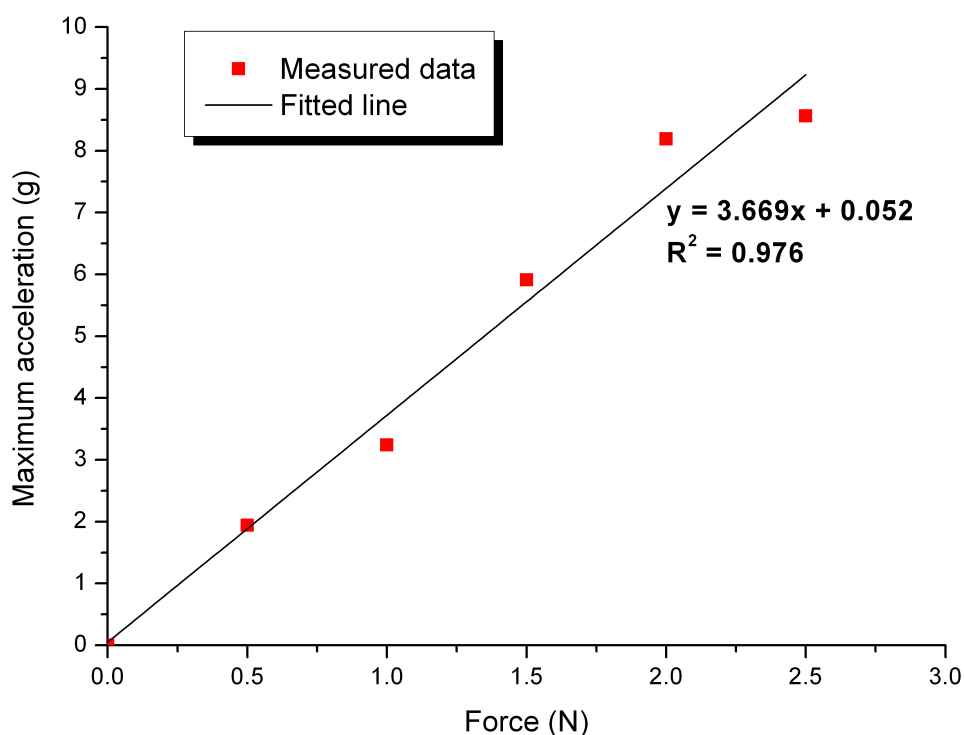


Figure 3.12 Maximum acceleration on the fingertip as a function of applied force feedback. A saturation effect can be noticed when force is greater than 2 N.

However, the force magnitude should also be adjusted according to users' preference and the appearance of the virtual button as suggested by [70]. Finally, this force feedback can also be applied to a Mole Attack game (illustrated in Figure 3.6 (a)): when the player tapped on the target mole, he obtained a vertical upward force resulted in an experience as if whacking on the mole with a hammer.

This effect made players felt immersive and entertaining.

User evaluation

An experiment was conducted to further understand the effect of force-enhanced haptic button on users' performance.

Task and experiment design: The experiment was designed according to the Task #1 (Tapping Task) described in the ISO 9241 standard, part 9 [112], which is an imitation of original Fitts' reciprocal tapping task. Participants proceeded to tap alternately between the two stripes of width W and separated by distance A .

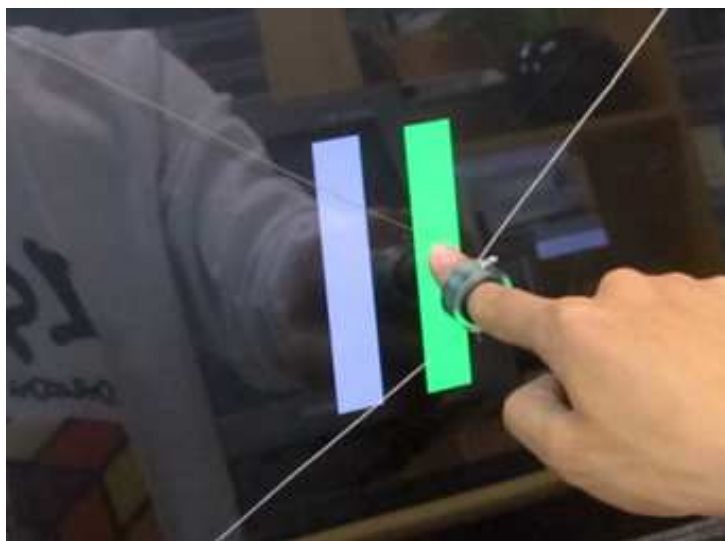


Figure 3.13 Reciprocal tapping task.

There were three feedback conditions – Visual-only, Haptic Wall and Haptic Button. In all three feedback conditions, the target stripe was displayed in green and the start stripe in grey, as shown in Figure 3.13. The opposite target would turn green only upon a successful tap on the target stripe. In the Visual-only condition, no haptic feedback was added.

In the Haptic Wall condition, the force feedback was a constant resistance against the finger's movement when it moved inside the feedback space (2 mm wide at the center of the target). It felt like a wall that helped participants stop at the center of the target (Figure 3.14 (a)). It may be noted that this feedback was applied before the participant tapped on the target. When the participants tapped

on the screen, they only felt the nature feedback from the screen.

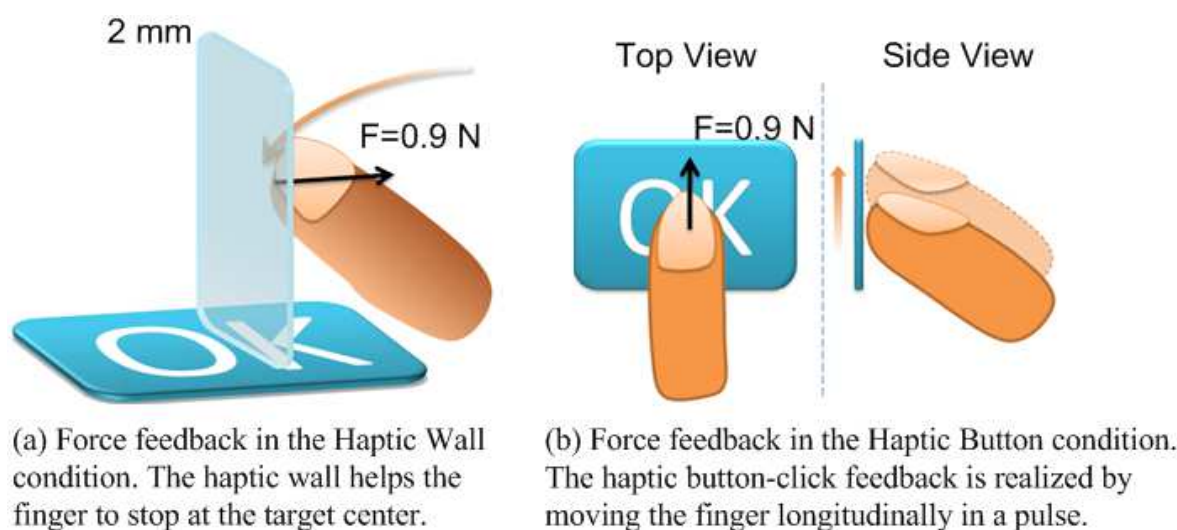


Figure 3.14 Force feedback in the experiment.

In the Haptic Button condition, force feedback was added after participants tapped successfully on the target. A button-click feeling was simulated by adding a pulse of 0.9 N force which pulled the participant's finger to move slightly longitudinally (Figure 3.14(b)). The button-click feeling felt like a "crisp click" and was recognized by the participants.

The experiment was a $3 \times 3 \times 3$ repeated-measures within-subjects design. The independent variables and levels were as follows: Feedback conditions (Visual-only, Haptic Wall, Haptic Button), Target Distance (A: 40, 80, 160 mm), and Target Width (W: 5, 10, 20 mm). The order of presentation of the three feedback conditions was counterbalanced using a Latin-squares design. Each participant implemented 3 blocks of trials for each of the feedback conditions. Within each block, participants performed 4 repetitions for each of the 9 A-W combinations, which were presented in random order. 12 right-handed participants (2 females and 10 males) between the ages of 24 and 29 took part in the experiment. Prior to each new feedback condition, participants were given a practice block. Breaks were allowed between blocks and between changes of feedback conditions. The entire experiment lasted approximately 30 minutes per participant. The task completion time (ms) and error rate (%) were recorded to

evaluate users' performance under the three feedback conditions.

Results: The mean task completion time and error rate in the experiment are presented in Figure 3.15. There was a significant effect of feedback conditions on target completion time ($F_{2,22} = 12.9, p < .0001$). The mean task completion times in the Visual-only condition, the Haptic Button condition and the Haptic Wall condition were 618 ms, 613 ms, and 592 ms respectively. The post-hoc Tukey test showed that there was no significant difference between the Haptic Button condition and the Visual-only condition ($p > .1$). However, the Haptic Wall led to a decrease in task completion time ($p < .0001$).

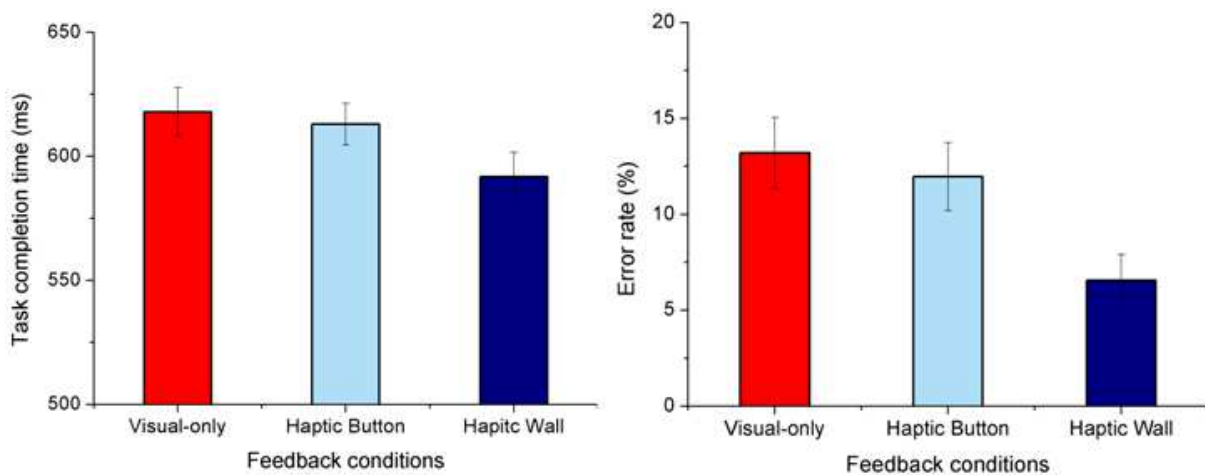


Figure 3.15 Mean task completion time and error rate in the tapping task, by feedback conditions. Error bars indicate 95% confidential interval.

Similarly, the error rate in the visual-only condition (mean = 13.2%) had no significant difference ($p > .1$) compared with the Haptic Button condition (mean = 12.0%). The Haptic Wall condition (mean = 6.6%), however, dramatically eliminated 50% of errors caused in the visual-only condition and 45% errors caused in the Haptic Button condition. The effect of feedback conditions on error rate was statistically significant ($F_{2,22} = 19.3, p < .0001$).

Discussion: In general, participants in the Haptic Wall condition outperformed those in other feedback conditions. Haptic feedback in the Haptic Wall condition worked in two ways. In the one, haptic feedback assured the participants that they had reached the target so that they were able to press on

the target without spending time aiming at its center. In the other, haptic feedback prevented participants from moving their fingers over the target. The force feedback in the Haptic Wall condition worked as a wall that fingers were “bounced off” as soon as they encountered the resistance. Then participants pressed on the target very close to the “wall” which was located at the center of the target. As a result, the error rate decreased significantly. By contrast, adding haptic feedback in the Haptic Button condition had no effect on users’ performance as compared with the visual-only feedback. Similar results have also been reported in number entering tests [12, 71] and Fitts’ tapping experiment [13, 66] on touch screens. This result is understandable. Because the haptic feedback worked after the interaction, it could not affect the user’s conduct at any stage of the interaction process. As far as users’ performance is concerned, it is more fruitful to add the Haptic wall rather than the Haptic button-click feedback in this task.

3.6.2. Knob manipulation

We evaluate the FingViewer-II device through a knob-control experiment. Using a physical knob as an input device outperformed a touch screen in navigating control tasks [113]. Moreover, the concrete feeling when gripping a physical knob to manipulate (rotate) virtual object [114] on touch screens is beneficial in providing natural and intuitive interactions between human and computer. Therefore, simulating a virtual knob with force feedback on touch screens is promising for combining these benefits: improving navigation control and enhancing intuitive interaction. Moreover, compared with physical knobs, the force feedback enhanced virtual knob is more visually-flexible. It can be transparent or appear as a very narrow ring when the user grips it so that it does not disguise part of the screen. To duplicate a physical knob on touch screen, we compare three designs of a virtual knob and offer guidelines on the design of this interface.

Participants : Twelve right-handed college students between the ages of 24 and 29

were volunteered to participate in the experiment. Three were female and nine male. They all had experience of handling normal touch screens but had never operated the force feedback touch screen before.

Procedure: The experiment was designed to simulate rotating a knob to navigate through a list with scrolling. A diagram of the task is presented in Figure 3.16. Subjects were asked to grasp and rotate the knob to shift the display of current item to the target item in the list as quickly and accurately as possible. This task is similar like scrolling a wheel on a mouse to navigate. The rotation of the knob was mapped with the shift of items on the list (2.5 degrees = 1 item). When the user rotated the knob to a corresponding item, the item was enlarged to twice of its size. There were 12 items in the list. The target item was marked by an arrow above the item.



Figure 3.16 Diagram of the virtual knob-control experiment.

In each trial, the subject was asked to select the target item from the start position. The display sequence of the target item was random. When the subject selected the target item, s/he pressed down the Space key to complete the trial. The center of the knob was fixed. The subject could only rotate at most 50 degrees in one direction each time due to the limitation of the rational workspace. However, s/he could release the knob after one rotation and keep rotating the knob successively. At the beginning of each trial, the knob was set to its normal

position. The size of the item was 15 mm × 22.5 mm. The diameter of the knob was 40 mm.

The experiment was conducted under three feedback conditions. The first was the visual-only condition (V). Subjects were asked to operate without any force feedback, relying solely on their vision to grip and rotate the knob. In the second, grasp force feedback was added (G). The stiffness of the grasp force was set at 0.25 N/mm. Subjects could feel the grasp force when they rotated the knob. In the third, in addition to the grasp force feedback, we added a torque feedback as soon as the user shifted from one item to the next (G + T). The torque feedback was a pulse of torque against the rotation of the knob with a magnitude of 30 Nmm. It made the subject feel bumps as if rotating a detent.

Each subject was asked to complete five sections of trials in each feedback condition. Each section consisted of 24 trials. Subjects were randomly divided into three groups. The order of presentation of the three feedback conditions was counterbalanced using a Latin-squares design between each group. In order to assess the system quantitatively, three variables were recorded and analyzed. They were: the task completion time, the overshoot rate (percentage of trials in which the user moved over the target item) and the mean grasp penetration depth. After the experiment, subjects were surveyed through a simple questionnaire to evaluate subjective preferences. The survey asked the participants to rank conditions using the Lickert scale ratings from 1 (worst) to 5 (best) [66]. All subjects were allowed to practice the trials for 5 minutes before the experiment. They were allowed to rest between sections. The experiment took about 40 minutes for each subject.

Results: Experimental results are presented in Figure 3.17. All data was analyzed with the one-way repeated measures ANOVA tests. Post-hoc Tukey tests were used when statistically significant interactions were found.

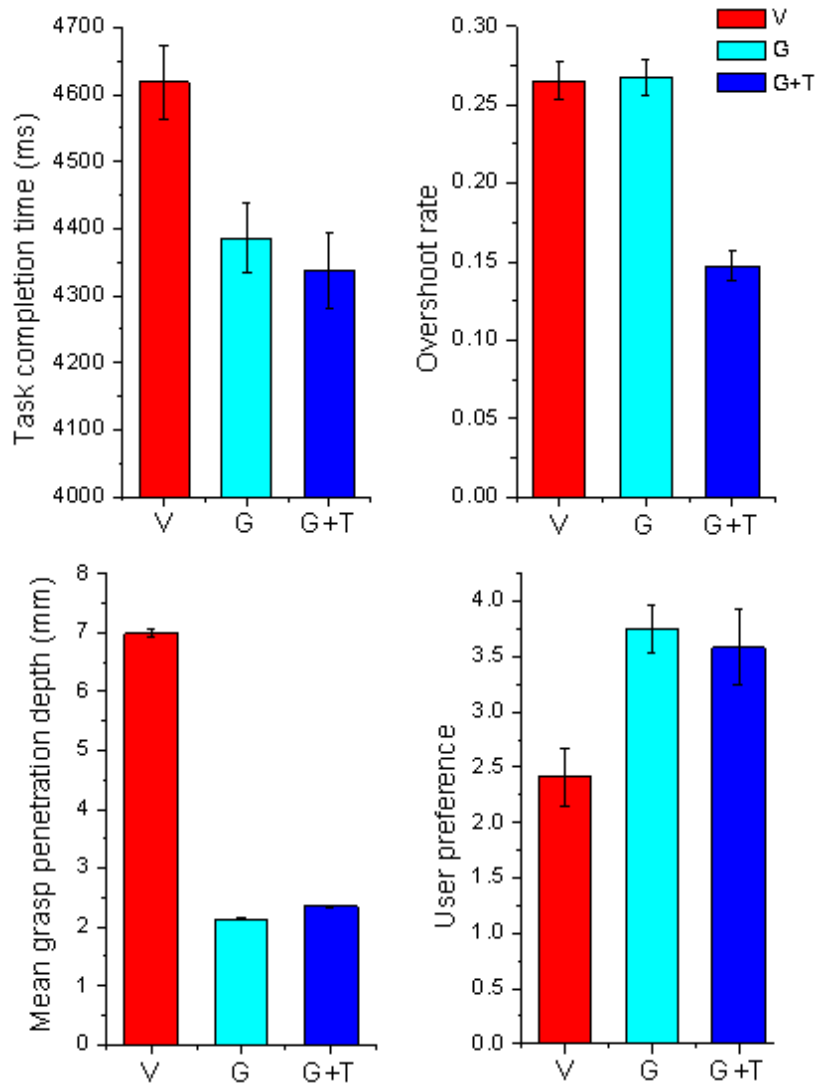


Figure 3.17 Aggregate results from 12 subjects demonstrating the effect of force feedback on their performance. The means and error bars with 95% confidence interval are plotted.

The feedback condition had a significant effect on the task completion time ($F_{2,22} = 8.97, p < .001$). There were 5.0% and 6.1% decreases in task completion in the G and G+T conditions respectively compared with the V condition ($p < .05$). However, the difference between the G and the G+T conditions was not statistically significant ($p > .5$).

The effect of feedback condition on the overshoot rate was statistically significant ($F_{2,22} = 39.8, p < .0001$). The G+T feedback condition reduced overshoots by 44.5% and 44.9% in the V and G conditions respectively ($p < .0001$). There was no statistically significant difference between the V and G conditions

($p > .5$).

The grasp force feedback reduced the grasp penetration depth dramatically compared with the visual-only condition. This effect was statistically significant ($F_{2,22} = 4501.4$, $p < .0001$). The mean grasp penetration depth in the V, G, and G+T conditions were 6.99 mm, 2.13 mm, and 2.34 mm respectively. The difference between the G and G+T conditions was statistically significant ($p < .0001$).

As far as user preference was concerned, conditions with force feedback won higher marks compared with the visual-only conditions ($p < .05$). However, there was no statistically significant difference between the G (Mean = 3.75) and G+T (Mean = 3.58) conditions ($p > .5$), though the G condition was slightly preferred.

Discussion: In general, force feedback improved users' performance and was preferred by them. In the experiment, the best way of completing the task was to watch the items and rotate the knob according to haptic feedback. However, in the visual-only condition, users had no sense of where the contours of the knob were when watching the items. This uncertainty caused users' hesitance even when they grasp the knob. As a result, they grasped "deeply" on the virtual knob, thus creating a greater penetration depth which resulted in a limitation of the knob size. If the radius of the knob had been smaller than the penetration depth, the user's fingers would have collided and thus caused a significant deterioration in simulation fidelity.

By contrast, after grasp force feedback was added, users were able to rely on the haptic feedback to grasp the knob and rotate it as if they were rotating a real one. The grasp force feedback increased users' confidence of grasping the knob and thus leading to an increase in task completion and a small grasp penetration. In addition, in the G+T condition, the torque which was against the rotation of the knob performed the function of reminding users that they had reached an item. As a result, this feedback reduced the noticeable overshoots existing in the V and G condition. Similar results were also found when adding vibration to indicate shift of items in a text selection task through tilting interface on a PDA [10]. However,

the torque feedback was not welcomed by all subjects. Seven of the twelve subjects who disliked it complained that it made it bulky to rotate the knob. They had to use greater force to grasp and rotate the knob. As a result, the mean grasp penetration depth in the G+T condition was greater than in the G condition. But there were also some subjects who were in favor of the torque feedback. They claimed that the feedback helped them select items accurately and suggested that the magnitude of the torque feedback should be increased. These opinions led us to further improve the feedback. A customized design of the feedback may be necessary to ensure that it is widely accepted.

Notably, our findings that the G+T condition outperformed the G condition but obtained less preference are also consistent with previous research [115] using a haptically enhanced physical knob. This indicates that our force feedback enhanced virtual knob is similar to a physical knob. The force feedback capability of the FingViewer is well applied. To further improve the virtual knob, we suggest increase the grasp force feedback but provide slight but perceivable haptic feedback when rotate the knob to shift items. A tactile feedback may also be a good choice.

As aforementioned, the virtual knob is visually-flexible. It can be transparent when the user grasps it to navigating while focusing on the document or webpage s/he is viewing. The addition of force feedback can reduce the visual load which is already very heavy when operating on touch screens.

3.7. Conclusion

In this chapter, we have presented the principle and performance of the FingViewer force feedback devices. These devices are capable of providing 3-DOF or 4-DOF force feedback to single-touch or multi-touch interaction. Two typical touch screen interactions, clicking a button and rotating a knob are enhanced with force feedback to evaluate the FingViewer-I and the FingViewer-II devices respectively.

In the button-click experiment, the finger acceleration was measured when the lateral force feedback was implemented. The acceleration was then compared with that in a key stroke on a physical button. With these measurements, we could adjust the magnitude of the force feedback to emulate a physical interaction. Preliminary results showed that players preferred the force feedback in a Mole Attack game.

A knob-control experiment has been conducted in order to evaluate the force feedback capability of the Fingviewer-II device. Experimental results showed that both the task completion time and the mean penetration depth are significantly reduced when grasp force feedback is added. Moreover, adding manipulation force feedback, which indicates users' movement, further reduces overshoot rates. Although the combination of grasp and manipulation force feedback further improves users' performance, it is not preferred by the majority of subjects. These findings that the G+T condition outperformed the G condition but obtained less preference are consistent with previous research [115] using a haptically enhanced physical knob. This indicates that our device is capable of providing force feedback required in manipulation of a virtual knob.

Appendix

The static Jacobian matrix in Section 3.4 is written as

$$\mathbf{A} = \begin{pmatrix} -s\theta_0 & -c\theta_1 & s\theta_2 & c\theta_3 \\ c\theta_0 & -s\theta_1 & -c\theta_2 & s\theta_3 \\ R \cdot s(\theta_0 - \varphi) & -R \cdot c(\theta_1 - \varphi) & R \cdot s(\theta_2 - \varphi) & -R \cdot c(\theta_3 - \varphi) \end{pmatrix}$$

where c and s represent \cos and \sin , respectively, $R = d/2$ (in case of FingViewer-I, R is the radius of the ring), and $\theta_0, \theta_1, \theta_2$, and θ_3 , which are presented in Figure 3.3, can be calculated by the kinematics of the mechanism.

Erreur ! Utilisez l'onglet Accueil pour appliquer 标题 1 au texte que vous souhaitez faire apparaître ici.. Design of the force feedback device

Chapter 4.

Design of the Tactile Feedback Device

Summary

4.1.	Introduction	84
4.1.1.	Squeeze Air Film Effect	84
4.1.2.	Motivation and difficulties of designing a large area tactile device	87
4.2.	Power consumption measurements	89
4.2.1.	Measurement Setup	90
4.2.2.	Dielectric Power Losses	90
4.2.3.	Mechanical Power Losses From the Resonator.....	92
4.2.4.	Power Losses in Electromechanical Conversion Stage.....	93
4.2.5.	Summary.....	95
4.3.	Power consumption modeling	96
4.3.1.	General Assumption	96
4.3.2.	Plate Deflection	96
4.3.3.	Power Calculation	99
4.3.4.	Variation Of The Piezoelectric Loss Tangent	104
4.3.5.	Effect Of The Actuator Layout	105
4.3.6.	Summary.....	105
4.4.	Design of a large tactile device.....	106
4.4.1.	Design Guidelines	106
4.4.2.	Implementation.....	107
4.4.3.	Modal analysis.....	108

4.4.4.	Experimental measurements	109
4.5.	Psychophysics evaluation of the tactile plate.....	113
4.5.1.	Motivation.....	113
4.5.2.	Method	115
4.5.3.	Results.....	120
4.5.4.	Discussion	121
4.6.	Conclusion	123

4.1. Introduction

This chapter presents the design of the tactile device. This research is based on the previous design of the STIMTAC tactile plate developed by the L2EP [116]. The principle of the device is to reduce the friction coefficient of the touch surface through the squeeze air film effect. In the following parts of this section, we first introduce the principle of the squeeze air film effect. Then, the motivation and difficulties of designing the large area tactile device are presented.

4.1.1. Squeeze Air Film Effect

The air in a small gap between a fixed plate and a plate moving perpendicular to the fixed plate at a high frequency will be compressed before it escapes from the gap. If the vibration frequency is high enough and the mean clearance between the two plates is small enough, the trapped air between the two plates will result in an average pressure higher than the atmospheric pressure. Thus, an air cushion is produced, which may reduce the friction coefficient between the two surfaces. Applied in the friction variable tactile device, the fixed plate is replaced by the fingertip and the moving plate is represented by the vibrating surface of the device, as shown in Figure 4.1. By that way, when the device vibrates at a very high frequency, the air pressure in the air gap between the fingertip and the device will be greater than the atmospheric one. As a result, the air will lift up the

finger so that the relative friction coefficient will be decreased. By changing the pressure of the squeezed air, different friction coefficients between the finger and the device can be realized. The friction coefficient is mapped to geometric features on virtual objects in order to simulate different tactile patterns.

The resultant overpressure in the air gap is difficult to calculate. However, an analytical expression may be obtained if we do the assumption that the air inside the gap is squeezable and behaves like a spring [25]. This assumption is fulfilled when the “squeeze number” σ expressed in (4.1) is large enough.

$$\sigma = \frac{12\eta\omega_0(l_0/2)^2}{p_0h_0^2} \quad (4.1)$$

where η is the air viscosity, ω_0 is the frequency of vibration, l_0 is the finger length in contact with the device, p_0 is the atmospheric pressure and h_0 is the mean clearance between the fingertip and the device [77].

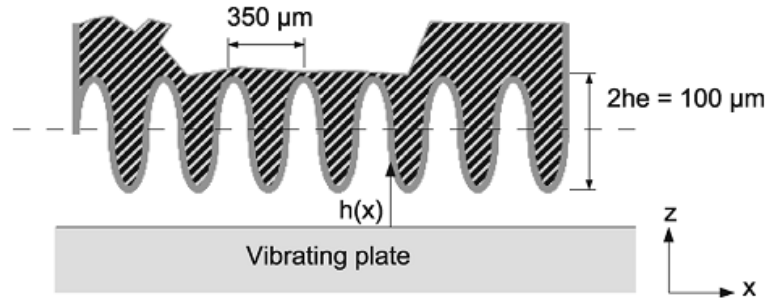


Figure 4.1 Schematic of epidermal ridges and the vibrating plate (adapted from [25]).

In the modal of squeeze film effect, the two plates are flat and smooth. However, when the squeeze film effect is applied in tactile devices, the epidermal ridges on the fingertip and the roughness of the vibrating plate should not be ignored [25]. Figure 4.1 presents geometrical properties of ridges and the plate. Taking into account of the epidermal ridges and the roughness of the plate, Equation (4.1) becomes

$$\sigma = \frac{12\eta\omega_0(l_0/2)^2}{p_0(h_{vib} + h_e + h_r)^2} \quad (4.2)$$

where h_{vib} is the vibration amplitude, h_e is the amplitude of the undulation of the fingerprint and h_r is the surface roughness. In (4.2), parameters η , l_0 , p_0 , h_e and h_r are constant. If the vibration amplitude, h_{vib} , is given, the squeeze number, σ , is in direct proportion to the vibration frequency w_0 . Usually, the vibration amplitude, h_{vib} , is about 1 μm and the roughness of the plate is 0.8 μm . They are comparatively much smaller than the undulation of the fingerprint, h_e , which is about 50 μm . As a result, the squeeze number depends almost entirely on the vibration frequency.

If the vibration frequency is high enough, namely above 25 KHz according to [25], the squeeze number will be greater than 10. In this case, the mean pressure of the squeezed air is greater than the ambient air pressure. The force N_s exerted on the fingertip by the squeezed air depends on the excursion ratio $\varepsilon (= h_{vib} / h_0)$ [77], as calculated by (4.3)

$$N_s = p_0 S \left(\sqrt{\frac{1 + \frac{3}{2} \varepsilon^2}{1 - \varepsilon^2}} - 1 \right) \quad (4.3)$$

where S is the contact area. Since $1 \geq \varepsilon \geq 0$, the force increases with the vibration amplitude.

When the squeeze film effect happens, the gapped air works as a spring. The pressure exerted on the fingertip by the air reduces the tangential force applied on a texture exploration task. The reduced friction coefficient is deduced as [77]

$$\frac{\mu'}{\mu} = 1 - \frac{N_s}{N_F} \quad (4.4)$$

where μ' and μ are the reduced and the original friction coefficient respectively and N_F is the normal force applied to the tactile plate by the finger in a texture exploration task.

In summary, in order to obtain an effective squeeze film effect, we must activate the tactile plate at an ultrasonic frequency (>25 kHz) so that a high squeeze number can be realized with inaudible vibration. The vibration amplitude is also important to decrease the friction coefficient. A minimum of $1\ \mu\text{m}$ is required to produce distinct tactile feedback according to our experience.



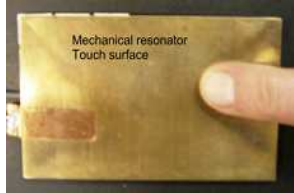

T-Pad [78]	LATPad [15, 117]	STIMTAC [25]	Transparent STIMTAC [118]
$\square 25\text{mm}$	$76.2\ \text{mm} \times 76.2\ \text{mm}$	$83\ \text{mm} \times 49\ \text{mm}$	$93\ \text{mm} \times 65\ \text{mm}$
			
Adapted from [119]	Adapted from [15]	Adapted from [25]	Adapted from [118]

Table 4.1 The touch area of the present variable friction tactile devices.

4.1.2. Motivation and difficulties of designing a large area tactile device

Several tactile devices have been developed based on the squeeze air film effect. Some glued piezoelectric actuators all over the underside of devices [25, 77, 78]. Some only attached actuators at two edges so that the middle part of the device can be transparent for applications as touch screens [117, 118]. By modulating the vibration amplitude, these devices have notably been used to simulate fine textures [78, 120] and facilitate pointing tasks [15, 80]. However, a limitation of these devices is that, their workspace is small (as shown in Table 4.1), as compared with the requirement of supporting multi-finger interaction and large display touch interfaces (e.g., tablet PC). Moreover, mainstream consumer

electronics need to satisfy consumers' requirement of large but portable touch screen electronics. For example, the Ipad [121] has a 9.7 inch touch screen, and the size of the screen is 197.1mm × 147.8mm. The Samsung's GALAXY Tab [122] has a 7 inch touch screen (154 mm × 87.2 mm). Therefore we intend to design a tactile interface with a similar size in order to realize tactile feedback on large but portable touch screen devices.

Developing a large area tactile interface based on the squeeze film effect is challenging. One main issue is to limit the power consumption. In fact, the dissipated power converts to heat which increases the temperature of the touch surface making the user uncomfortable. Moreover, the heat also changes the resonance frequency of the tactile plate, reducing the vibration amplitude and further degrading the perception of tactile feedback. Furthermore, much power consumption needs powerful power supply which is not applicable to portable mobile devices. In previous researches, we found that the power consumption could be reduced by using thin resonator and thin piezoelectric actuators [123, 124]. These studies were carried out in cases that piezoelectric actuators were glued all over the underside of the device. This device was the STIMTAC display from Université Lille1 [125]. Recent research begins gluing piezoelectric actuators only at the edges of the device, reducing the number of piezo-actuators [117, 118]. However, to obtain a methodological approach, it is necessary to analyze the effect of the number and the layout of piezo-actuators on power consumption. In this chapter, we develop an approach for the power consumption modeling of the STIMTAC tactile device. The model takes into account the number and the layout of piezoelectric actuators. Based on this model, we are able to offer guidelines on how to use minimum piezoelectric actuators to develop a large area tactile device operating with squeeze film effect and to make an accurate estimation of the power consumption.

In this research, our objective is to develop a large area tactile device based on the squeeze film effect with minimum power consumption and minimum

piezoelectric actuators. To achieve this, we first conducted a series of measurements to investigate the source of the power consumption of the STIMTAC device (Section 4.2). Then, we developed an analytical model to estimate the power (Section 4.3). We found that when vibration amplitude is constant, the power consumption is not related to the number of piezoelectric actuators but related to their layouts. With this result, we designed a large area tactile plate with very few piezoelectric actuators (Section 4.4). Finally, the device was evaluated in a psychophysics experiment to validate its capability of tactile feedback (Section 4.5).

4.2. Power consumption measurements

In previous researches in Univeristé Lille1, we optimized the geometric parameters of the tactile plate [123]. We noted that the power consumption of the tactile plate was in proportion to the thickness of the resonator and the piezoceramics [124]. However, these analyses were based on the device whose resonator was fully glued with piezoceramics. The number and layout of piezoceramics were not taken into account. In this study, we aim to answer the question that if reducing the number of piezoceramics will reduce the power consumption. Therefore, we conducted a series of measurements to reveal the source of the power consumption. The tactile plate consists of three major parts: the resonator, the piezoceramics, and the glue bonding. Considering these components, we assume that the power consumption of the tactile plate includes three parts: mechanical power losses, electrical power losses and electro-mechanical power losses. The mechanical power losses may be due to the vibration of the whole device (including the resonator, the piezo-ceramics and the glue). The electrical power losses may come from the hysteresis losses in dielectric, and the electro-mechanical power losses come from the hysteresis cycle in the piezoelectric coupling energy [126]. In the following measurements, we investigate the source of the power consumption by analyzing each possibility.

4.2.1. Measurement Setup

In the measurements, we recorded the voltage applied to the piezoceramics, the vibration speed of the resonator and the power consumption. We used a waveform generator (Agilent 33120A) to generate sinusoid wave. The frequency of the sinusoid signal was tuned at the resonance frequency of each measured tactile plate. The sinusoid signal was amplified 20 times by a high speed amplifier (NF HAS 4052) to actuate the tactile plate. The vibration speed was measured by a single-point Laser Doppler Vibrometer (Model OFV-505, Polytec GmbH, Waldron, Germany). The power consumption and vibration speed were read through an oscilloscope (Tektronix TDS 3054B).

We made several tactile plates with different number and layout of piezoceramics glued under the resonator so as to obtain feasible conclusions over the relevant number and layout of piezoceramics. In the first two measurements, the dimensions for the aluminum resonator were 76 mm \times 41 mm \times 1 mm. Each piezoceramic column contained 4 pieces of piezoceramics. The dimension of the piezoceramics was: 5 mm \times 9 mm \times 0.5 mm. Material details of the piezoceramics can be found in [127]. A sketch of the materials is listed in Table 4.4. All tactile plates worked at the (9, 0) mode with the mode shape of a standing wave.

4.2.2. Dielectric Power Losses

Method. To study the dielectric power losses, we assume that the mechanical power losses are proportional to the square of the vibration speed, and the dielectric power losses are proportional to the square of the applied voltage [126]. To study the changes of dielectric power losses, we kept the mechanical power losses to be constant through keeping the same vibration speed. Firstly, we recorded the vibration speed at the resonance as v_0 and the corresponding power as P_0 . Then we slightly changed the frequency of the applied voltage apart from the resonance frequency without changing the mode shape. As a consequence, the

vibration speed decreased. Then, we applied a higher voltage to regain the vibration speed v_0 and record the power needed at this state as P_t . If P_t does not increase significantly, we can deduce that the dielectric power losses are negligible.

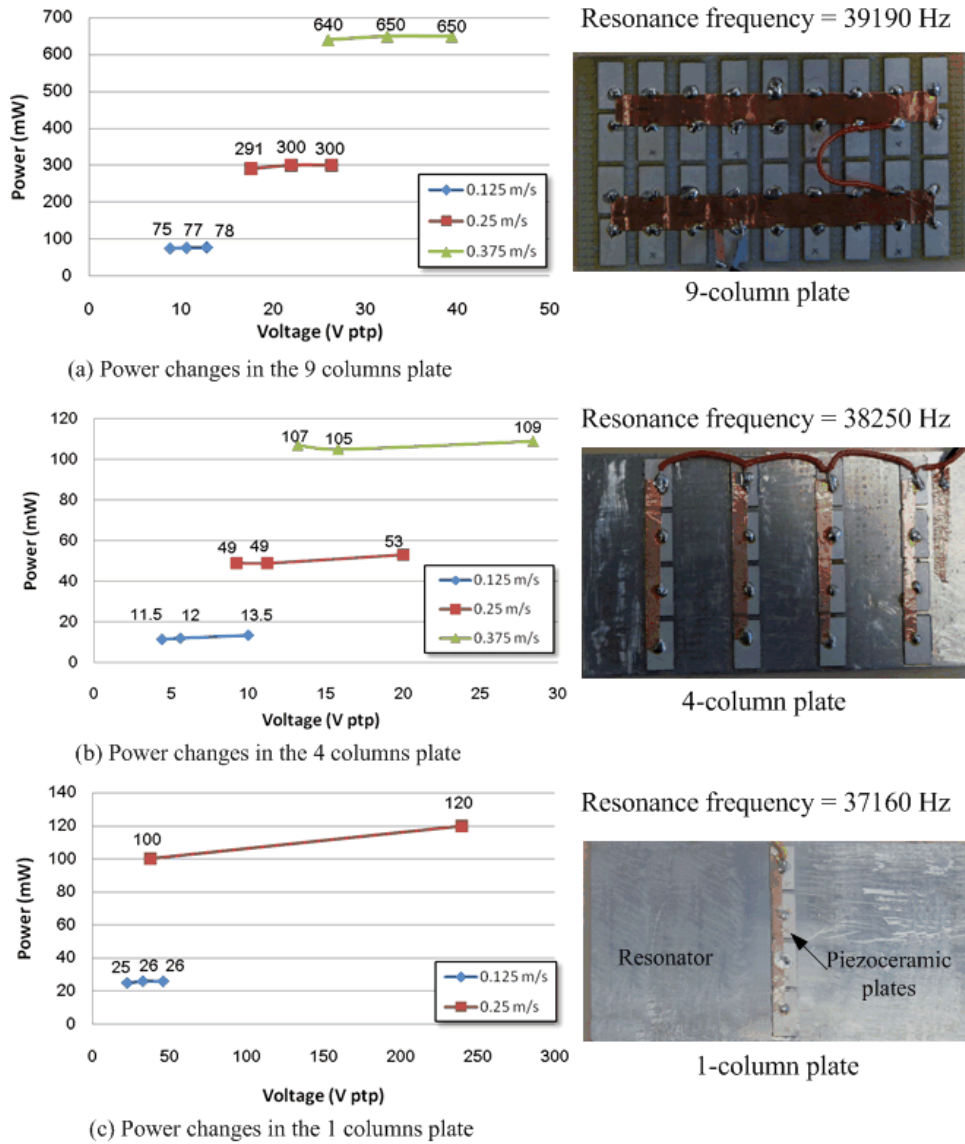


Figure 4.2 Power changes in the three tactile plates. Piezoceramics were glued on the resonator to excite the resonance vibration.

We studied three tactile plates with 1 column, 2 columns and 9 columns of piezoceramics (Figure 4.2, right column). We found that decrease or increase frequency symmetrically to the resonance cause similar power losses. Therefore we only present the power changes through increasing the frequency. Accordingly,

we record P_i when the vibration speed was regained from 80%, 60% and 50% of the speed at resonance. We applied three vibration speed levels (0.125 m/s, 0.25 m/s, and 0.375 m/s) in the measurements. Accordingly, high driving voltage was required to obtain high vibration speed.

Results. Experimental results are presented in Figure 4.2, left column. It should be noted that the measurement of power was conducted by integrating the applied voltage cross the current on the oscilloscope. There may be a 10% error due to this operation. According to the first two measurements (Figure 4.2 (a) and (b)), we found that the power needed to regain resonance speed did not change significantly. This indicated that the dielectric power losses are negligible. To further confirm this conclusion, we increased the applied voltage frequency of the 1 column tactile plate (from 37180 Hz to 37560 Hz) so that a much higher voltage needed to be applied to regain the vibration speed. We intended to check if P_i varied significantly in this process. As shown in Figure 4.2 (c), we found that P_i increased from 100 mW to 120 mW when voltage was increased from 37.6 V to 240 V. We therefore infer that the dielectric power losses are only noticeable when applied voltage is high. However, in our application, we do not apply voltage above 100 V. Therefore, the dielectric power losses are negligible in our tactile plate.

4.2.3. Mechanical Power Losses From the Resonator

Method. In the second step, we analyzed mechanical power losses due to the resonator's vibration in the air: we intended to check if the resonator was damped by the air while vibrating. In this experiment, we compared power consumption when changing the size of the resonator. In order to exclude the influence of the glue and the piezoceramics, we used the 1 column tactile plate and cut certain lengths from each edge of the resonator symmetrically in each measurement. We conducted three measurements with the lengths of the resonator shortened from 75 mm to 59mm, and finally 28mm. We applied the voltage with same amplitude

(20V, ptp) but tuned frequency (at resonance) to the piezoceramics in the three cases and measured the power and vibration speed at the center of the tactile plate.

Results. Measurement results are listed in Table 4.2. We found that the size of resonator did not change the power or the speed significantly. Therefore we infer that the resonator does not contribute to the mechanical power losses. In fact, the vibration speed was higher at the edges than at the centre of the 1 column tactile plate. We cut off the edges of the tactile plate and measured at the center of the tactile plate. If the edges of the resonator cost power, then the changes of power should be significant. However, we did not notice this effect in our measurement. This inference strengthened the assumption that the power losses were not due to the damping of the resonator.

Item \ Size	75x41 (9 antinodes)	59x41 (7 antinodes)	28x41 (3 antinodes)
Frequency (Hz)	37160	37180	35130
Voltage (V, ptp)	20	20	20
Power (mW)	27	23	25
Speed (m/s, ptp)	0.175	0.188	0.188

Table 4.2 Measurement results according to the length of the resonator.

4.2.4. Power Losses in Electromechanical Conversion Stage

Method. According to our aforementioned measurements, we found that the power losses were neither due to the dielectric power losses nor to the vibration of the resonator. We supposed that the power losses were caused by the piezoceramics where the electromechanical energy conversion occurs. However, we did not know if the losses were due to the electrical field that was applied to the piezoceramics or due to the mechanical losses such as damping in the glue bonding between the piezoceramics and the resonator. To figure out this question, we made a tactile plate with one column of piezoceramics and compared it with a 2-column tactile plate, as shown in Figure 4.3. The dimension of the aluminum

resonator was 76×41×1.2 mm while that of the piezoceramics was 5×9×0.5 mm.

The measurements were conducted in two steps. We first applied voltage to only one column of piezoceramics on the 2-column tactile plate, and applied the same voltage to the 1-column tactile plate. Then, we applied half of the voltage to both columns of piezoceramics on the 2-column tactile plate. The measurements included resonance frequency, power, and average vibration speed and amplitude along the antinodes where the piezoceramics were glued.



(a) One column at the edge



(b) Two columns at the edges

Figure 4.3 Two tactile plates with piezoceramics glued at the edges.

Tactile plate	1	2-columns	2-columns
Item	column	1-powered ^a	2-powered
Frequency (Hz)	43792	44810	44720
Voltage (V, ptp)	24	24	12
Power (mW)	115	112	100
Speed (m/s, ptp)	0.30	0.26	0.27
Amplitude (μm, ptp)	1.08	0.92	0.96

^aThe other column of piezoceramics was open.

Table 4.3 Measurements of the 1-column and 2-column tactile plates.

Results. Measurement results are presented in Table 4.3. If there were mechanical power losses in the piezoceramics, when the same voltage was applied, the vibration speed of the half powered 2-column tactile plate (only one column of piezoceramics was powered) should be much smaller than that of the 1-column tactile plate. Moreover, the power consumption of the 2-column tactile plate should be twice of the 1-column to keep the same vibration speed. However, we found that both the power and the vibration speed were similar in these two conditions. This result indicated that the un-powered column of piezoceramics did not take any power. The bonding of the extra column of piezoceramics did not cause any mechanical power losses. Therefore, the power losses were mainly caused by the electrical field on piezoceramics.

Moreover, we also noticed a linear accumulation effect of the number of powered piezoceramics on the vibration amplitude according to our measurement in Table 4.3. Namely, the vibration amplitude was in proportion to the number of powered piezoceramics and the applied voltage voltage

$$A \propto n_c \square V \quad (4.5)$$

where A is the vibration amplitude, n_c is the number of powered piezoceramics, and V is the applied voltage.

We also measured the condition when one column of the piezoceramics was short-circuited while the other one was powered for comparison with the condition in the last column of Table 4.3. We found that there was only a slight change of frequency rather than amplitude or power. This result excluded the assumption that the connection mode (short or open) of piezoceramics causes power losses.

4.2.5. Summary

According to our measurements, we find that the power losses of the tactile plate are mainly due to the powered piezoceramics. Dielectric power losses and the mechanical power losses within the resonator can be negligible when analyzing the power losses. Since these factors are excluded, we suppose that the

power losses are mainly due to the hysteresis losses during piezoelectric coupling. Based on this assumption, we develop an analytical model to analyze the power losses.

4.3. Power consumption modeling

4.3.1. General Assumption

According to our measurement results, we inferred that the power consumption was mainly due to the electro-mechanical conversion. Therefore, we assume that the electrical power provided to the device is fully dissipated into the piezoelectric layer. Moreover, the power losses due to acoustic radiation are assumed to be negligible.

In the following parts, we will analyze the deformation of the piezoceramics and calculate the power consumption of the tactile device. We intend to find out the effect of the layout and number of piezoelectric actuators on the power consumption.

4.3.2. Plate Deflection

At resonance, a uniform standing wave is created across the resonator. To simplify the analysis, we consider the bond section of the piezoceramics and the resonator with the width of $\lambda/2$ and the length of b (see Figure 4.4). The deflection surface is assumed to be cylindrical since the length of the section is much longer than its width. The Plate Theory is applied to solve the cylindrical bending of the plate [128].

The cross section of the bended plate is presented in Figure 4.4. It is the assembly of the piezoceramics layer and the resonator layer. The two layers are glued together. We assume this assembly is perfect, which amounts to considering that the thickness of adhesive is zero and that the strains are continuous on the resonator–piezoceramic interface.

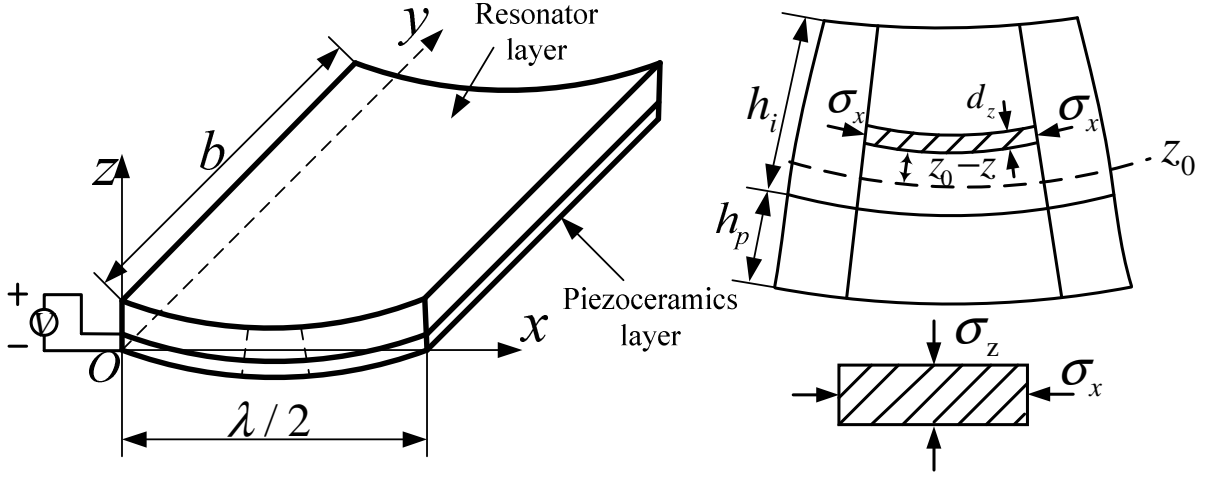


Figure 4.4 A half-wavelength section of the bended plate. h_i and h_p are thickness of the resonator layer and piezoceramics layer respectively.

When calculating the bending stress, we assume that cross sections of the plate remain plane during bending, so that they undergo only a rotation with respect to the middle surface. Then, the curvature of the deflection curve is assumed to be d^2w/dx^2 , which is equal to the inverse of the radius of curvature, $1/\rho$. The deflection, w , is assumed to be small compared with the width of the plate, $\lambda/2$. Then the strain of a fiber parallel to the x axis, S_x , is proportional to its distance from the middle surface

$$S_x = \frac{z_0 - z}{\rho} = \frac{(z_0 - z)d^2w}{dx^2} \quad (4.6)$$

According to Hooke's law, the relationship between strain, S , and stress, T , acting on the shaded element shown in Figure 4.4 are

$$\begin{aligned} S_x &= \frac{T_x}{E_x} - \frac{\nu T_y}{E_y} \\ S_y &= \frac{T_y}{E_y} - \frac{\nu T_x}{E_x} = 0 \end{aligned} \quad (4.7)$$

where E and ν are Young's module and Poisson's ratio respectively. The lateral strain in the y direction must be zero in order to maintain continuity in the plate during bending. Substituting the second equation into the first equation of

(4.7), we obtain

$$T_x = \frac{ES_x}{1-\nu^2} = \frac{E(z_0 - z)}{1-\nu^2} \frac{d^2w}{dx^2} \quad (4.8)$$

In our case, the resonator is considered to be isotropic. Substituting the material properties of the resonator into (4.8), we obtain

$$T_i = E_i' S_x \quad (4.9)$$

where $E_i' = E_i / (1 - \nu_i^2)$. As for the piezoelectric part of the plate, the coupling between the mechanical and the electrical part of the system is described by the constitutive relationships between the stress, strain, and applied electrical fields in terms of the piezoelectric stress relations

$$\begin{aligned} T &= c^E S - e^t E \\ D &= eS + \varepsilon^S E \end{aligned} \quad (4.10)$$

where E and D are, respectively, the electric field intensity vector and the electric flux density vector. The terms c^E , e , and ε^S are, respectively, the elastic constants short circuit matrix, the voltage coefficient matrix, and the dielectric constants matrix.

Thus, the stress distribution across the tactile plate due to an applied electric filed in the z-direction can be summarized as

$$T_x(z) = \begin{cases} E_i' S_x(z) & h_p \leq z \leq h_p + h_i \\ c_{11}' S_x(z) - e_{31} E_3 & 0 \leq z < h_p \end{cases} \quad (4.11)$$

where $c_{11}' = c_{11}^E / (1 - \nu_p^2)$, E_3 is the electric field in the z-axis. The moment yielded by the piezoceramic causes the resonator to bend. This relationship can be described by

$$\begin{aligned} M_p &= M_i \\ \int_{h_p}^{h_p+h_i} (z_0 - z) T_x(z) b dz &= \int_0^{h_i} (z_0 - z) T_x(z) b dz \end{aligned} \quad (4.12)$$

Substituting (4.6) and (4.11) into (4.12), we can obtain

$$\int_{h_p}^{h_p+h_i} \frac{(z_0-z)^2}{\rho} E_i' dz = \int_0^{h_i} \frac{(z_0-z)^2}{\rho} c_{11}' dz - \int_0^{h_i} (z_0-z) e_{31} E_3 dz \quad (4.13)$$

By integrating (4.13), we deduce that the deflection curvature can be expressed as follows

$$\frac{1}{\rho} = \frac{d^2 w}{dx^2} = \frac{3}{2} \frac{d_{31} E_3}{h_p a} \quad (4.14)$$

where

$$\frac{1}{a} = \frac{1-2f_0}{1-3f_0+3f_0^2-\alpha(3\beta+3\beta^2+\beta^3)-6\beta f_0-3\beta^2 f_0+3\beta f_0^2}$$

and

$$\alpha = \frac{E_i'}{c_{11}'}, \quad \beta = \frac{h_i}{h_p}, \quad d_{31} = \frac{e_{31}}{c_{11}'}, \quad f_0 = \frac{z_0}{h_p} \quad (4.15)$$

The above equations calculate the deflection in a static model. At resonance, the strain is enhanced by a dynamic amplification factor, Q . Moreover, according to our measurement, the strain is also amplified by the number of actuated piezoceramics, n_c (see (4.5)). Therefore, the dynamic strain is deduced as

$$S_x = n_c Q \frac{3d_{31}(z_0-z)}{2h_p a} E_3 \quad (4.16)$$

4.3.3. Power Calculation

The power losses in the piezoceramics are assumed to include two parts:

$$P_l = P_m + P_d \quad (4.17)$$

where P_m and P_d represent the mechanical part and the electrical part of the power losses in the piezoelectric layer respectively. These two powers are deduced to calculate the real power of the piezoelectric layer

$$P_m = \iiint \frac{1}{2} \text{Re}(T\dot{S}^*) dV \quad (4.18)$$

$$P_d = \iiint \frac{1}{2} \text{Re}(E\dot{D}^*) dV \quad (4.19)$$

As shown in Figure 4.4, the piezoceramic layer is powered in the z-direction and it yields a movement along the x-direction. According to (4.11) and (4.16), the stress in the piezoelectric layer is

$$\begin{aligned} T_1 &= c_{11}' S_x - e_{31} E_3 \\ &= n_c Q c_{11}' \frac{3d_{31}(z_0 - z)}{2h_p a} E_3 - d_{31} c_{11}' E_3 \end{aligned} \quad (4.20)$$

The electric displacement is written as

$$\begin{aligned} D_3 &= e_{31} S_x + \epsilon_{33} E_3 \\ &= n_c Q c_{11}' \frac{3d_{31}^2(z_0 - z)}{2h_p a} E_3 + \epsilon_{33} E_3 \end{aligned} \quad (4.21)$$

where ϵ_{33} is the dielectric constant in z-direction, and E_3 is the electric field in the z-direction.

Taking the Laplace transform and then the Inverse Laplace transform of \dot{S}_x and \dot{D} , we can obtain their forms in the frequency domain

$$\dot{S}_x = n_c Q \frac{3d_{31}(z_0 - z)}{2h_p a} j\omega E_3 \quad (4.22)$$

$$\dot{D} = (n_c Q c_{11}' \frac{3d_{31}^2(z_0 - z)}{2h_p a} + \epsilon_{33}) j\omega E_3 \quad (4.23)$$

Since we found that piezoceramics only cost power when they were powered with voltage, we assumed that the power consumption was caused by hysteresis losses in piezoelectric coupling. Therefore, a complex parameter, d_{31}^* , is introduced to calculate the power losses

$$d_{31}^* = d_{31}(1 - j \tan \theta') \quad (4.24)$$

where θ' is the phase delay of the strain when an electric field is applied, or the phase delay of the electric displacement when an applied stress is applied.

Substitute the complex piezoelectric constant d_{31}^* and (4.22) to (4.18), we can calculate the mechanical part of power losses as

$$\begin{aligned}
 P_m &= \iiint \frac{1}{2} \text{Re}(T\dot{S}^*) dV \\
 &= \iiint \frac{1}{2} \text{Re} \left(\begin{array}{l} d_{31}(1-j \tan \theta') \left[n_c Q c_{11} \frac{3(z_0-z)}{2h_p a} E_3 - c_{11} E_3 \right] \\ \times n_c Q \frac{3d_{31}(1+j \tan \theta')(z_0-z)}{2h_p a} (-j)\omega E_3 \end{array} \right) dV
 \end{aligned}$$

Since $d_{31}(1-j \tan \theta') \times d_{31}(1+j \tan \theta') \times (-j) = -j|d_{31}|^2 \notin \Re$, there is no real part in the above equation. As a result, the mechanical part of power losses in the piezoelectric layer equals to zero.

Similarly, we can also calculate the electrical part of power losses as

$$\begin{aligned}
 P_d &= \iiint \frac{1}{2} \text{Re}(E\dot{D}^*) dV \\
 &= \iiint \frac{1}{2} \text{Re} \left(\begin{array}{l} E_3 \times (n_c Q c_{11} \frac{3d_{31}(1+j \tan \theta')^2(z_0-z)}{2h_p a} + \epsilon_{33}) \\ (-j)\omega E_3 \end{array} \right) dV
 \end{aligned}$$

Integrating the above equation over one piece of piezoceramics, we can obtain the electrical part of power losses as

$$P_d = V^2 n_c Q \tan \theta' \frac{3b\lambda}{8} \pi f d_{31}^2 c_{11}' \left(\frac{2z_0 - h_p}{h_p^2 a} \right) \quad (4.25)$$

Considering that there are n_c pieces of piezoceramics glued on the resonator, the total power is calculated as

$$\begin{aligned}
 P &= n_c P_d \\
 &= V^2 n_c^2 Q \tan \theta' \frac{3b\lambda}{8} \pi f d_{31}^2 c_{11}' \left(\frac{2z_0 - h_p}{h_p^2 a} \right) \quad (4.26)
 \end{aligned}$$

According to this model, the power losses are in proportion to the square of the number of piezoceramics and the applied voltage. This result is consistent with our measurements (see Table 4.3).

In our application, the tactile plate must vibrate at ultrasonic frequency in order to generate the Squeeze air film effect. Moreover, instead of the applied voltage, we care more about the vibration amplitude which should be above 1 μm [25]. Therefore, we need to deduce the relationship between power and the

vibration amplitude.

Assume the vibration across the x axis is presented as

$$w(x) = A \sin\left(\frac{2\pi}{\lambda} x\right) \quad (4.27)$$

where A is the maximum amplitude at the antinodes. The strain in the piezoceramic layer is then deduced as

$$S_x = \frac{z_0 - z}{\rho} = -\frac{(z_0 - z)d^2 w}{dx^2} = (z - z_0) \left(\frac{2\pi}{\lambda}\right)^2 A \sin\left(\frac{2\pi}{\lambda} x\right) \quad (4.28)$$

By substituting the strain to (4.21) we can obtain the total power as in (4.25):

$$P = n_c P_d = 2n_c A V f b d_{31} c_{11}' \tan \theta' (2z_0 - h_p) \frac{\pi^2}{\lambda} \quad (4.29)$$

From (4.29) and (4.26), which give the same result, we can deduce the relationship between the maximum amplitude, A , and the applied voltage, V , as

$$A = V n_c Q \frac{3\lambda^2}{16\pi} \left(\frac{d_{31}}{h_p^2 a}\right) \quad (4.30)$$

Then, we can write the power losses using only the vibration amplitude A :

$$P = \frac{A^2}{Q} \tan \theta' f b c_{11}' (2z_0 - h_p) \frac{32\pi^3 h_p^2 a}{3\lambda^3} \quad (4.31)$$

The above equation indicates that the power is in proportion to the square of vibration amplitude. This result is also consistent with our measurement results, as shown in Table 4.3. In our application of providing tactile feedback, we need the device to work at constant vibration amplitude rather than constant voltage [124]. According to (4.31), when vibration amplitude is constant, the power consumption is independent of the number of piezoceramics. Namely, we can use very few piezoelectric actuators to excite the resonator while costing the same amount of power. The reduction of the number of piezoceramics will reduce the cost and weight of the tactile plate. This result is significant for the design of a large but compact tactile device.

However, the values of two parameters in (4.31) are unknown. One is the piezoelectric loss tangent, $\tan \theta'$. The other is the amplification factor, Q . To

obtain these data and to analyze their sensitivity, we made six other small tactile plates that varied in actuator layout and resonator thickness. We intended to use the data obtained from these small tactile plates to estimate the power consumption of large tactile plates. Figure 4.5 shows the aluminum resonator with different layouts of the piezoceramics. The dimension of these aluminum resonators was 76×41 mm varying in thickness (2mm and 1.2mm). The size of piezoceramics was $5 \times 9 \times 0.5$ mm. In the following section, we present the measurement results of the piezoelectric loss tangent and the amplification factor.

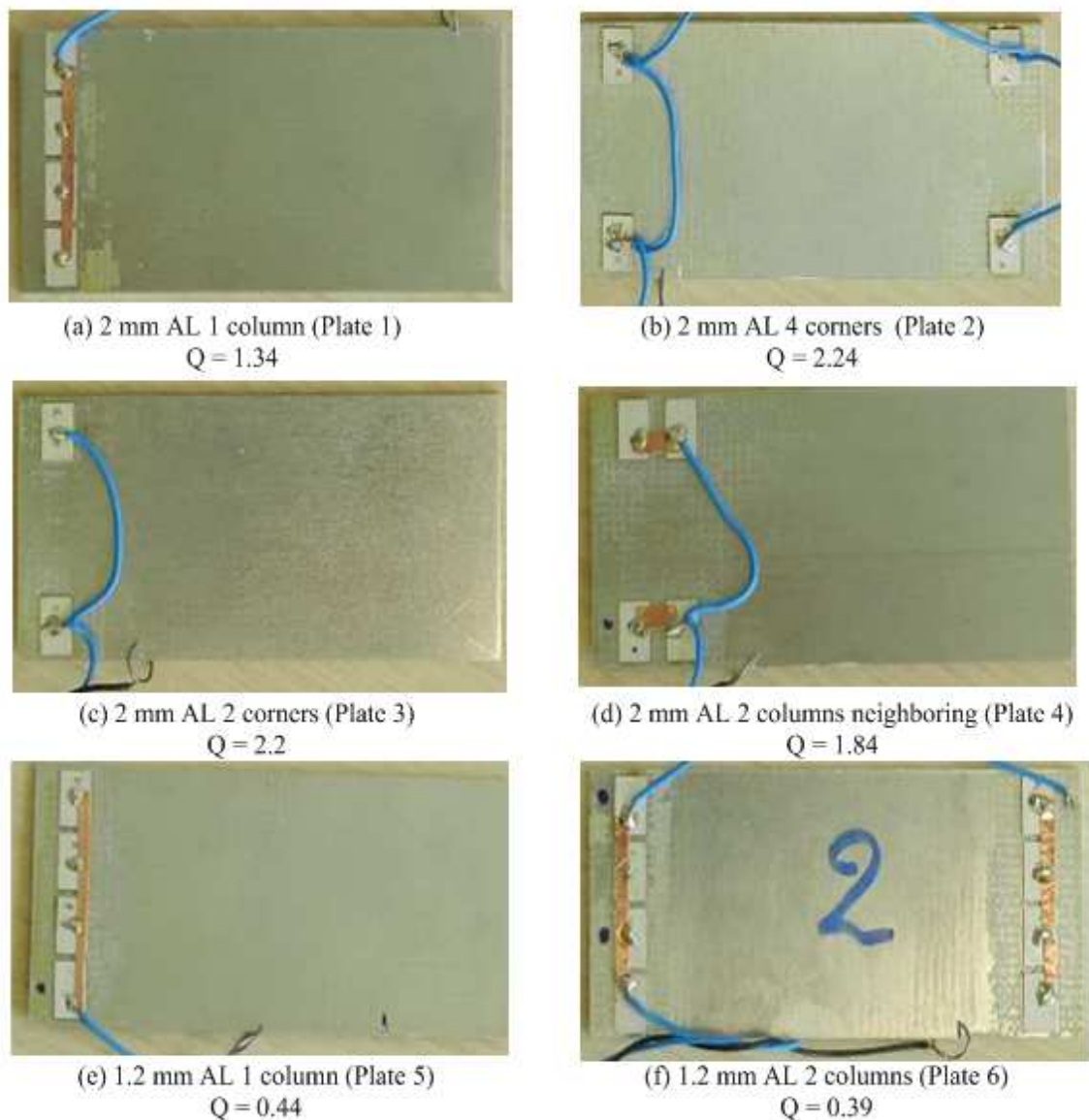


Figure 4.5 Aluminum resonators with different piezoceramics layouts. The amplification factor (Q) has been measured in each condition, as explained further.

4.3.4. Variation Of The Piezoelectric Loss Tangent

The piezoelectric loss tangent is calculated by dividing the product of $Q \tan \theta'$ by Q . The product of $Q \tan \theta'$ is obtained from (4.26). In (4.26), all the other parameters are known and the power is measured. As for the amplification factor Q , it is obtained from (4.30) where we just need to measure the vibration amplitude, the voltage and the wavelength. Measurement results are presented in Figure 4.6.

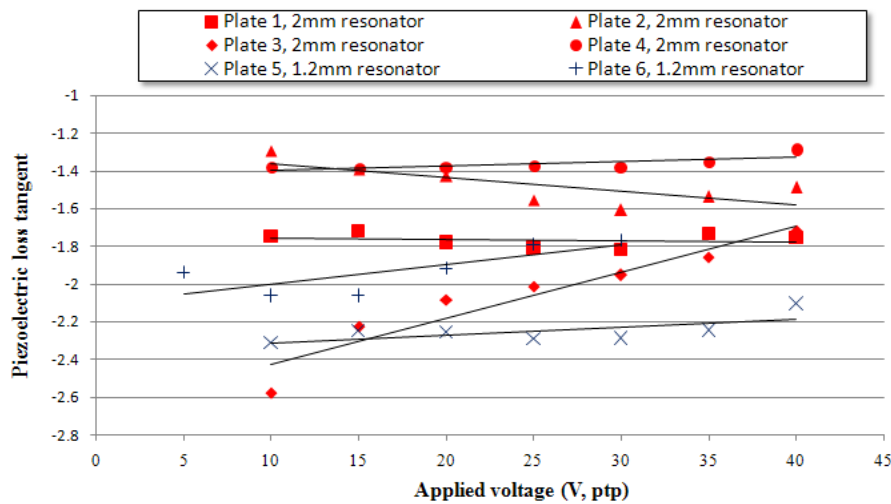


Figure 4.6 Piezoelectric loss tangent in different tactile plates as a function of applied voltage.

In Uchino et al.'s research, the piezoelectric loss tangent increased about 60% when the applied voltage was increased from 0.5 KV/mm to 0.9 KV/mm [126]. Nevertheless, the applied voltage was relatively low (lower than 100 V) in our application and resulted in a small electric field (<0.2 KV/ mm). In this range, we found that the piezoelectric loss tangent only changed slightly with the applied electric field. Therefore, we assume that the influence of applied voltage on the piezoelectric loss tangent is negligible. Moreover, we did not find any constant relationship between the layout of the piezoceramics and the $\tan \theta'$. So, we assume the actuator layout does not affect the piezoelectric loss tangent in our application.

Generally, we suppose that the piezoelectric loss tangent is a constant which does not vary with the resonator. However, we found that $\tan\theta'$ was in general varying with the thickness of the resonator. The mean $\tan\theta'$ with 2 mm resonator was -1.65 (SD = 0.14) while that with the 1.2 mm was -2.16 (SD = 0.06). These data will be used to estimate the power consumption of the large area tactile plate whose resonator has the same thickness (1.2mm or 2 mm).

4.3.5. Effect Of The Actuator Layout

Assuming that $\tan\theta'$ did not vary with layout of the piezoceramics, we found that the layout of the piezoceramics had a significant effect on the amplification factor, Q . Comparing Plate 1 with Plate 3, we found that removing the two pieces of piezoceramics along the width of the resonator increased the amplification factor by almost twice of its value. Similarly, we also found that removing the two pieces of piezoceramics that were neighboring along the length of the resonator also increased the amplification factor (comparing Plate 3 with Plate 4). According to these results, we conclude that piezoceramics should not be placed close to each other in order to increase the amplification factor.

We also noticed that duplicate the same layout of actuators of each column to a column that was far away from the neighboring column did not change the amplification factor (see Plate 2 and Plate 3, Plate 5 and Plate 6). This result indicates that we can place piezoceramics at the two opposite edges of the resonator if we need to glue many actuators on the tactile plate. This design will not deteriorate the amplification factor.

4.3.6. Summary

We have developed an analytical model to estimate the power consumption of the tactile plate. According to this model, the power consumption of the tactile plate is irrelevant to the number of piezoceramic actuators. This result makes it

possible to reduce the number of actuators. However, we notice that the layout of the piezoceramic actuators affects the amplification factor significantly. Optimal layout is realized by placing the piezoceramics far away from each other, for instance, placing them at the four corners of the resonator. Otherwise, placing piezoceramics close to each other will deteriorate the amplification factor thus increasing the power. We also find that the piezoelectric loss tangent may vary with the thickness of the resonator but not with the layout of actuators. These findings offer guidelines for the design of a large but compact tactile plate. Moreover, we can also use the data obtained through measuring the small tactile plates to estimate the power consumption of large tactile plates. In the following section, we present the design of a large tactile plate and the power estimation of it to validate the analytical power modeling.

4.4. Design of a large tactile device

4.4.1. Design Guidelines

We intend to design a large but portable tactile interface which is able to provide programmable friction coefficient. Therefore, the design should satisfy several requirements due to the considerations from different aspects. First of all, the STIMTAC tactile plate is based on the Squeeze air film effect. The squeeze number should be above 10 so as to realize an efficient tactile feedback [129]. As a result, we need to excite the tactile plate at an ultrasonic frequency (>25 kHz) with an amplitude above $1 \mu\text{m}$ [25]. Secondly, ultrasonic vibration modes exhibit nodal lines. Along the nodal lines, squeeze film effect is diminished. To minimize this effect, we use a standing wave mode shape with the half wavelength similar to the width of fingertip [118]. Thirdly, we intend to design a large tactile plate whose workspace is similar to that of mainstream consumer electronics such as the Apple Ipad. Finally, we use the minimum number of piezoelectric actuators by placing them as the optimal layout to reduce cost and power. These requirements are summarized as follows,

Squeeze air film effect: resonance frequency > 25 kHz, vibration amplitude > 1 μm

Mode shape: uniform standing wave, half wave length ≤ 15 mm .

Workspace: about 200 mm \times 150 mm.

Actuator layout: glue piezoceramics at the four corners of the resonator.

4.4.2. Implementation

The resonator is made of aluminum for its light weight and easy manufacture. The size is 198 mm \times 138 mm. The thickness of the resonator should be as thin as possible to minimize power consumption [124]. However, the tactile plate shall also have sufficient rigidity to preclude deformation during user's exploration. Therefore, we use the 2 mm thick resonator as a trade-off between mechanical resistance and power consumption. Moreover, the 2 mm thick resonator can produce a high frequency (above 50 KHz) standing wave mode so that the user cannot hear the noise when it works. It may be noted that we did not use glass resonator in this prototype. The first reason is that the aluminum resonator is easy to manufacture. Secondly, our primary motivation in this research is to validate our power modeling instead of developing a tactile touch screen. However, it is possible to replace the resonator with a transparent one, such as glass [118] and off the shell capacitance touch screens [116].

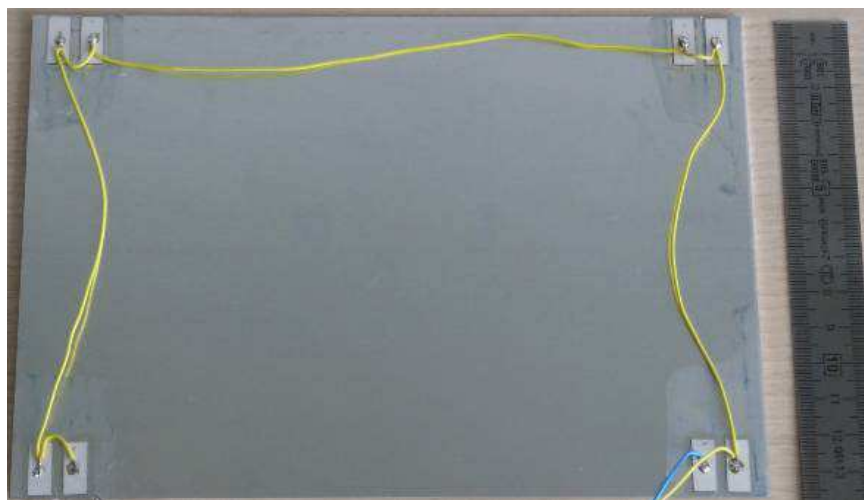


Figure 4.7 The layout of the eight piezoceramics on the big tactile plate.

Mechanical properties of the aluminum resonator		
Young's module	E_i	$67 \times 10^9 \text{ N/mm}^2$
Poisson's ratio	ν_i	0.34
Density	ρ_i	2790 kg/m^3
Mechanical properties of NCE 41 piezoceramics		
Charge constant	d_{31}	$-130 \times 10^{-12} \text{ C.N}^{-1}$
Elastic constant	c_{11}^E	$80 \times 10^9 \text{ N.m}^{-2}$
Density	ρ_p	7900 kg/mm^3
Poisson's ratio	ν_p	0.33

Table 4.4 Material parameters of the big tactile plate

Eight PZT piezoceramics (NCE 41, Noliac Inc.) are glued at the backside of the resonator, as shown in Figure 4.7. The half wavelength is designed to be 9 mm. The piezoceramics are chosen with a dimension of 6 mm \times 14 mm \times 0.5 mm. They are placed equally at the four corners of the resonator to minimize the power consumption. In fact, we can use only four pieces of them. However, the fewer number of piezoceramics we use, the higher voltage is needed to excite the plate (see (4.30)). Moreover, we also need one piece of the piezoceramics as a vibration sensor to set up a close-loop control of the vibration. Therefore, we glue extra four pieces of piezoceramics symmetrically on the resonator. To minimize their effects on the amplification factor, they are glued in a neighboring mode as Plate 4 in Figure 4.7. The material properties are presented in Table 4.4.

4.4.3. Modal analysis

A modal analysis is conducted to further verify the performance of the new tactile plate. There are three parameters to check in the modal analysis. Firstly, we check if there is a uniform standing wave mode with 21 antinodes as we

designed. Secondly, we check if the corresponding resonance frequency of the tactile plate is above 25 KHz which is a requirement of generating efficient squeeze film effect. Finally, we need to check if the frequencies of the neighboring modes are too close to the standing wave mode (i.e. less than 0.1 KHz). If so, we may have difficulties to obtain an accurate tactile feedback: usually, the resonance frequency of the tactile plate varies slightly according to the temperature changes (such as changes caused by the heating of the tactile plate and the environment). If several resonance modes are close to each other, a small shift may excite neighboring modes that are not expected and that may weaken the quality of the vibration.

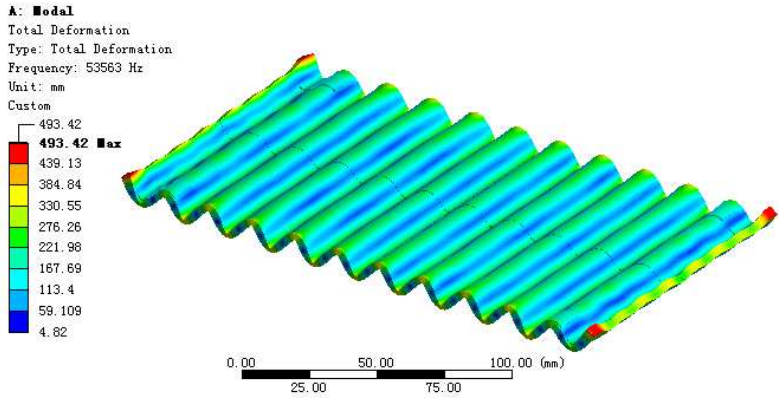


Figure 4.8 Modal analysis of the big tactile plate by ANSYS Workbench: deformed shape at (21, 0) mode.

The deformed shape of the (21, 0) mode of the tactile plate is presented in Figure 4.8. The resonance frequency is 53563 Hz which satisfies the frequency requirement (above 25 KHz). The frequencies of the neighboring modes are 53.2 KHz and 53.7 KHz respectively. The differences are above 0.1 KHz indicating that the mode interference is not likely to happen.

4.4.4. Experimental measurements

We conduct several measurements to validate its design and the power modeling. The measurement setup is the same as the one we presented in Section 4.2.1. Before the measurements, we adjusted the waveform generator to activate the tactile plate at the desired resonance frequency. We then applied several

voltages to the tactile plate and measured its vibration amplitude with a Laser Doppler Vibrometer. The power consumption and the vibration speed of the tactile plate were read from an oscilloscope.

(a) Mode shape and vibration amplitude

The expected (21, 0) mode shape was found at the resonance frequency of 52.4 KHz. To further confirm the mode shape, we made cartography of the tactile plate. The tactile plate was placed softly on a servo-controlled x-y platform. The platform moved with a step of 2 mm along either the x or y direction. We measured and record the vibration amplitude of each sample point of the tactile plate and made the cartography, as shown in Figure 4.9.

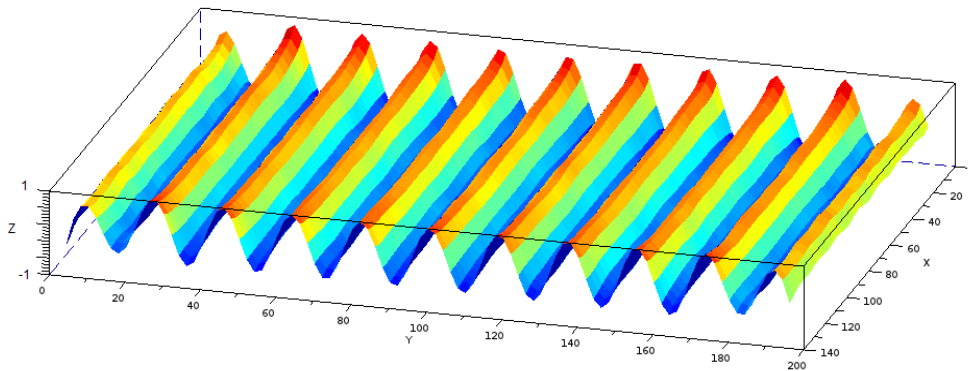


Figure 4.9 Cartography of the big tactile plate.

The cartography indicates that the mode shape is uniform across the tactile plate. This shape is good to provide a homogeneous tactile feedback to users. Then, we measured the relationship between vibration amplitude and the applied voltages. The measurement was carried out at the center of the tactile plate since the area was explored most frequently. The measurement result is presented in Figure 4.10. The vibration amplitude has a linear relationship with the applied voltage. This result agrees with our model in (4.30).

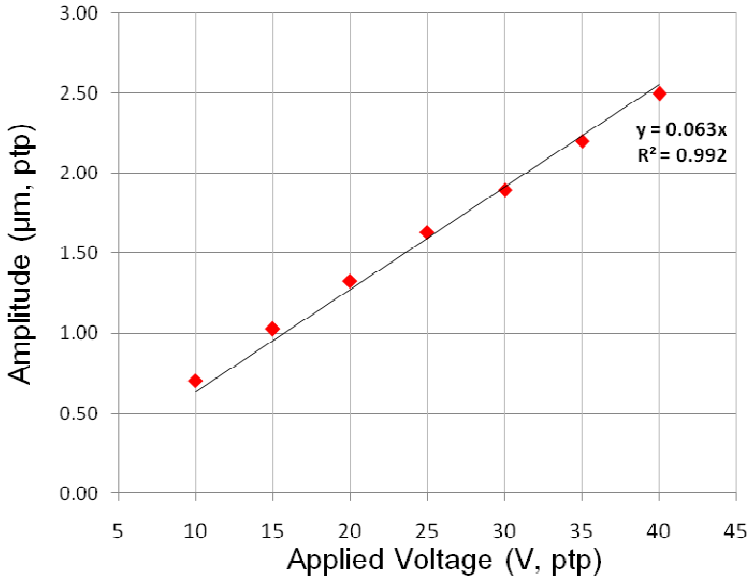


Figure 4.10 Vibration amplitude as a function of applied voltage.

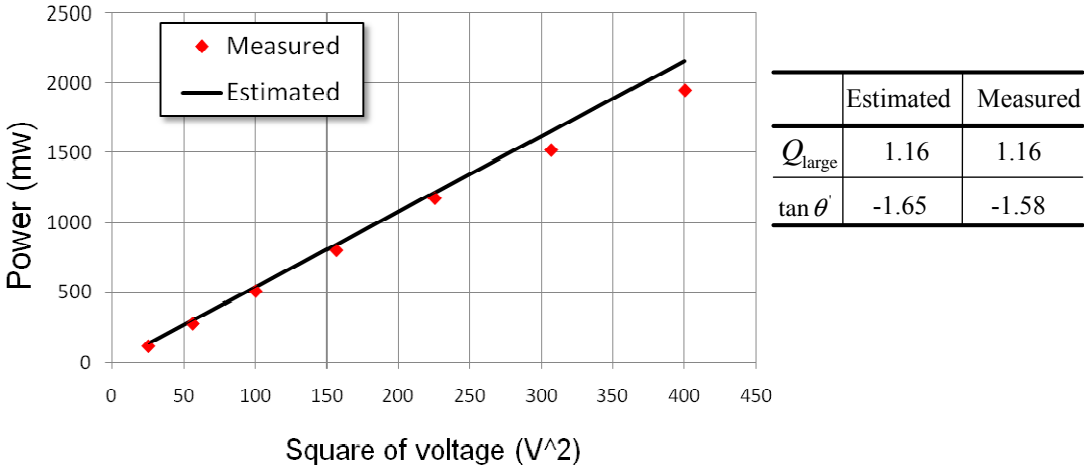


Figure 4.11 Measured and estimated power as a function of the square of voltage. The measured and estimated amplification factor and piezoelectric loss tangent are also listed (The estimated values are obtained according to the measurement results on the small samples).

(b)Power consumption

As presented in section 4.3, we have developed a model to estimate the power consumption of the tactile plate. However, the piezoelectric loss tangent and the amplification factor are difficult to be obtained through modeling. Instead, we intend to obtain them through our measurement results, as described in Section 4.3.4 and Section 4.3.5. We assume that the piezoelectric loss tangent does not change if the resonator of our large tactile plate has the same thickness (2 mm AL)

as the small tactile plates. Then, $\tan \theta$ equals to -1.65 , as the average value of the results. The amplification factor varies with the piezoelectric actuator layout. The layout of the big tactile plate is the same as the Plate 4 (Figure 4.5), by duplicating four groups of piezoceramics at the four corners. Therefore, we use the amplification factor of the Plate 4 which also has the layout of placing piezoceramics at the neighboring antinodes. Moreover, we have also found that the longer the piezoceramics are, the lower the amplification factor is (Figure 4.5, Plate 1 and 3). We suppose this effect is linear. With these hypotheses, we calculate the amplification factor of the large tactile plate as

$$Q_{\text{large}} = Q_{\text{small}} \times \frac{b_{\text{small}}}{b_{\text{large}}} \quad (4.32)$$

where Q_{small} is the amplification factor obtained from the small tactile plates, b_{small} is the length of the piezoceramics used in the small tactile plates ($b_{\text{small}} = 9$ mm), b_{large} is the length of the piezoceramics used in the large tactile plate ($b_{\text{large}} = 14$ mm). With these data, we can estimate the power consumption of the large tactile plate according to (4.26). The estimated and measured power as a function of the square of voltage is presented in Figure 4.11. The estimated power consumption is very close to the measured data with an average error of 7.29%. This result validates our analytical model of power estimation. According to Figure 4.10 and Figure 4.11, we can infer that this tactile plate needs only 1.3 W@32 V_{rms} to excite a distinct friction reduction with the vibration amplitude above 1 μm .

Figure 4.12 and Figure 4.13 show two other large tactile plates we developed with different piezoceramics layouts and their power estimation results. The mean errors of power estimation for these two tactile plates are both less than 10%.

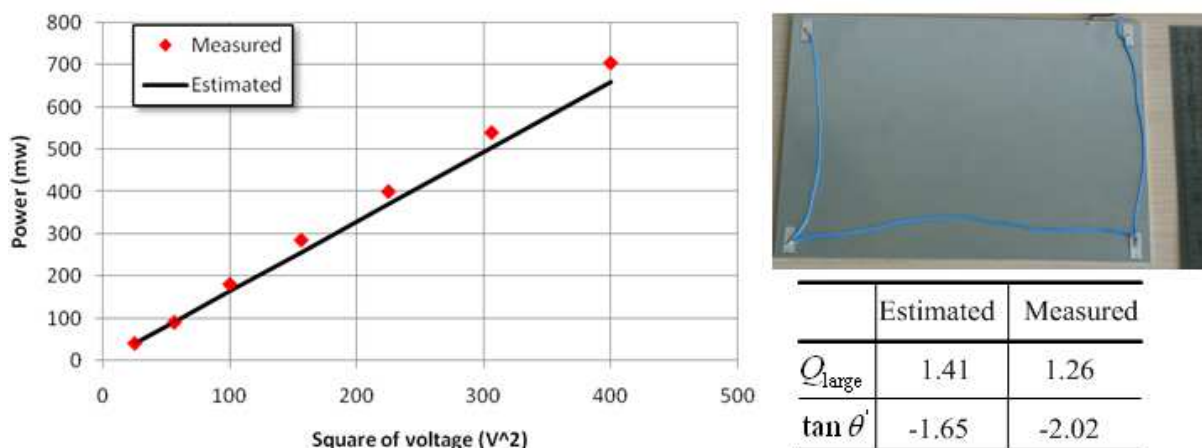


Figure 4.12 Measurement result of a 4 piezoelectric actuators tactile plate. The mean error between the measured power and estimated power is 6.3%.

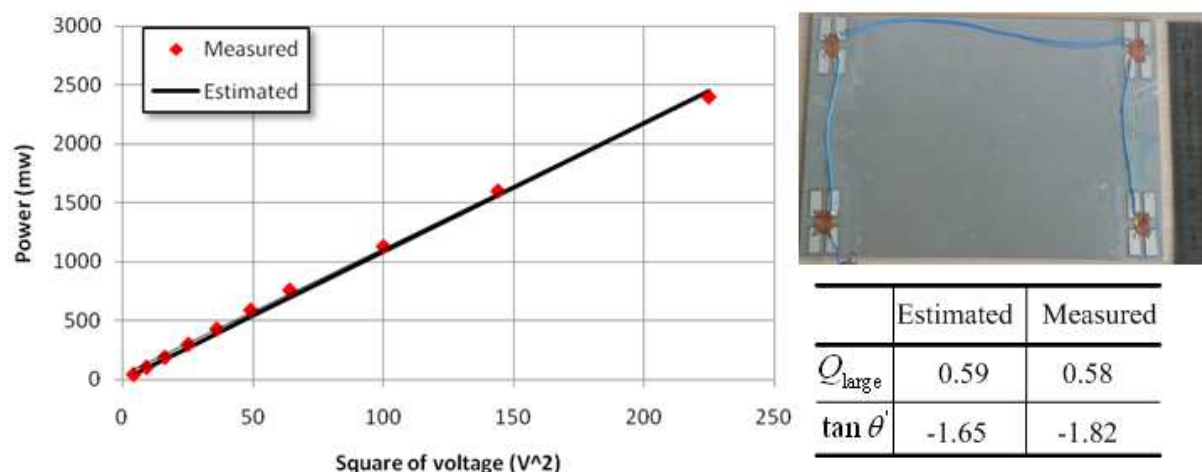


Figure 4.13 Measurement result of a 16 piezoelectric actuators tactile plate. The mean error between the measured power and estimated power is 5.96%.

4.5. Psychophysics evaluation of the tactile plate

4.5.1. Motivation

The STIMTAC tactile plate takes advantage of the Squeeze air film effect to generate tactile feedback. Previous research shows that the increase of amplitude reduces the friction coefficient [78] and users' perception of smoothness increases with the vibration amplitude [25]. However, there is little research indicating how much difference of vibration amplitude can produce perceivable friction variation. Moreover, this datum is important not only for designing efficient user interfaces

[15, 80] but also for designing the tactile plate itself.

Usually, users explore on the STIMTAC in two ways according to interaction tasks. In one way, they move their fingers continuously on the tactile plate to perceive tactile feedback, such as in texture exploration [120], scrolling [130] and pointing [80] tasks. This type of exploration is referred as continuous exploration. In these tasks, an efficient way to use the STIMTAC tactile plate is to present the shift between rough (low vibration amplitude) and smooth (high vibration amplitude). Examples include presenting grating textures by shifting between high and low friction coefficient [120] and rendering targets as rough and environment as smooth in dragging tasks [15, 80]. To generate a perceivable shift of friction coefficient, we need to know how much vibration amplitude difference is required when the user explores across the two stimuli (high and low vibration amplitude).

In the other way of exploration, users explore several areas on the tactile plate when these areas are mapped with different tactile feedback. For example, in a drawing application, different paints are mapped with different friction coefficients. When the user dips in any grid of paints, he will be able to tell the friction coefficient of that color. This type of task is referred as *distributed* exploration. In such a task, the user needs to identify different friction coefficients separately. The difference of vibration amplitude that is required to produce this effect is needed before designing such an application.

According to these considerations, we conducted two psychophysics experiments to evaluate the capability of the large STIMTAC tactile plate. The first experiment evaluates users' ability to detect a step (shift) of friction coefficient. We intended to know how many levels of friction coefficients can be generated by the device to produce detectable step stimulus. The second experiment evaluates users' discrimination of friction reduction. This experiment investigated how much vibration amplitude was needed to enable users to discriminate reduced friction coefficient from the tactile plate's actual friction

coefficient. These data described the resolution of friction variation and offers important reference to the use of the STIMTAC device.

4.5.2. Method

(a) Apparatus and stimuli

In the experiments, the large STIMTAC which uses eight piezoceramics was evaluated. The size of the device was 198 mm × 138 mm. The device worked at resonance frequency of 52.2 KHz and generated the maximum vibration amplitude of 1.3 μm. Four force sensors were placed asymmetrically at the four corners of the tactile plate to track the finger position [118]. One of the eight pieces of piezoceramics was used as a vibration sensor to detect the vibration amplitude. The large tactile plate was controlled by a custom-made controller based on a DSP (Piccolo control stick from Texas Instrument). The board of the DSP included FTDI circuit, which enabled communication through an emulated RS232 link. The controller was connected with the master PC with a USB port which also supplied power to the piezoceramics due to the low power consumption of the device. More details of the controller can be found in [118]. The experiment application was coded in C++ and OpenGL. The tactile feedback was update at a frequency of 1 KHz. The device is presented in Figure 4.14.

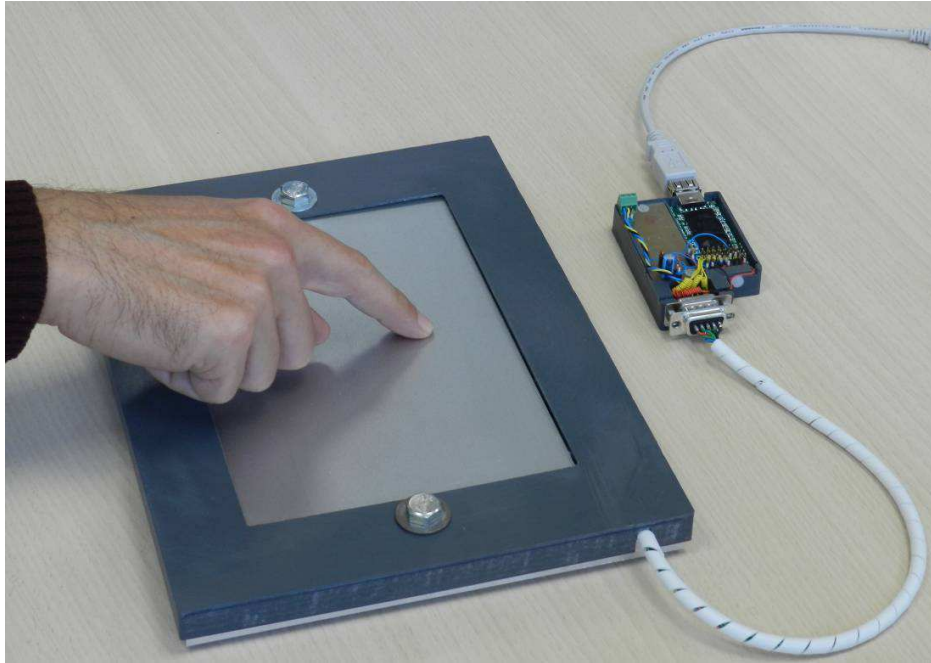


Figure 4.14 The large STIMTAC and its controller.

Two forms of stimuli corresponding with the *continuous* and *distributed* exploration modes were investigated in the experiments. One was a *step* signal. When the participants moved their finger across the center of the device, they perceived the step (shift) between roughness and smoothness). This kind of stimulus was used to estimate the minimum perceivable threshold in the *continuous* exploration mode. The other one was a *constant* stimulus. Namely, the tactile feedback was uniform across the workspace of the tactile plate. This kind of stimulus simulated the *distributed* exploration mode in which tactile feedback only varied at different touching areas.

(b) Procedure

We used a well-established one-up/two-down adaptive staircase method to obtain the detection threshold and the discrimination threshold. This transformed adaptive method is good for estimating high performance level (70.7%) threshold with relatively few trials [131]. We also employed the three-alternative forced-choice (3AFC) procedure to present the stimuli for its high efficiency and less bias in low threshold estimation [132].

On each trial, one test stimulus and two reference stimuli (the three

“alternatives”) were presented to the participants in a random order. Participants were asked to identify which stimulus was different from the other two. The three stimuli were numbered 1, 2 and 3. Participants pressed the Space key to progress to the next stimulus. They were not allowed to return to the previous stimulus. On each alternative, participants were asked to use their dominant index finger to explore the tactile device back and forward at least three times in the lateral direction. After exploring all the three alternatives, participants pressed the “1”, “2” or “3” key on the keyboard to make their selection. This was a forced-choice experimental paradigm. Participants had to select one stimulus even if they had no idea and made a guess. It should be noted that in the *Step Detection* tasks, the step was presented in an alternative as the test stimulus. In the two other alternatives, only constant stimuli with the reference amplitude were presented. The stimuli in the experiments are depicted in Figure 4.15.

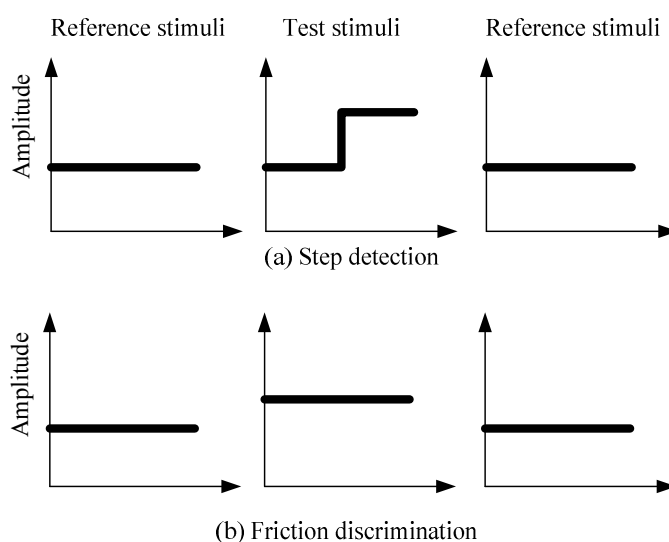


Figure 4.15. Stimuli in the experiments. The x-axis represents the workspace while the y-axis represents the vibration amplitude. The test and reference stimuli were presented to the participants in a random order.

The experiment application was added with game elements to make the experiment enjoyable and less tedious [133]. The three stimuli were mapped with three identical ghosts on the screen. One of the ghosts was a cursed human being. He could not be identified by vision but had different tactile feedback. The task

was to save him by selecting the ghost with different tactile feedback from the two others. There was no feedback about if the selection was right or wrong.

At the start of the Friction Discrimination task, the test stimulus was set to be the maximum vibration amplitude (1.3 μm) while the reference stimulus was 0 μm (no vibration). In the first round Step Detection task, the reference stimuli were 0 μm (no vibration). The test stimulus was a step function of the vibration amplitude: the initial value was the same as the reference stimulus (0 μm) and the step value was the maximum vibration amplitude (1.3 μm). Then, in the second round, the threshold obtained in the first round was used as the reference stimuli while the step value of the test stimulus was kept as 1.3 μm . This method was to find the number of friction reduction steps that the device could produce.

In the experiments, the test stimulus was reduced by 0.6 dB after the participant made two consecutive correct responses. If the participant made a wrong response, the test stimulus was increased by 0.6 dB. The change of test stimulus from decreasing to increasing and vice versa was referred as reversal. After the first three reversals, the step size of the test stimulus change was reduced to 0.3 dB. The big step size enabled the vibration amplitude to converge fast to the expected threshold and the small step size guaranteed the fine resolution of the threshold estimation. The session was ended after 11 reversals at the 0.3 dB step size. The last 8 peaks and valleys were then averaged to calculate the estimate threshold. A typical trial session of a participant in the Step Detection task is illustrated in Figure 4.16.

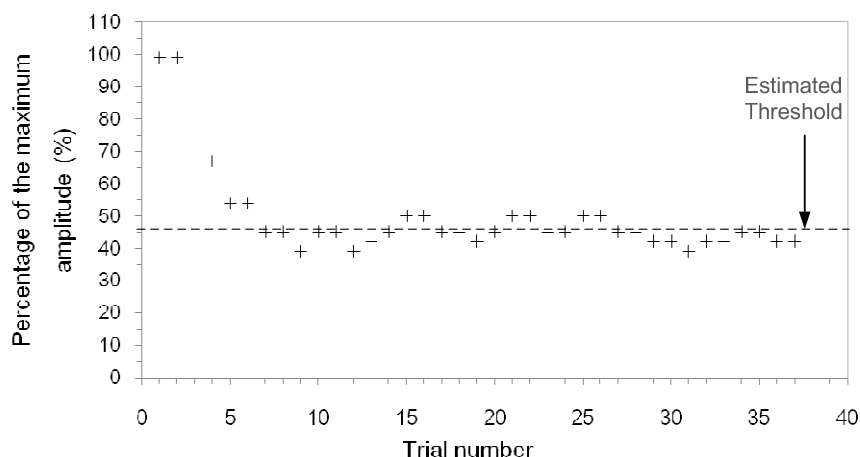


Figure 4.16 A typical series of trials of a participant in the Step Detection task

(c) Pretest

Before the experiment, we conducted a pretest to evaluate the participants. We asked them to explore the easiest perceivable stimuli. Namely, a step made of $1.3 \mu\text{m}$ and $0 \mu\text{m}$ stimuli before the Step Detection task and respective $1.3 \mu\text{m}$ and $0 \mu\text{m}$ constant stimuli before the Friction Discrimination task. We intended to preclude participants who were not able to perceive the most apparent stimuli before the experiment. They were asked to explore the stimuli as many times as they wished and asked if they could perceive the step and the friction coefficient difference before and after friction was reduced.

21 volunteers aged between 22 to 31 were recruited from the laboratory to implement the pretest. However, only 7 of them could easily perceive the step. Most participants reported that they hardly decode the step or did not feel anything at all. For the constant stimuli, none of the participants reported that they could easily distinguish the difference when the friction coefficient was reduced. This result may be due to the relatively low vibration amplitude which made the squeeze film effect not very easy to be perceived. In a preliminary study, Samur et al. found the squeeze film effect on the TPad started to be felt when the vibration amplitude was around $1.5 \mu\text{m}$ [134]. However, according to our experience on the small STMTAC devices [116], the squeeze film effect was noticeable even when vibration amplitude was about $1 \mu\text{m}$. A possible explanation may be that the finger pad damped the vibration of the device weakening the

actual squeeze film effect. This possibility needed further investigation.

(d) Participants

The seven relatively sensitive participants (three female, four male, mean age = 26.3, Standard Deviation = 2.1) took part in the formal tests. They conducted the Step Detection task first and implemented the Friction Discrimination task after a week's interval. Each session of the Step Detection task included 25 to 35 trials, taking about 20 minutes. The amplitude detection task included 35 to 57 trials, taking 20 to 30 minutes. Participants were asked to put on earplug to eliminate any audible clue in the judgment¹⁰.

4.5.3. Results

In the first round of the Step Detection task, we presented a step made of the maximum amplitude (1.3 μm) and no vibration. The test stimulus was reduced from 100% of the maximum amplitude while the reference stimulus was 0 all the time. The threshold was obtained as 49.3% of the maximum amplitude (0.64 μm , SD = 10%). This result indicated that, to generate a detectable step between rough and smooth, the vibration amplitude of the tactile plate needed to be increased from 0 to at least 49.3% of the maximum amplitude (i.e. above 0.64 μm). In other word, weak vibration (below 0.64 μm) was not sufficient for users to distinguish the friction reduction effect from the tactile plate's actual friction coefficient. The threshold defined the first level of friction reduction that could be used to create a step.

We intended to find the second level of friction reduction that could be distinguished from the first level. Therefore, we used the first level threshold as the reference stimuli in the second round Step Detection task. However, we could not obtain a convergence trial session as we obtained in Figure 4.16. We supposed the second level threshold was around 1.3 μm which was the maximum vibration

¹⁰ Although the device worked at ultrasonic frequency, when vibration was activated as a step function there was still a weak sound caused by the deformation of the piezoceramics. Some sensitive participants could hear it.

amplitude of the large STIMTAC. Therefore, stronger vibration was needed to find the threshold.

As for the Friction Discrimination task, only four of the seven participants completed the experiments successfully. The other data did not show convergence. The average discrimination threshold was 0.63 μm , with the Weber's ratio of 51.5%. In Samur et al's study[134], they found the Weber's ratio of friction coefficient was 18% (though it was obtained from only one subject). However, we did not measure the friction coefficient in the experiment. Further investigation is needed to compare these data.

It seems that the threshold in the Step Detection task was very similar to that in the Friction Discrimination task. Due to very limited number of data, statistics analysis does not make sense. However, we reckon that the threshold in the Step Detection task was smaller than the Friction Discrimination threshold, because the seven participants reported that they could easily detect the step but they hardly discriminate the friction reduction in the Friction Discrimination task. Interestingly, they performed the experiment quite well, although they said they conducted it mainly by guess.

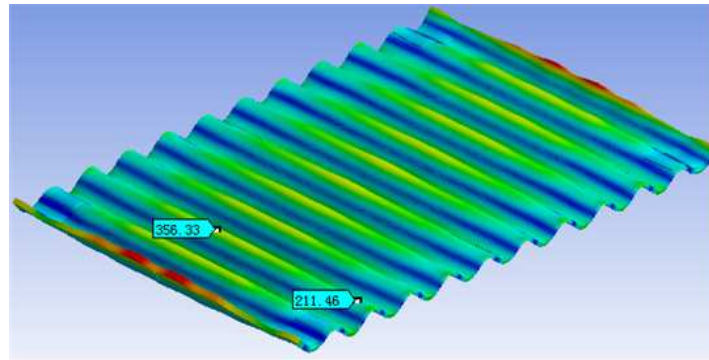
4.5.4. Discussion

The results indicated that the capability of the current tactile plate was limited. It could generate a detectable step which required the tactile plate to vibrate from 0 to at least 0.64 μm (49.3% of the maximum amplitude). The current maximum vibration amplitude was not sufficient to produce various levels of distinct feelings of friction reduction. The maximum vibration amplitude needed to be increased to expand the measurement of discrimination thresholds.

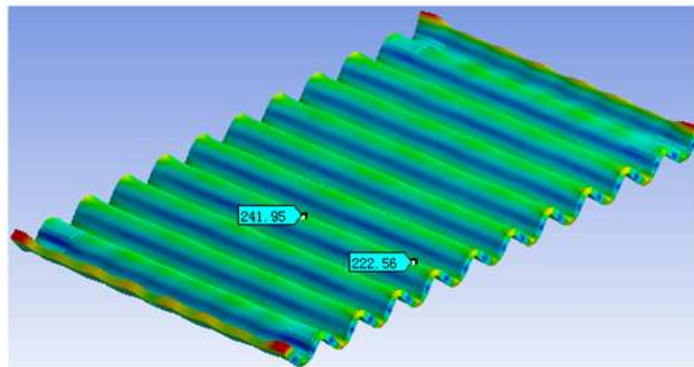
The data obtained from the experiment also offers important reference for the design of the STIMTAC. For instance, we sometimes find that the mode shape of the tactile plate is not a uniform standing wave. For example, Figure 4.17 shows a transverse mode which causes variation of amplitude along the width direction of the tactile plate. If the amplitude variation is great enough, users will be able to

detect the difference between the center and the edge when they explore these two areas. If the difference of amplitude cannot be detected, we do not have to modify the design. In the inverse case, we have to compensate the amplitude difference or even abandon the design. Similar problem also exists in the design of the large tactile plates with very few piezoceramics. According to our observation, when the user presses on the large tactile plate, the vibration amplitude of the tactile plate sometimes decreases due to the damping of the finger. If a user explores on a tactile plate which is not damped and then explore on a large tactile plate whose amplitude is damped, will she/he perceive the difference between these two tactile plates? The amount of amplitude decrease helps us to decide whether or not to compensate it.

According to our results, we can infer that if the vibration amplitude has a difference of up to about 50%, the difference can be detected. In this case, if a mode shape has a 50% amplitude variation along the antinodes, the design should be eliminated. Moreover, if the finger on the tactile plate damps the vibration by more than 50%, the user may perceive this difference, thus more power is needed to compensate the damping. In that case, a close-loop control of vibration amplitude may be needed to provide constant tactile feedback to users.



(a) Transverse mode shape



(b) Standing wave mode shape

Figure 4.17. Transverse and standard standing wave mode shapes. The labels in the pictures indicating the variation of amplitude along the width direction of the tactile plate.

It may be noted that the current threshold was evaluated based on the vibration amplitude of the tactile plate rather than on the friction coefficient. The purpose was to evaluate the new tactile plate and to obtain data on how to control the device to produce detectable tactile patterns. The human perception capability which is based on the friction coefficient was not evaluated. This should also be included in the future work in order to compare with Samur et al's work [134].

4.6. Conclusion

This chapter has presented the design of a large area tactile device which is based on the squeeze air film effect. A key issue in enlarging the workspace of the device is to minimize its power consumption. To achieve this objective, in the first step, we conducted a series of measurements to investigate the source of the power consumption. We found the power comes from the powered piezoelectric actuators. We then develop an analytical model based on the piezoelectric

hysteresis to estimate the power. The model shows that, when vibration amplitude is constant, the power consumption is not related to the number of piezoelectric actuators but related to their layouts. The optimal layout is to place the piezoelectric actuators far away from each other, e.g., at the four corners of the resonator. According to this result, we design a large area tactile plate (198mm × 138mm) with only eight piezoelectric actuators. The device needs only 1.3 W@32 V_{ptp} to excite a distinct friction reduction with the vibration amplitude above 1 μm. Moreover, the power consumption is well estimated by the analytical model with an average error of less than 10%.

Two psychophysics experiments have also been conducted to evaluate the tactile feedback capability of the device. According to the experimental results, producing a detectable reduction of friction requires the vibration amplitude to be at least 0.64 μm. This is under the capability of the new device. However, the maximum vibration amplitude of the current design is limited to 1.3 μm, thus only a limited friction level can be realized.

Chapter 5.

Evaluation of the Coupled Haptic Device

Summary

5.1.	Introduction	126
5.2.	Apparatus.....	130
5.3.	Experiment 1: Perception of a boundary simulated by a step function of force feedback.....	132
5.3.1.	Task and stimuli.....	132
5.3.2.	Design.....	133
5.3.3.	Participants	134
5.3.4.	Results and discussion.....	135
5.4.	Experiment 2: Perception of a boundary simulated by a coupled haptic feedback..	137
5.4.1.	Experiment details	137
5.4.2.	Results and discussion.....	139
5.4.3.	Limitations of the current research.....	144
5.5.	Conclusion.....	146

This chapter presents the evaluation of the integrated haptic interface. The evaluation is carried out by comparing the simulation of a haptic boundary by means of using force feedback and coupled haptic feedback (force feedback + tactile feedback) respectively. After the introduction of the motivation and

background of this research, we present the two experiments to evaluate the coupled haptic device and draw conclusion at the end of this chapter.

5.1. Introduction

Boundaries are fundamental elements that distinguish one object from others. Touch screen GUI boundaries separate keys on a virtual keyboard, distinguish icons from background, and separate items in a menu so that users' actions of pointing at a position can be interpreted as an interaction with a particular GUI element. However, the boundaries or edges of these GUIs are basically presented by visual feedback. The lack of haptic feedback when user explores on the touch surface has been shown to be a significant limitation of touch interaction [1, 2, 135], as we have introduced in Chapter 1.

Haptic enhanced boundaries are important for users' operation on touch screens. The haptic feedback enables users to feel around the touch surface and to know when they are on a GUI element or moving between other GUI elements [14]. A typical implementation of this function is to add vibrotactile feedback when the user moves across the boundaries of an item, such as using a period of semantic vibration [14] or simply using a pulse signal to produce a short but distinct vibration [10, 13, 48, 136, 137]. This feedback enhances users' perception of a boundary and thus improves the user respond speed [10, 48, 66] and reduces errors caused by unawareness of passing or slipping off the target [3, 14]. Moreover, the effect of assisting users to locate GUIs of haptic edges is significant especially when visual feedback is unavailable due to social or physical reasons [138] (such as when driving a car, having a meeting or the target is occluded by the fat finger [139]). In this case, haptic feedback becomes an important clue to help users interact with touch screen GUIs [13, 47, 140].

Besides informing the user if he is coming in or leaving a GUI widget, haptic boundaries can also physically help users reach the target accurately and efficiently. This effect is usually realized by adding a resistant force feedback

when the user gets inside the target [49, 141]. The resistant force is like a brake which helps users stop accurately and fast inside the target, thus reducing the stop time [49]. Although this method is effective in single target or target-aware situations, the undesirable force feedback will deteriorate users' performance in multi-target tasks [37, 40]. An alternative method is to modulate the friction coefficient of the target and the background instead of providing resistant force feedback [15, 80, 83]. This method has been shown to be able to improve users' performance not only in single-target task but also when distracters are presented [80]. However, the magnitude of haptic feedback exerted by providing variable friction coefficient is weak and limited. It cannot replace the force feedback to stop users' movement in particular situations (e.g., getting access to the Delete button, keep scrolling at the end of a list). By contrast, using a step function of force to simulate an edge also has problems. If the magnitude of the force is small, the boundary feels very smooth. This does not satisfy users' preference of sharp, crisp and clear boundaries [68]. On the contrary, if the force magnitude is great, users' performance is degraded [42, 43]. In this research, we intend to address this problem by combining the programmable friction feedback with force feedback. The hypothesis of this research is that, a programmable friction feedback plus a small force feedback can produce a stiff boundary that requires a great force to simulate. To implement this idea, the interaction between force feedback and programmable friction feedback needs to be understood at first.

Since the programmable friction feedback is essentially based on modulating friction on the touch surface, we focus on quantify it to an amount of equivalent lateral force. We are interested in if adding the programmable friction feedback to a small lateral force feedback can produce the perception of a great force. Moreover, we also investigate if the amount of perceived force increment equals to the friction produced by changing the friction coefficient of the touch surface. In the following sections of this chapter, two experiments are presented to answer these questions. The first experiment quantifies the differential threshold of the stiffness of boundary simulated solely by force feedback. This is done to establish

the human resolution (JND, Just Noticeable Difference) to perceive kinesthetically rendered edge simulated by a step function of force feedback. The second experiment determines the added effect that programmable friction has on the perceived force magnitude when presented in combination with force feedback. The second experiment realizes this by matching the coupled haptic feedback to an equivalent lateral force feedback. The increment of perceived force is used to quantify the level that variable friction coefficient feedback can substitute for force feedback.

Our research is very close to Provancher and Sylvester's work on quantifying the effect of skin stretch on friction perception [22]. They used the PHANToM force feedback device to render normal force and kinesthetic resistance. In addition, they added a Contact Location Display to render skin stretch. The Contact Location Display was a radiused (about 1 cm) rubber-coated contact block pulled or pushed by an extra linear actuator fixed on users' forearm (as shown in Figure 5.1).

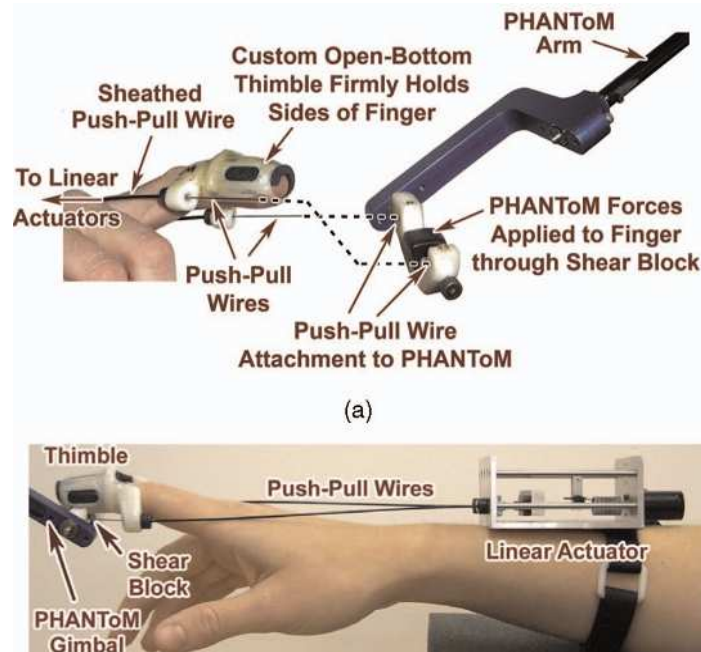


Figure 5.1 The Contact Location Display and its assembly with a PHANToM device (adapted from [22]).

When simulating friction, the integrated device produced kinesthetic rendered friction plus a skin stretch caused by the lateral movement of the

Contact Location Display. To investigate the effect of skin stretch on friction rendering, they compared the friction rendered solely by force feedback with that by a reduced force feedback plus a skin stretch (0.25-0.75 mm). They found that the small amount of skin stretch lead to a statistically significant increase in friction perception. This indicated that the skin stretch could be used to replace a certain level of force feedback to render a same level of friction simulated solely by force feedback device. This research successfully associated friction to skin stretch imposed by the Contact Location Display. However, the amount of force exerted by the linear actuator to produce the skin stretch was not quantified to the amount of perceived friction increment caused by the skin stretch. In our research, by contrast, we quantify the perceived force increment caused by modulating the friction coefficient to an amount of lateral force. Moreover, we find that the perceived force increment may equal to the amount of friction increment due to the increase of friction coefficient. This result paves the way for coupling the programmable friction based tactile feedback and force feedback by revealing that the effect of programmable friction based tactile feedback could be considered as an equivalent lateral force.

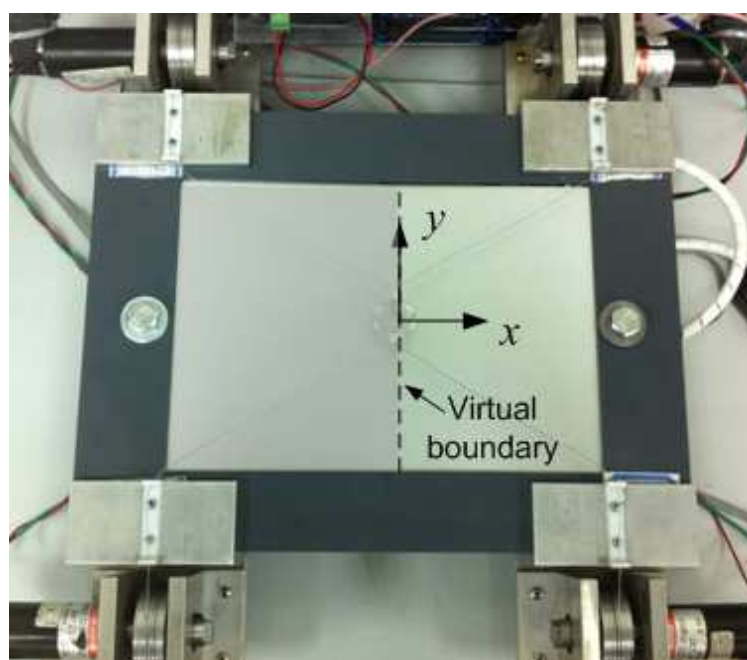


Figure 5.2 The coupled haptic device. In the experiment, the device was used to simulate a boundary located at the center. The gray patch indicates where haptic feedback was exerted.

5.2. Apparatus

The FingViewer-I force feedback device and the large STIMTAC tactile display were integrated in this study to provide coupled haptic feedback. The four actuator-units of the FingViewer-I were fixed at the four corners of the frame of the large STIMTAC, as shown in Figure 5.2.

Users wore the ring of the FingViewer-I device at about their distal joints of the index finger to operate the device. The position of the finger is tracked by the FingViewer-I through the forward kinematics of the mechanism. The cable tensions to exert force feedback were calculated accordingly. When the users touched on the large STIMTAC, the four force sensors that were located on the four corners of the device [118] measured the normal force applied on the touch surface and thus identify the contact status of the finger. The vibration amplitude was then modulated to control the vibration of the large STIMTAC. It should be noted that we used the force feedback device to track the finger position instead of using the force sensors on the tactile device for the purpose of high positioning accuracy. Figure 5.3 shows the control architecture of the integrated device.

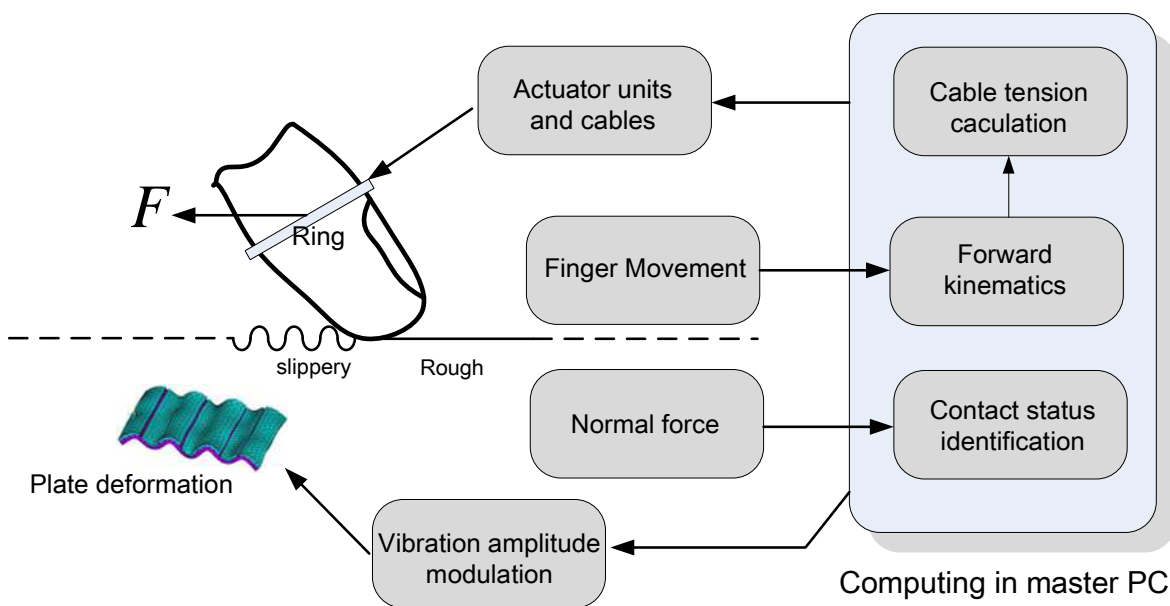


Figure 5.3 Control architecture of the integrated haptic device.

According to Pakkanen et al's research on comparing three designs of haptic

edges, the most preferable edge was simulated with fast, crisp and sharp haptic stimuli [68]. How crisp of a boundary may be defined by the perceived force over a period of time, as dF/dt . In this sense, a step function of stimulus would be perceived as “the most crisp”. Therefore, we use a step function of resistant force to simulate a crisp and stiff boundary. Theoretically, the output of a step function of force requires the rigidity of the force feedback device to be infinite, or it will vibrate. In practice, we found that output a small force did not make our device vibrate. Therefore, the range of output force in this study was limited from 0.3 N to 1.2 N. The maximum output is sufficient to be perceived as a crisp and stiff boundary. Within this range, the force error was less than 5% of the demanded output.

Similarly, the output of the tactile feedback device was also a step increase of friction coefficient for the simulation of a boundary. This was realized by reducing the friction coefficient of the touch surface through activating the squeeze film effect by a 52.2 KHz, 1.6 μm vibration before the user touched the boundary. When the user moved across the boundary, the vibration was stopped immediately restoring actual friction coefficient of the touch surface. The shift between low and high friction coefficient was well used to simulate rectangular grating textures [120].

To obtain a high resolution force feedback, the force feedback device was controlled by a custom-designed controller and amplified by an amplifier. The processor of the controller was a ARM Cortex M3 MCU (STM32F103). The controller communicates with the master PC through Ethernet. The maximum data transmission rate was 100 Mbyte/s. The amplifier could realize accurate control of current with a resolution of 10 mA, causing the force resolution of 0.016N. The large STIMTAC device that we developed in Chapter 4 was used to provide tactile feedback. In the experiments, the update rate for the haptic interaction was 1 KHz.

5.3. Experiment 1: Perception of a boundary simulated by a step function of force feedback.

The objective of the first experiment is to establish the difference thresholds for the stiffness of a boundary simulated solely by a step function of resistant force feedback. The thresholds provide references for the second experiment to evaluate the adding effect of variable friction coefficient on substituting a certain level of force feedback.



Figure 5.4 Experiment setup for both experiments. In the training session of the second experiment, a slider was shown on the computer monitor to represent the normal force. Participants were instructed to maintain the normal force in the green area which indicated the gauge output of 1-1.5 N. The slider was hidden when the experiment started.

5.3.1. Task and stimuli

We employed the method of constant stimuli with a paired-comparison, forced-choice test paradigm to obtain accurate differential thresholds [142]. The task requires participants to discriminate the stiffness of a pair of boundaries. The boundary was simulated solely by a step function of force feedback. Once the

finger moved across the boundary, the user could feel a constant resistant force feedback. On the contrary, there was no force feedback outside the boundary. The boundary was set at the center of the touch surface along the y -axis, as shown in Figure 5.2. In the experiment, the participants were seated in front of a computer screen and a keyboard with the wrist of the dominant arm rested on a comfortable support. They wore the ring of the force feedback device on their index finger of the dominant hand. Participants were asked to move the finger on the touch surface towards to the boundary along the x -axis. They were instructed to ‘tap’ actively on the boundary to perceive its stiffness and retreat their finger as soon as they felt the existence of the boundary. This was designed to avoid vibration of the force feedback device due to the burst output of force. Moreover, tapping was shown to be more precise than pressing in stiffness discrimination task [143].

In each trial, two boundaries were presented in temporal order. They were marked as 1 and 2. One of the stimuli was a standard stimulus while the other was a comparison stimulus. Participants were asked to select the boundary which had a “greater” stiffness by pressing the number key 1 or 2 on a keyboard with their non-dominant hand. They could switch between the two stimuli as many times as they wished and tapped several times on each. As soon as one boundary was selected, a new trial was presented. No feedback was provided to indicate if the selection was correct or not. During the experiment, Over-the-Head earmuffs (3M Peltor Optime 105) were worn by all participants. Training was provided initially so that participants understood the procedure of the experiment, which typically lasted a few minutes. Data collection began when the participant indicated that s/he was ready.

5.3.2.Design

There were three standard force levels: 0.6 N, 0.8 N and 1.0 N. For each standard stimulus, there were eight comparison stimulus values (four higher than the reference and four lower). The standard stimuli and comparison stimulus values are shown in Table 5.1. The step change for the 0.6 N standard force was

8% which was higher than step changes for the other two standard stimuli (5%) because higher discrimination threshold was found for that level of force magnitude [144].

Standard force (N)	Comparison force (N)							
0.6	0.408	0.456	0.504	0.552	0.648	0.696	0.744	0.792
	(-32%)	(-24%)	(-16%)	(-8%)	(+8%)	(+16%)	(+24%)	(+32%)
0.8	0.64	0.68	0.72	0.76	0.84	0.88	0.92	0.96
	(-20%)	(-15%)	(-10%)	(-5%)	(+5%)	(+10%)	(+15%)	(+20%)
1.0	0.8	0.85	0.9	0.95	1.05	1.1	1.15	1.2
	(-20%)	(-15%)	(-10%)	(-5%)	(+5%)	(+10%)	(+15%)	(+20%)

Table 5.1 Experiment 1 comparison stimuli for force levels.

All combinations of standard and comparison stimulus were repeated 15 times, which amounted to 360 (3 standard forces \times 8 comparisons \times 15 repetitions) trials for each participant. The experiment was split to 3 sessions corresponding to the 3 levels of standard stimuli. Each session consisted of 5 blocks of trials. Each block contained 24 (1 standard \times 8 comparisons \times 3 repetitions) trials of comparisons. The three levels of force comparison were counterbalanced across participants with a balanced Latin Square design. The order that the standard stimulus presented to the participants as 1 or 2 was randomized. Breaks were enforced between blocks for avoiding muscular fatigue. A session lasted between 30 to 40 minutes for each participant. The sessions were separated by about one day.

5.3.3. Participants

9 unpaid volunteers (2 females and 7 males) between the ages of 24 and 30 were recruited from the laboratory. All participants were right-handed.

5.3.4. Results and discussion

The JND of each participant at each force level was calculated via methods outlined by Gescheider [142]. These methods converted the recorded proportions of “greater” response to z-scores, and established a linear fit to the data points, solving for the PSE (point of subjective equality), upper and lower JNDs.

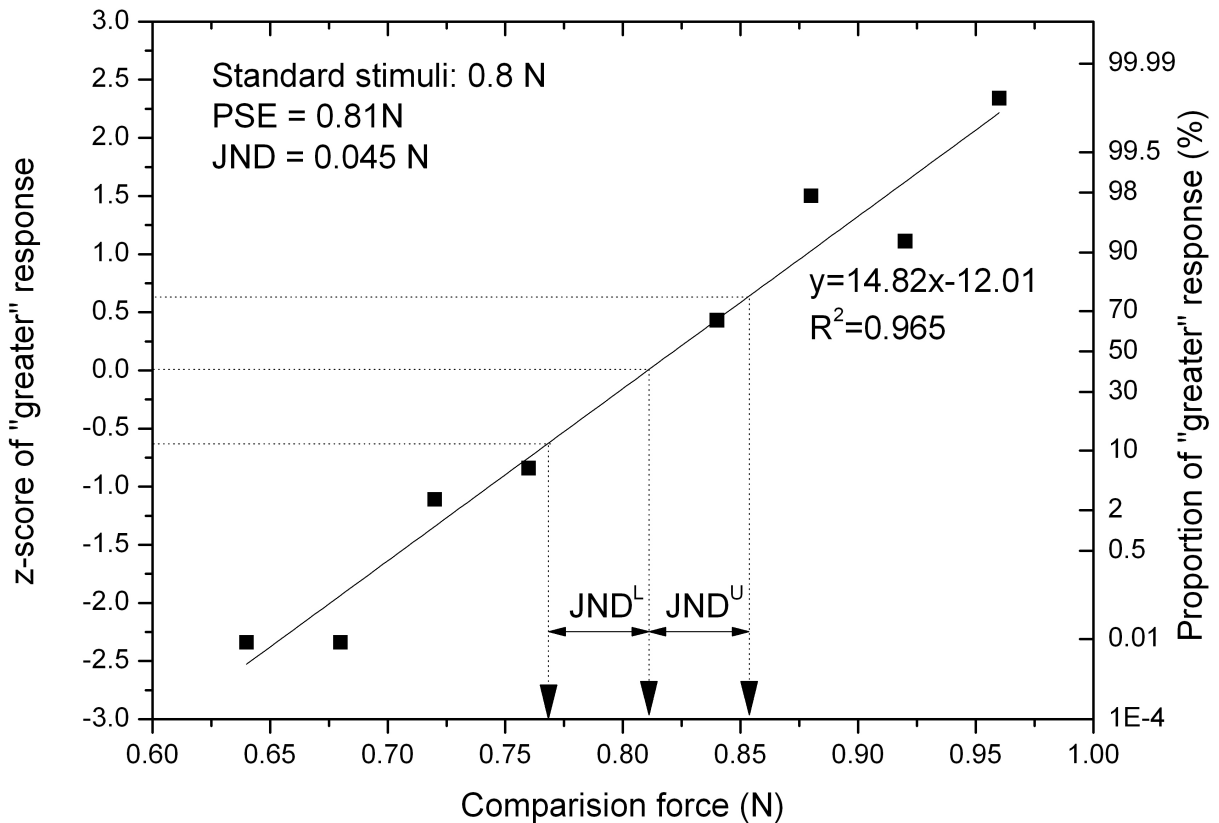


Figure 5.5 Typical response of a participant at the level of 0.8N.

Figure 5.5 shows a typical response of a participant at the level of 0.8 N in the first experiment. The psychometric function in which the proportion of “greater” responses are expressed as z-scores and are fitted as a linear function of the comparison stimuli. The dashed lines mark z-scores of 0.67, 0 and -0.67 correspond to the points where the upper JND, PSE and lower JND are calculated. The average JND of the nine participants are summarized in Table 5.2. The average Weber’s fractions were 10.3%, 6.6%, and 6.4% for 0.6 N, 0.8 N and 1.0 N force levels respectively, as shown in Figure 5.6. An ANOVA test showed that

there was a significant effect of standard force on the Averaged JND % ($F_{2,16} = 19.34, p < 0.001$). Pairwise post-hoc means comparisons showed that the JND% in the 0.6 N level was higher than the other two levels ($p < 0.001$).

Standard Force (N)	Average JND	Standard Deviation	Average JND %
0.6	0.064	0.008	10.3%
0.8	0.053	0.008	6.6%
1.0	0.063	0.012	6.4%

Table 5.2 Average JNDs for the three standard force levels.

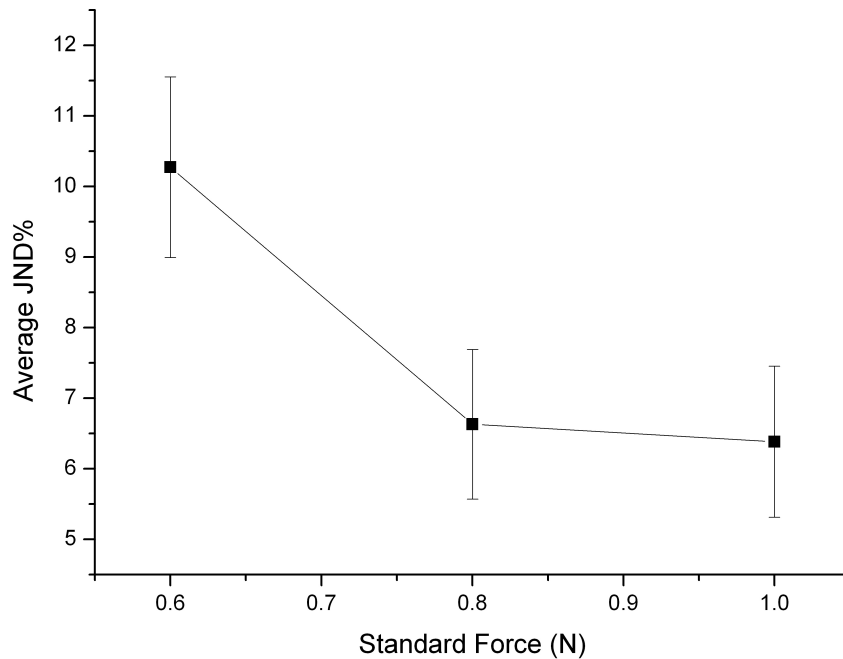


Figure 5.6 Average Weber's fraction for the three standard force levels. Error bars represent 95% confidence interval.

It should be noted that, although we asked participants to compare which boundary was felt stiffer, the boundary was actually simulated by a step function of force. Therefore, the participants were essentially comparing the magnitude of force in the task. In this sense, our results are coincident with previous research. Past studies of haptic signals using a discrimination paradigm have established a

Weber fraction of 5-10% [145] for force magnitude: with lower fraction (7%) [146] for greater force (2.5~10 N) and higher fraction (10%) for smaller force (around 0.5 N) [144].

Pang, Tan and Durlach found that the force magnitude JND% was not affected by squeezing distance and speed [146] when discriminating force magnitude by squeezing. Our result showed that the force magnitude could also be perceived in a short period (by tapping), indicating that the force magnitude perception might not be affected by the time that the force was presented.

5.4. Experiment 2: Perception of a boundary simulated by a coupled haptic feedback.

The second experiment investigated the perception of a boundary simulated by a step function of force feedback and variable friction coefficient. We intended to study if the addition of variable friction coefficient could enable participants to perceive a stiffer boundary as compared with using the force feedback alone.

5.4.1. Experiment details

The task in the second experiment was the same as in the first one. The participants were asked to judge which of the paired stimuli had a greater stiffness. The standard stimuli consisted of tactile inputs based on variable friction coefficient generated by the large STIMTAC combined with force feedback provided by the FingViewer-I force feedback device. In addition to the step increase of resistant force, the participants perceived a step increase of friction coefficient when they moved their index fingers across the boundary. The increase of friction coefficient was realized by reducing the vibration amplitude of the STIMTAC device from 1.6 μm to 0. A schematic of this stimulus is presented in Figure 5.7.

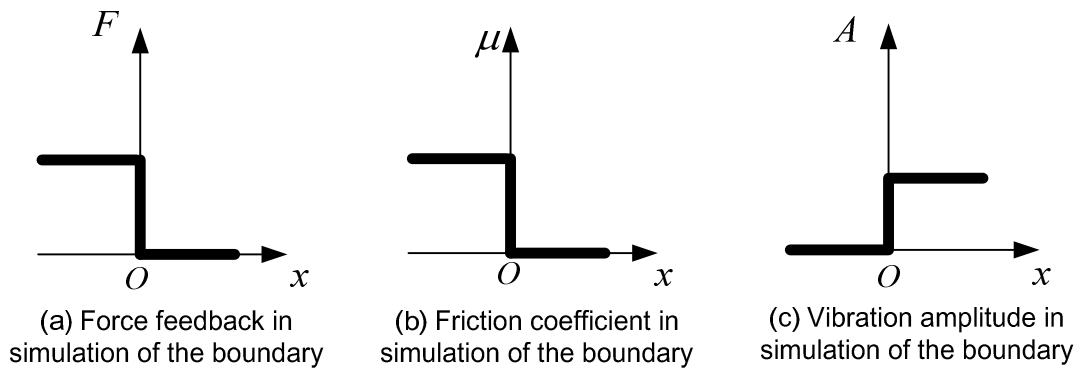


Figure 5.7 Haptic feedback in simulation of a boundary.

Standard stimuli	Comparison stimuli (N)								
0.4 N + T*	0.408	0.456	0.504	0.552	0.6	0.648	0.696	0.744	0.792
	(-32%)	(-24%)	(-16%)	(-8%)		(+8%)	(+16%)	(+24%)	(+32%)
0.6 N + T	0.64	0.68	0.72	0.76	0.8	0.84	0.88	0.92	0.96
	(-20%)	(-15%)	(-10%)	(-5%)		(+5%)	(+10%)	(+15%)	(+20%)
0.8 N + T	0.8	0.85	0.9	0.95	1.0	1.05	1.1	1.15	1.2
	(-20%)	(-15%)	(-10%)	(-5%)		(+5%)	(+10%)	(+15%)	(+20%)

*Tactile feedback: a step increase of friction coefficient. Accordingly, vibration amplitude was reduced from 1.6 μm to 0.

Table 5.3 Experiment 2 comparison stimuli for force levels.

The comparison stimuli were rendered solely by the force feedback device as we described in the first experiment. The effect of variable friction coefficient was quantified by matching the boundary stiffness simulated by a smaller force feedback plus a variable friction coefficient feedback to that simulated by a greater force feedback. Our hypothesis was that a stiff boundary simulated by a small force feedback plus a variable friction coefficient feedback could be perceived as stiff as that rendered by a great force feedback. The force feedback in the standard stimuli was chosen to be 0.2 N smaller than the average force feedback in the comparison stimuli (33.3%, 25% and 20% of the comparison stimuli respectively). The 0.2 N interval was chosen since it was much greater

than the JND we obtained in the first experiment. Moreover, we found that the amount of force that the variable friction coefficient feedback could substitute was approximate to 0.2 N in a pilot test. In this case, the distribution of the comparison stimuli should be symmetric to the standard stimuli. The stimuli in the second experiment are presented in Table 5.3.

Unlike the first experiment, there were 9 comparison stimuli in the second experiment so that the step interval of the comparison stimuli was equal. As a result, the number of trials that each participant conducted was increased to 405 (3 standard forces \times 9 comparisons \times 15 repetitions). In the training session of the second experiment, participants were trained to apply a normal force of 1-1.5 N in the discrimination task to avoid the effect of distributed normal force. A slider was shown on the computer monitor to represent the normal force, as shown in Figure 5.4. Participants were instructed to maintain their normal force in the green area which indicated the gauge output of 1-1.5 N. In the experiment, the slider was hidden so as not to disturb participants' judgment.

Due to the vibration amplitude limitation ($<1.6 \mu\text{m}$) of the large STIMTAC, only a limited number of subjects were able to detect a step increase of friction coefficient as we showed in Chapter 4. A prerequisite of the second experiment was that the participants could perceive the step increase of friction coefficient. Therefore, six participants (2 female, 4 male aged between 24 and 29) who had the capacity took part in the second experiment. All participants were right-handed. They all had taken part in the first experiment. The second experiment was conducted three days after the first experiment. The sessions of the experiment were separated by a day.

5.4.2. Results and discussion

The same methods used to calculate the discriminate threshold in the first experiment were mirrored in the second experiment. The recorded proportions of "greater" response was converted to z-scores and fitted as a linear function of the comparison stimuli to solve for the PSEs and JNDs [142]. Among the six

participants, we found two groups of results. Three of the participants judged the stiffness of the boundaries solely on force feedback. This was indicated by their data that the proportion of “greater” response was 100% in the majority of the comparison pairs. This was due to the fact that the force feedback in the standard stimuli was 2 or 3 JNDs (Table 5.2) smaller than the average comparison stimuli as shown in Table 5.3. By contrast, the other three participants compared the stiffness of the boundary by taking into account both the force feedback and the tactile feedback. Their results were similar to the example showed in Figure 5.5. The proportion of “greater” response increased gradually with the comparison stimuli.

To further confirm the inference, we interviewed the three participants who were assumed to have compared the boundary stiffness only by the magnitude of force feedback. Two of the participants reported that they did not feel the tactile feedback in the experiment and confirmed that they judged the stiffness by force feedback only, as they did in the first experiment. However, these two participants reported that they were able to perceive the tactile simulated boundary when no force feedback was provided before the experiment. We further analyzed the perception sensitivity of the two participants who had also taken part in the step detection experiment as presented in Chapter 4. We found that the two participants needed the large STIMTAC to vibrate at 33.4% and 16.2% higher amplitude respectively than the other participants to detect a friction step simulated by changing the vibration amplitude of the device. This indicated that the tactile sensitivity of these two participants was lower than others. Although the tactile simulated step could be perceived without force feedback, for the two participants, the adding effect of tactile feedback was hidden by force feedback. The other participant who compared the stiffness of boundary by force magnitude confirmed that he could clearly perceive the tactile feedback in the experiment. However, he reported that he could not combine the force feedback at the distal joint with the tactile feedback at the fingertip. Therefore, he decided to compare

the stiffness of the boundary simply by the force magnitude as he did in the first experiment.

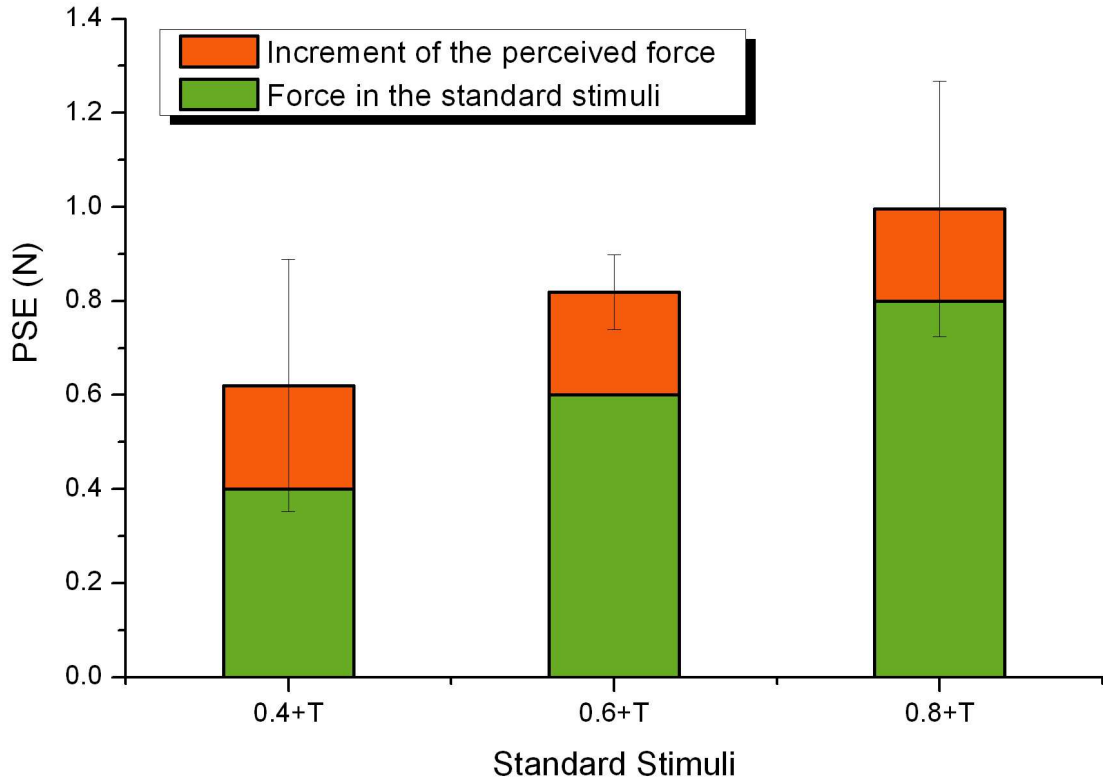


Figure 5.8 The PSEs at the three standard stimuli levels. Error bars represent 95% confidence interval. The force feedback magnitudes in the standard stimuli are also plotted as a reference to indicate the increment of perceived force due to the addition of tactile feedback.

The rest three participants took into account the tactile feedback in combination with force feedback to discriminate the boundary stiffness. Figure 5.8 shows the average PSE obtained for the three participants over the three standard stimuli levels. The PSE indicated how much the comparison stimuli were perceived equal to the standard stimuli. According to Figure 5.8, the additional tactile feedback enhanced the perceived boundary stiffness, making a boundary simulated by a small force perceived as one simulated by a great force. Moreover, an ANOVA test showed that the force feedback in the standard stimuli had no significant effect on the increment of perceived force ($F_{2,4} = 0.07$, $p = 0.93$). The amount of perceived force increment was always greater than the JNDs of the corresponding force feedback in the standard stimuli according to our data obtained in the first experiment. This indicated that the tactile feedback was

distinctively discriminated as a force increment.

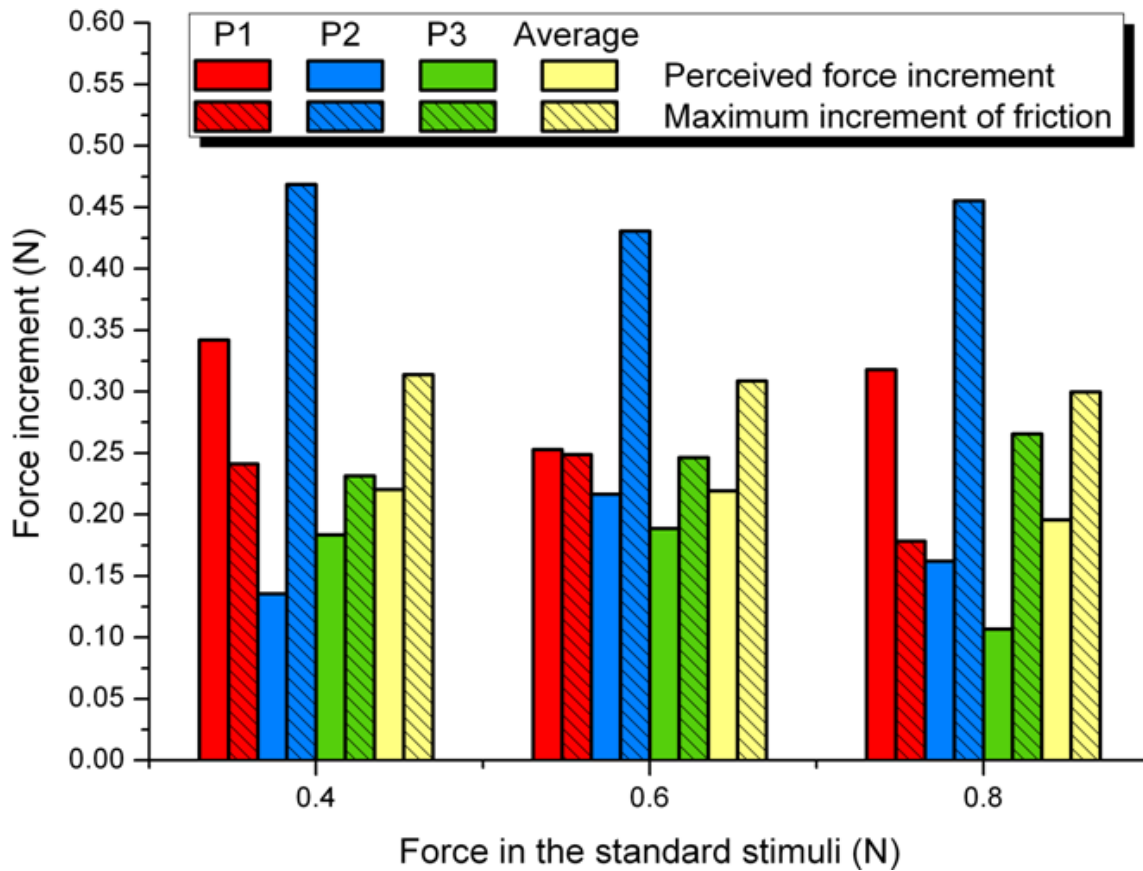


Figure 5.9 The perceived force increment and the maximum increment of friction in the second experiment.

The effect of the tactile feedback was assumed to be an increment of force. The perceived force increment for each participant and the average are presented in Figure 5.9. In addition, the maximum increment of friction caused by increasing the friction coefficient for each participant and the average are also plotted. The maximum friction increment, f , was calculated according to the Coulomb's friction model

$$f = \Delta\mu N$$

where N represents the normal force which was obtained by the force sensors on the large STIMTAC during the experiment. Assuming that the friction coefficient was reduced to zero by the vibration of the STIMTAC, the maximum friction coefficient reduction, $\Delta\mu$, equaled to the dynamic friction coefficient of the touch

surface when the device was static. The dynamic friction coefficients of the three participants were measured on a small plate with the same covering plastic film as the large STIMTAC. The small plate was fixed on an ATI force sensor. The participant was asked to move the index finger back and forth on the plate as they did in the experiment. The average quotient between the lateral force and normal force was recorded as the friction coefficient¹¹. The perceived force increment and the maximum friction coefficient in the experiment are listed in Table 5.4.

	Perceived force increment (N)	Maximum friction increment (N)	Dynamic friction coefficient, μ	Normal force (N)
P1	0.285 (SD=0.032)	0.223 (SD = 0.03)	0.25	0.89 (SD=0.12)
P2	0.189 (SD = 0.027)	0.452 (SD = 0.014)	0.35	1.29 (SD = 0.10)
P3	0.148 (SD=0.041)	0.248 (SD = 0.012)	0.25	0.99 (SD = 0.18)
Average	0.212 (SD = 0.062)	0.307 (SD = 0.096)	–	1.06 (SD = 0. 21)

Table 5.4 Perceived force increment and maximum friction increment in the second experiment. Data are averaged across standard stimuli levels.

In fact, we should measure the lateral force exerted by the participants in the discrimination task to analyze the effect of adding the tactile feedback. However, the large STIMTAC was too big and very heavy (due to the aluminum support) to be mounted on an accurate force sensor (such as the ATI nano 17). Therefore, we only used the maximum increment of friction to roughly evaluate the adding effect of the tactile feedback.

¹¹ Since the friction coefficient was not measured directly on the large tactile device, the result of the friction coefficient in the two experiments may have difference.

As we can infer from Figure 5.9, the perceived force increment was smaller than the maximum friction increment except for P1. The average difference between the perceived force increment and the maximum friction increment was 0.1 N (SD = 0.006 N). In fact, the squeeze film effect could reduce the friction coefficient to a very low level but not to 0. Current published minimum friction coefficient produced by the squeeze film effect was 0.1 [78, 134]. The average normal force in the experiment was 1.06 N (SD = 0.21 N). The difference between the perceived force increment and the maximum friction increment thus may be explained by the difference between the actual friction reduction limit (0.1) and the ideal friction reduction limit (0). In this case, the adding effect of tactile feedback may be explained by the increase of friction caused by the variable friction coefficient. However, this conclusion should be drawn carefully since we did not actual measure the friction increment in the experiment.

5.4.3. Limitations of the current research.

Although we found that the tactile feedback based on varying friction coefficient was able to produce perceivable force increment in combination with a force feedback, there are some points that need further investigation.

Spatial separation of force feedback and tactile feedback.

In the experiment, the force feedback was delivered through the ring which was worn on the distal joints of participants' index fingers, while the tactile feedback was felt through the finger pads. The two feedbacks were spatially separated. As a result, at least one participant reported difficulties in coupling the two feedbacks in the discrimination task. Although previous research showed that the haptic integration with spatial separation could also improve user's perception of boundaries [147, 148] and shapes [23], the effect of spatial distance between the locations where the two feedbacks are applied needs to be further investigated.

The rising time of the step function of haptic feedback.

In our study, the boundary was simulated by a step function of resistant force and an increase of friction coefficient. Thus, the stiffness of the boundary was discriminated by the magnitude of force. This also agrees with Tan et al's finding that the discrimination of stiffness was based on the magnitude of the terminal force [149]. However, the rising time of the step response may also affect the stiffness discrimination. For example, in a softness discrimination task, LaMotte found that the greater the magnitude *and* the rate of compression force produced by tapping against an object with a stylus, the harder the object was perceived [143]. In our experiment, the rising time of the friction coefficient was around 5 ms according to our previous measurement. However, the mean rising time for the force feedback was about 70 ms. Therefore, we cannot draw a conclusion whether the increment of the perceived force is due to the magnitude of friction increment or to the fast response of the tactile feedback.

Levels of friction coefficient.

Only one level of friction coefficient was applied in the experiment due to the capability of the large STIMTAC. The average increment of force due to the increase of friction coefficient was perceived to be 0.2 N with an average normal force of 1 N. Imagine if the friction coefficient could be reduced from 1 to 0.1¹² (as did in [134]), the increment of perceived force would be greater. If this hypothesis holds true, the tactile feedback can be added to enhance the output of force feedback device whose capability is limited. Moreover, since the power consumption of the squeeze film based device is low (as analyzed in Chapter 4), the combination with this type of tactile device would significantly reduce power consumption of a force feedback device which requires great power to drive motors, links etc. However, the increment merit of larger friction variance needs to be

¹² Due to the low friction coefficient of the plastic film we applied, the friction coefficient measured on a small STIMTAC device was 0.2 at static mode and could be reduced to around 0.15 when the vibration amplitude was increased to 1.3 μm . However, No data have been obtained on the large one, though they used the same plastic film.

proved.

5.5. Conclusion

This chapter evaluated the coupling of force feedback and tactile feedback for the simulation of crisp and stiff GUI boundaries. The boundaries were simulated by a step function of resistant force and friction coefficient. In the first experiment, we measured the discriminate threshold of stiffness for force feedback simulated boundaries. The Weber's fraction of the stimuli agrees with previous research on force magnitude perception. In the second experiment, we quantify the effect of variable friction coefficient by adding it with a reduced force feedback and compared the coupled feedback to a greater force feedback. We found that the increase of friction coefficient produced a perceived force increment of 0.2 N. Moreover, this amount of increment may equal to the amount of friction increment caused by the increase of friction coefficient. Therefore, the effect of tactile feedback can be converted to a certainly level of force feedback in order to enhance the lateral force feedback. This result can help us to quantify the design of coupled force feedback and tactile feedback in simulating boundaries.

This result indicated that the combination of programmable friction feedback and force feedback was based on the perception of lateral force

Conclusion

This thesis presents an integrated haptic interface designed for enhancing interactions with touch screens. The device is composed of a cable-driven force feedback device and a squeeze-film effect based tactile device. The chapters of this dissertation cover the design and evaluation of each component device and also the effects of coupling force feedback and tactile feedback on enhancing touch screen GUI elements.

In the second chapter, we review research on adding haptic feedback to touch interactions. The physiology of human touch sensation has been summarized at first, including how touch sensation is categorized and perceived. According to the survey, we show that both force feedback and tactile feedback are necessary for user's interaction with touch screens. Then, previous research on adding haptic interfaces to indirect interactions with GUIs and adding tactile feedback to direct touch interactions are introduced. The features, applications and effects of each haptic interface are summarized. The review shows that tactile feedback has been widely added in touch interaction but little research has incorporated force feedback at the same time; how to incorporate the integrated haptic feedback with touch interaction needs to be investigated.

In Chapter 3, we present the design of the cable-driven force feedback device. The device is used to provide force feedback to user's fingers. The cable-driven force feedback device is applied due to its low inertia, simple structure and most importantly, transparent and scalable workspace. The device is based on a reconfigurable mechanism which can provide force feedback to either a single finger or two fingers. In this case, we can add force feedback to single-touch or multi-touch interactions. Then, the kinematics and cable tension control of the

device are presented to illustrate how the device works. Finally, two experiments are conducted to evaluate the force feedback device. The first experiment evaluates the single-touch interaction with a button simulation task. A button-click feedback is simulated and compared with a physical button. Then, in the second experiment, we evaluate the multi-touch force feedback in a knob control experiment. Experimental results show that the device is capable to produce the force feedback required in the tasks.

In Chapter 4, we demonstrate the design of the large area tactile feedback device which is based on the squeeze air film effect to reduce the friction coefficient of the touch surface. A key issue in enlarging the workspace of the device is to minimize its power consumption. Therefore, in this chapter, the power consumption of the tactile device has been analyzed and modeled. The model shows that, when vibration amplitude is constant, the power consumption is not related to the number of piezoelectric actuators but related to their layouts. The optimal layout is to place the piezoelectric actuators far away from each other, e.g., at the four corners of the resonator. According to this result, a large area tactile plate (198mm × 138mm) has been designed with only eight piezoelectric actuators. The device needs only 1.3 W@32 V_{rms} to provide a distinct friction reduction with the vibration amplitude above 1 μm. Moreover, the power consumption is well estimated by the analytical model with an average error of less than 10%. Two psychophysics experiments have also been conducted to evaluate the tactile feedback capability of the device. According to the experimental results, producing a detectable reduction of friction requires the vibration amplitude to be 0.64 μm at least. This can be achieved by the new device.

Chapter 5 focuses on the evaluation of the integrated haptic device. Two psychophysics experiments are conducted to investigate the merit of applying simultaneous force feedback and tactile feedback to the simulation of a crisp and stiff boundary. The boundaries were simulated by step functions of resistant force and friction coefficient. In the first experiment, we measured the discriminate threshold of stiffness for force feedback simulated boundaries. The Weber's

fraction of the stimuli follows previous research for force magnitude perception (5%-10%). In the second experiment, we quantified the effect of variable friction coefficient by adding it with a reduced force feedback and compared this combination with a greater force feedback. Experimental result shows that using a small amount of force feedback plus a tactile feedback can simulate a boundary which feels as stiff as the one simulated by a large force feedback. Moreover, the perceived force increment may equal to the amount of friction increment due to the increase of friction coefficient. This result shows that the combination of programmable friction feedback and force feedback is based on the perception of lateral force. Thus, the integrated haptic device can take advantage of this effect to broaden the output and produce more expressive haptic effect than using a single type haptic device.

Future work

In the current research, the integrated haptic interface is only used to enhance the simulation of a boundary, which is a basic element of GUI widgets. The coupled haptic feedback can also be applied to enhance other elements. For example, a main problem of touch screen is that it does not support eye-free interactions. When using a conventional handheld device, such as a music player, a user can select the track of songs, pause or play the music and change the volume without looking at the display screen (some do not even have screens). Users do not have to take the device out of their pockets since the haptic feedback of the buttons provides sufficient clues for them to make operations. On the contrary, users have to look at the touch screen if there is no physical buttons on the device. The haptic feedback on a button includes the feeling of its boundary, shape and the button-click feedback. All these requirements may be achieved by our device: simulating boundaries with coupled haptic feedback (soft or stiff), simulating button shape (concave or convex) by modulating lateral force [104, 105], and providing button-click feedback through a pulse of lateral force feedback as presented in Chapter 3. Moreover, the large STIMTAC device is able to

simulate various textures [120]. The textures can be used to distinguish home keys from others. In this way, the combination of haptic simulated textures, shapes and boundaries can be used to create distinguishable buttons on touch screens. The effect of haptic enhanced buttons on users' performance is worth investigating.

The objective of this research is to develop a haptic interface to incorporate with touch interaction. Currently, the large STIMTAC is not yet transparent due to the use of an aluminum resonator. The aluminum resonator is used for its ease of manufacturing. We have also developed small STIMTAC devices that are compatible with capacitive touch screens [116]. Therefore, it is possible to modify an off-the-shelf touch screen to develop a haptic touch screen. Moreover, the friction coefficient variation range of the large STIMTAC is limited in the research. One possible solution to extend the range is to further reduce the power consumption through an optimization based on our power modeling. Then, the vibration amplitude of the large STIMTAC will be increased at the same supply voltage. In that way, levels of friction reduction produced by the device will also increase and more interesting tactile patterns may be generated. Finally, we can investigate more levels of friction substitution in the second experiment presented in Chapter 5 to broaden the output capability of the integrated device.

During the development and evaluation of the large STIMTAC device, we noticed that the vibration amplitude might also be damped by finger press on the device. We have conducted some preliminary tests on this factor. Currently, we found that the damping was not only affected by the normal force on the tactile plate but also by the skin properties and the posture to press on the device. Moreover, the damping was not significant when many piezoceramics were glued to activate the small STIMTAC device. We have proposed a close-loop control method to compensate the finger damping by applying higher voltage. Although this method is promising, more work is needed to implement and evaluate the method.

Another problem we met was the long attenuation time of the large STIMTAC

device. Ideally, the attenuation of the vibration is instant. Namely, when the supply voltage was shut off, the vibration amplitude should stop immediately. However, the problem of the large tactile plate is that the attenuation speed is slow. For example, the attenuation time for the 2 mm-thick-4-actuator large tactile plate (in Figure 4.12) was 7.9 ms. As a result, in the simulation of a step by shifting vibration amplitude, users felt that the step was smooth rather than sharp. To solve this problem, we proposed a “brake” method to stop the vibration: when the activating voltage was stopped, we applied a reverse voltage to the tactile plate for a short period of time. The reverse voltage could effectively stop the vibration in about 5 ms. When the vibration stopped in this period, users would feel a sharp step (boundary). However, we still do not know how the attenuation speed affects users’ perception of roughness and how long is the maximum attenuation time to create effective friction shift. This question needs to be answered before the design of a large tactile plate with a few pieces of piezoelectric actuators.

Glossary

\mathbf{A}	static Jacobian matrix
d	distance between the cable connections
d_0	original length of the spring
k_s	spring constant
\mathbf{F}_w	manipulation force
\mathbf{F}_G	grasp force
F_s	magnitude of the spring tension
\mathbf{T}	manipulation torque
\mathbf{t}_i	tension vector on the i^{th} cable
\mathbf{t}_{Gi}	cable tension to balance the grasp force
\mathbf{t}_{Si}	cable tension to balance the spring tension
\mathbf{t}_{Wi}	cable tension to balance the wrench
t_{\min}	magnitude of the minimum cable tension
\mathcal{S}^w	the wrench of the grasped object
φ	orientation angle
A	vibration amplitude
E_3	electric field in the z-direction
l_0	finger length in contact with the device
n_c	number of powered piezoceramic plates
p_0	atmospheric pressure

Q	dynamic amplification factor
S_x	strain of a fiber parallel to the x axis
T_1	stress of the piezoceramic plate in the x -direction
V	applied voltage
w	deflection
Y	admittance
σ	squeeze number
η	air viscosity
ω_0	frequency of vibration
$1/\rho$	inverse of the radius of curvature
θ'	phase delay of the strain when an applied electric field is applied

Reference

- [1] M. Levin and A. Woo, "Tactile-feedback solutions for an enhanced user experience," *Information Display*, vol. 25, pp. 18-21, 2009.
- [2] B. Banter, "Touch screens and touch surfaces are enriched by haptic force-feedback," *Information Display*, vol. 26, pp. 26-30, 2010.
- [3] S. Brewster, F. Chohan and L. Brown, "Tactile feedback for mobile interactions," San Jose, CA, United states, 2007, pp. 159-162.
- [4] S. Lee and S. Zhai, "The performance of touch screen soft buttons," in *Proceedings of the SIGCHI Conference on Human Factors in Computing Systems*, Boston, MA, USA, 2009, pp. 309-318.
- [5] R. W. Lindeman, J. N. Templeman, J. L. Sibert, and J. R. Cutler, "Handling of Virtual Contact in Immersive Virtual Environments: Beyond Visuals," *Virtual Reality*, vol. 6, pp. 130-139, 2002.
- [6]<http://www.fastcompany.com/1684713/apples-netbook-killer-most-appealing-as-a-netbook>
- [7] <http://ipad.tgbus.com/zt/ipad-cs/design.shtml>
- [8] <http://labs.teague.com/2010/04/20/physical-touchscreen-knobs>
- [9] M. Fukumoto and T. Sugimura, "Active click: tactile feedback for touch panels," in *Proceedings of the SIGCHI Conference on Human Factors in Computing Systems*, 2001, pp. 121-122.
- [10] I. Poupyrev, S. Maruyama and J. Rekimoto, "Ambient touch: designing tactile interfaces for handheld devices," in *Proceedings of the 15th annual ACM symposium on User interface software and technology*, Paris, France, 2002, pp. 51-60.
- [11] S. A. Brewster and A. King, "The design and evaluation of a vibrotactile progress bar," in *Proceedings of the World Haptics 2005*, 2005, pp. 499- 500.

-
- [12] R. Leung, K. MacLean, M. B. Bertelsen, and M. Saubhasik, "Evaluation of haptically augmented touchscreen gui elements under cognitive load," in *Proceedings of the 9th international conference on Multimodal interfaces*, Nagoya, Aichi, Japan, 2007, pp. 374-381.
- [13] C. Forlines and R. Balakrishnan, "Evaluating tactile feedback and direct vs. indirect stylus input in pointing and crossing selection tasks," in *Proceeding of the twenty-sixth annual SIGCHI conference on Human factors in computing systems*, Florence, Italy, 2008, pp. 1563-1572.
- [14] E. Hoggan, S. A. Brewster and J. Johnston, "Investigating the effectiveness of tactile feedback for mobile touchscreens," in *Proceeding of the twenty-sixth annual SIGCHI conference on Human factors in computing systems*, Florence, Italy, 2008, pp. 1573-1582.
- [15] V. Levesque, L. Oram, K. MacLean, A. Cockburn, N. D. Marchuk, D. Johnson, J. E. Colgate, and M. A. Peshkin, "Enhancing physicality in touch interaction with programmable friction," in *Proceedings of the 2011 annual conference on Human factors in computing systems*, Vancouver, BC, Canada, 2011, pp. 2481-2490.
- [16] H. Chen, J. Park, S. Dai, and H. Z. Tan, "Design and Evaluation of Identifiable Key-Click Signals for Mobile Devices," *IEEE Transactions on Haptics*, vol. 4, pp. 229 -241, 2011.
- [17] S. P. Parikh and J. M. Esposito, "Negative Feedback for Small Capacitive Touchscreen Interfaces: A Usability Study for Data Entry Tasks," *IEEE Transactions on Haptics*, vol. 5, pp. 39-47, 2012-01-01 2012.
- [18] K. Yatani and K. N. Truong, "SemFeel: a user interface with semantic tactile feedback for mobile touch-screen devices," in *Proceedings of the 22nd annual ACM symposium on User interface software and technology*, Victoria, BC, Canada, 2009, pp. 111-120.
- [19] Y. Ikei and M. Shiratori, "TextureExplorer: a tactile and force display for virtual textures," in *Proceedings of Haptics Symposium 2002*, pp. 327-334.
- [20] D. K. A. G. Ki-Uk Kyung, "A Novel Interactive Mouse System for Holistic Haptic Display in a Human-Computer Interface," *International Journal of*

Human Computer Interaction, 20(3), 247–270, 2006.

[21] C. R. Wagner, D. P. Perrin, R. L. Feller, R. D. Howe, O. Clatz, H. Delingette, and N. Ayache, "Integrating Tactile and Force Feedback with Finite Element Models," in *Proceedings of the 2005 IEEE International Conference on Robotics and Automation*, 2005, pp. 3942-3947.

[22] W. R. Provancher and N. D. Sylvester, "Fingerpad Skin Stretch Increases the Perception of Virtual Friction," *IEEE Transactions on Haptics*, vol. 2, pp. 212-223, 2009.

[23] A. Frisoli, M. Solazzi, F. Salsedo, and M. Bergamasco, "A Fingertip Haptic Display for Improving Curvature Discrimination," *Presence: Teleoperators & Virtual Environments*, vol. 17, pp. 550-561, 2008.

[24] Z. Tao, F. Giraud, B. Lemaire-Semail, and M. Amberg, "Haptic perception of curvature through active touch," in *World Haptics Conference (WHC), 2011 IEEE*, 2011, pp. 533-538.

[25] M. Biet, F. Giraud and B. Lemaire-Semail, "Squeeze film effect for the design of an ultrasonic tactile plate," *IEEE Transactions on Ultrasonics, Ferroelectrics and Frequency Control*, vol. 54, pp. 2678-2688, 2007.

[26] K. J. Kuchenbecker, "Characterizing and controlling the high-frequency dynamics of haptic interfaces," Ph.D thesis, Stanford University, 2006.

[27] ISO: Ergonomics of human-computer interaction—Part910: Framework for tactile and haptic interaction.

[28] E. E. Hoggan, "Crossmodal audio and tactile interaction with mobile touchscreens". Ph.D. thesis, University of Glasgow, 2010.

[29] U. Proske and S. Gandevia, "The kinaesthetic senses," *The Journal of Physiology*, vol. 587, pp. 4139-4146, 2009.

[30] V. G. Chouvardas, A. N. Miliou and M. K. Hatalis, "Tactile displays: Overview and recent advances," *Displays*, vol. 29, pp. 185-194, 2008.

[31] K. Yatani, "Spatial Tactile Feedback Support for Mobile Touch-screen Devices," Ph.D thesis, University of Toronto, 2011.

[32] R. S. Johansson, "Receptive field sensitivity profile of mechanosensitive units

innervating the glabrous skin of the human hand," *Brain Res*, vol. 104, pp. 330-334, 1976.

[33] Kandel, E. R. and Jessell, T. M., "Touch," in *Principles of Neural Science*. Eds. E. R. Kandel, J. H. Schwartz, and T. M. Jessell. New York: Oxford University Press, 1991, pp. 349 - 414.

[34] K. Hinckley, "Input technologies and techniques," in *The human-computer interaction handbook*, J. A. Jacko and A. Sears, Eds.: L. Erlbaum Associates Inc., 2003, pp. 151-168.

[35] L. Rosenberg and S. Brave, "Using force feedback to enhance human performance in graphical user interfaces," in *Conference companion on Human factors in computing systems: common ground*, Vancouver, British Columbia, Canada, 1996, pp. 291-292.

[36] I. Oakley, M. R. McGee, S. Brewster, and P. Gray, "Putting the feel in "look and feel"," in *Proceedings of the SIGCHI conference on Human factors in computing systems*, The Hague, The Netherlands, 2000, pp. 415-422.

[37] I. Oakley, S. Brewster and P. Gray, "Solving multi-target haptic problems in menu interaction," in *CHI '01 extended abstracts on Human factors in computing systems*, Seattle, Washington, 2001, pp. 357-358.

[38] I. O. Alison, A. Adams, S. Brewster, and P. Gray, "Guidelines for the Design of Haptic Widgets," In *Proceedings of British HCI 2002*, 2002, pp. 195--212.

[39] J. T. Dennerlein, D. B. Martin and C. Hasser, "Force-feedback improves performance for steering and combined steering-targeting tasks," in *Proceedings of the SIGCHI conference on Human factors in computing systems*, The Hague, The Netherlands, 2000, pp. 423-429.

[40] J. T. Dennerlein and M. C. Yang, "Haptic Force-Feedback Devices for the Office Computer: Performance and Musculoskeletal Loading Issues," *Human Factors: The Journal of the Human Factors and Ergonomics Society*, vol. 43, pp. 278 -286, 2001-01-01 2001.

[41] T. N. Smyth and A. E. Kirkpatrick, "A new approach to haptic augmentation of the GUI," in *Proceedings of the 8th international conference on Multimodal*

interfaces, Banff, Alberta, Canada, 2006, pp. 372-379.

[42] L. Vanacken, J. De Boeck and K. Coninx, "Force Feedback Magnitude Effects on User's Performance during Target Acquisition: A Pilot Study," in *Proceedings of INTERACT 2009*, pp. 5-8, 2009.

[43] J. De Boeck, L. Vanacken and K. Coninx, "Target Acquisition with Force Feedback: The Effect of Different Forces on the User's Performance," in *Lecture Notes in Computer Science*, 2009, pp. 11-20.

[44] C. Jay and R. Hubbard, "Delayed visual and haptic feedback in a reciprocal tapping task," in *Proceedings of World Haptics 2005*, 2005, pp. 655- 656.

[45] C. S. Campbell, S. Zhai, K. W. May, and P. P. Maglio, "What You Feel Must Be What You See: Adding Tactile Feedback to the Trackpoint," In *Proc. of INTERACT'99*, 1999, pp. 383--390.

[46] A. Cockburn and S. Brewster, "Multimodal feedback for the acquisition of small targets," *Ergonomics*, vol. 48, pp. 1129-1150, 2005.

[47] J. Pasquero and V. Hayward, "Tactile feedback can assist vision during mobile interactions," in *Proceedings of the 2011 annual conference on Human factors in computing systems*, Vancouver, BC, Canada, 2011, pp. 3277-3280.

[48] M. Akamatsu, I. S. Mackenzie and T. Hasbroucq, "A comparison of tactile, auditory, and visual feedback in a pointing task using a mouse-type device," *Ergonomics*, vol. 38, pp. 816-827, 1995.

[49] . Akamatsu and I. S. MacKenzie, "Movement characteristics using a mouse with tactile and force feedback," *International Journal of Human-Computer Studies*, vol. 45, pp. 483-493, 1996.

[50] K. Dong-Soo, Y. Tae-Heon and C. JoonYeon, "Trend & prospects of haptic technology in mobile devices," in *Proceedings of the IEEE International Symposium on Industrial Electronics (ISIE)*, 2010, pp. 3778-3783.

[51]" Touchsense Tactile Feedback Overview", Immersion Corporation.
<http://www.immersion.com/products/touchsense-tactile-feedback/index.html>

[52] T. Pakkanen, R. Raisamo, K. Salminen, and V. Surakka, "Haptic numbers: three haptic representation models for numbers on a touch screen phone," in

International Conference on Multimodal Interfaces and the Workshop on Machine Learning for Multimodal Interaction, Beijing, China, 2010, pp. 1-4.

[53] K. Ki-Uk, Y. L. Jun and P. Jun-Seok, "Pen-like Haptic Interface and Its Application on Touch Screen," in *Proceedings of The 16th IEEE International Symposium on Robot and Human interactive Communication*, 2007, pp. 9-13.

[54] M. Sun, X. Ren and X. Cao, "Effects of Multimodal Error Feedback on Human Performance in Steering Tasks," *Information and Media Technologies*, vol. 6, pp. 193-201, 2011.

[55] G. Park, S. Choi, K. Hwang, S. Kim, J. Sa, and M. Joung, "Tactile effect design and evaluation for virtual buttons on a mobile device touchscreen," in *Proceedings of the 13th International Conference on Human Computer Interaction with Mobile Devices and Services*, Stockholm, Sweden, 2011, pp. 11-20.

[56] R. Hendrik, E. Ronald, C. Deisler, and A. Butz, "HapTouch and the 2+1 State Model: Potentials of Haptic Feedback on Touch Based In-Vehicle Information Systems," in *Proceedings of the 1st international Conference on Automotive User interfaces and interactive Vehicular Applications (AutomotiveUI '10)*. ACM, November 11-12, 2010, Pittsburgh, Pennsylvania, 2010.

[57] S. Brewster and L. Brown, "Tactons: structured tactile messages for non-visual information display," in *Proceedings of the 5th Australasian User Interface Conference (AUIC2004)*, Dunedin, 2004, pp. 15-23.

[58] L. M. Brown, S. A. Brewster and H. C. Purchase, "A First Investigation into the Effectiveness of Tactons," in *Proceedings of the First Joint Eurohaptics Conference and Symposium on Haptic Interfaces for Virtual Environment and Teleoperator Systems*, 2005, pp. 167-176.

[59] L. M. Brown, S. A. Brewster and H. C. Purchase, "Multidimensional tactons for non-visual information presentation in mobile devices," in *Proceedings of the 8th conference on Human-computer interaction with mobile devices and services*, Helsinki, Finland, 2006, pp. 231-238.

[60] E. Hoggan, S. Anwar and S. A. Brewster, "Mobile multi-actuator tactile

displays," in *Proceedings of the 2nd international conference on Haptic and audio interaction design*, Seoul, South Korea, 2007, pp. 22-33.

[61] Y. Tae-Heon, K. Sang-Youn, H. K. Chong, K. Dong-Soo, and W. J. Book, "Development of a miniature pin-array tactile module using elastic and electromagnetic force for mobile devices," in *Proceedings of the World Haptics 2009*, 2009, pp. 13-17.

[62] K. Seung-Chan, Y. Tae-Hon, H. Byung-Kil, and K. Dong-Soo, "Interaction with a display panel - An evaluation of surface-transmitted haptic feedback," in *Proceedings of the International Conference on Control, Automation and Systems*, 2008, pp. 278-283.

[63] J. C. Lee, P. H. Dietz, D. Leigh, W. S. Yerazunis, and S. E. Hudson, "Haptic pen: a tactile feedback stylus for touch screens," in *Proceedings of the 17th annual ACM symposium on User interface software and technology*, Santa Fe, NM, USA, 2004, pp. 291-294.

[64] T. Kaaresoja, "Snap-Crackle-Pop: Tactile Feedback for Mobile Touch Screens," in *Proceedings of Eurohaptics 2006*, 2006, pp. 565--566.

[65] P. Laitinen and J. Mawnpaa, "Enabling mobile haptic design: piezoelectric actuator technology properties in hand held devices," in *Proceedings of the IEEE International Workshop on Haptic Audio Visual Environments and their Applications*, 2006, pp. 40-43.

[66] I. Poupyrev, M. Okabe and S. Maruyama, "Haptic feedback for pen computing: directions and strategies," in *Proceedings of the CHI '04 extended abstracts on Human factors in computing systems*, Vienna, Austria, 2004, pp. 1309-1312.

[67] I. Poupyrev and S. Maruyama, "Tactile interfaces for small touch screens," in *Proceedings of the 16th annual ACM symposium on User interface software and technology*, Vancouver, Canada, 2003, pp. 217-220.

[68] T. Pakkanen, R. Raisamo, J. Raisamo, K. Salminen, and V. Surakka, "Comparison of three designs for haptic button edges on touchscreens," in *Proceedings of the Haptics Symposium*, 2010, pp. 219-225.

[69] J. Rantala, R. Raisamo, J. Lylykangas, V. Surakka, J. Raisamo, K. Salminen,

T. Pakkanen, and A. Hippula, "Methods for Presenting Braille Characters on a Mobile Device with a Touchscreen and Tactile Feedback," *IEEE Transactions on Haptics*, vol. 2, pp. 28-39, 2009.

[70] E. Hoggan, T. Kaaresoja, P. Laitinen, and S. Brewster, "Crossmodal congruence: the look, feel and sound of touchscreen widgets," in *Proceedings of the 10th international conference on Multimodal interfaces*, Chania, Crete, Greece, 2008, pp. 157-164.

[71] E. Koskinen, T. Kaaresoja and P. Laitinen, "Feel-good touch: finding the most pleasant tactile feedback for a mobile touch screen button," in *Proceedings of the 10th international conference on Multimodal interfaces*, Chania, Crete, Greece, 2008, pp. 297-304.

[72] K. Ki-Uk, L. Jun-Young and M. A. Srinivasan, "Precise manipulation of GUI on a touch screen with haptic cues," in *Proceedings of the World Haptics 2009*, 2009, pp. 202-207.

[73] H. Shin, J. Lim, J. Lee, K. Kyung, and G. Lee, "Tactile feedback for button GUI on touch devices," in *CHI '12 Extended Abstracts on Human Factors in Computing Systems*, Austin, Texas, USA, 2012, pp. 2633-2636.

[74] C. Harrison and S. E. Hudson, "Providing dynamically changeable physical buttons on a visual display," in *Proceedings of the 27th international conference on Human factors in computing systems*, Boston, MA, USA, 2009, pp. 299-308.

[75] "Tactus," <http://www.tactustechnology.com/index.html>.

[76] K. Sang-Ho, K. Sekiyama, T. Fukuda, K. Tanaka, and K. Itoigawa, "Development of Dynamically Re-formable Input Device in Tactile and Visual Interaction," in *Proceedings of the International Symposium on Micro-NanoMechatronics and Human Science, 2007*. 2007, pp. 544-549.

[77] T. Watanabe and S. Fukui, "A method for controlling tactile sensation of surface roughness using ultrasonic vibration," in *Proceedings of the IEEE International Conference on Robotics and Automation*, 1995, pp. 1134-1139 vol.1.

[78] L. Winfield, J. Glassmire, J. E. Colgate, and M. Peshkin, "T-PaD: Tactile Pattern Display through Variable Friction Reduction," in *Proceedings of the*

World Haptics 2007. 2007, pp. 421-426.

[79] V. Lévesque, L. Oram, K. E. MacLean, A. Cockburn, N. D. Marchuk, D. Johnson, J. E. Colgate, and M. A. Peshkin, "Enhancing physicality in touch interaction with programmable friction.," in *Proceedings of the 2011 annual conference on Human factors in computing systems*, Vancouver, BC, Canada, 2011, pp. 2481-2490.

[80] G. R. Casiez, N. Roussel, R. Vanbelleghem, Fr, D, and R. Giraud, "Surfpad: riding towards targets on a squeeze film effect," in *Proceedings of the 2011 annual conference on Human factors in computing systems*, Vancouver, BC, Canada, 2011, pp. 2491-2500.

[81] H. Ji, I. Oakley, J. Kang, and J. Ryu, "Exploring the perceptual space of a novel slip-stick haptic surface display," in *CHI '12 Extended Abstracts on Human Factors in Computing Systems*, Austin, Texas, USA, 2012, pp. 2231-2236.

[82] H. Kotani, M. Takasaki and T. Mizuno, "Surface Acoustic Wave Tactile Display using a Large Size Glass Transducer," in *Proceedings of the International Conference on Mechatronics and Automation, 2007*. 2007, pp. 198-203.

[83] O. Bau, I. Poupyrev, A. Israr, and C. Harrison, "TeslaTouch: electrovibration for touch surfaces," in *Proceedings of the 23rd annual ACM symposium on User interface software and technology*, New York, New York, USA, 2010, pp. 283-292.

[84] O. Bau and I. Poupyrev, "REVEL: tactile feedback technology for augmented reality," *ACM Trans. Graph.*, vol. 31, pp. 1-11, 2012.

[85] G. Wintergerst, R. Jagodzinski, F. Hemmert, A. Müller, and G. Joost, "Reflective Haptics: Enhancing Stylus-Based Interactions on Touch Screens," in *Haptics: Generating and Perceiving Tangible Sensations*, 2010, p. 360.

[86] D. Xiaowei, J. E. Colgate and M. A. Peshkin, "LateralPaD: A surface-haptic device that produces lateral forces on a bare finger," in *Proceedings of the Haptics Symposium (HAPTICS), 2012 IEEE*, 2012, pp. 7-14.

[87] J. J. Kaye, "Sawtooth planar waves for haptic feedback," in *Adjunct proceedings of the 25th annual ACM symposium on User interface software and technology*, Cambridge, Massachusetts, USA, 2012, pp. 5-6.

-
- [88] Y. Jansen, T. Karrer and J. Borchers, "MudPad: localized tactile feedback on touch surfaces," in *Adjunct proceedings of the 23rd annual ACM symposium on User interface software and technology*, New York, New York, USA, 2010, pp. 385-386.
- [89] J. Alexander, M. T. Marshall and S. Subramanian, "Adding haptic feedback to mobile tv," in *Proceedings of the 2011 annual conference extended abstracts on Human factors in computing systems*, Vancouver, BC, Canada, 2011, pp. 1975-1980.
- [90] M. Weiss, C. Wacharamanotham, S. Voelker, and J. Borchers, "FingerFlux: near-surface haptic feedback on tabletops," in *Proceedings of the 24th annual ACM symposium on User interface software and technology*, Santa Barbara, California, USA, 2011, pp. 615-620.
- [91] M. E. Altinsoy and S. Merchel, "Electrotactile Feedback for Handheld Devices with Touch Screen and Simulation of Roughness," *IEEE Transactions on Haptics*, vol. 5, pp. 6-13, 2012.
- [92] Massie, T.H., Salisbury, J.K, "The phantom haptic interface: A device for probing virtual objects, "In *Proceedings of the ASME Winter Annual Meeting, Symposium on Haptic Interfaces for Virtual Environment and Teleoperator Systems* (1994)
- [93] S. Kim, M. Ishii, Y. Koike, and M. Sato, "Development of tension based haptic interface and possibility of its application to virtual reality," in *Proceedings of the ACM symposium on Virtual reality software and technology*, Seoul, Korea, 2000, pp. 199-205.
- [94] M. Sato, M. Isshiki, L. Lin, and A. Katsuhito, "Spidar-mouse: A Design of Open Source Interface for SPIDAR," in *IEICE Tech. Rep.*, 2009.
- [95] C. Bonivento, A. Eusebi, C. Melchiorri, M. Montanari, and G. Vassura, "WireMan: a portable wire manipulator for touch-rendering of bas-relief virtual surfaces," in *Proceedings of the 8th International Conference on Advanced Robotics*, 1997, pp. 13-18.
- [96] C. Gosselin, R. Poulin and D. Laurendeau, "A planar parallel 3-dof

cable-driven haptic interface," in *Proceedings of the 12th World Multi-Conference on Systemics, Cybernetics and Informatics: WM-SCI '08*, Orlando, Florida, USA, 2008, pp. 266-271.

[97] G. Rosati, D. Zanotto and A. Rossi, "Performance Assessment of a 3D Cable-Driven Haptic Device," in *Proceedings of the ASME 2008 ASME International Mechanical Engineering Congress and Exposition*, pp. 597-606, 2008.

[98] R. LINDEMANN and D. TESAR, "Construction and demonstration of a 9-string 6 DOF force reflecting joystick for telerobotics," in *Proceedings of the NASA Conference on Space Telerobotics*, Vol. 4, pp. 55-63, 1989.

[99] Y. Hirata and M. Sato, "3-dimensional Interface Device For Virtual Work Space," in *Proceedings of the IEEE/RSJ International Conference on Intelligent Robots and Systems*, 1992, pp. 889-896.

[100] M. Ishii and M. Sato, "A 3D interface device with force feedback: a virtual work space for pick-and-place tasks," in *Proceedings of the IEEE Virtual Reality Annual International Symposium*, 1993, pp. 331-335.

[101] S. Walairacht, K. Yamada, S. Hasegawa, Y. Koike, and M. Sato, "4 + 4 fingers manipulating virtual objects in mixed-reality environment," *Presence: Teleoper. Virtual Environ.*, vol. 11, pp. 134-143, 2002.

[102] S. Kim, J. J. Berkley and M. Sato, "A Novel Seven Degree of Freedom Haptic Device for Engineering Design," *Virtual Reality*, vol. 6, pp. 217-228, 2003.

[103] T. Butnaru, C. Antonya and D. Talaba, "A Wired Haptic System for Multimodal VR Interaction," *Product Engineering*, pp. 243-258, 2008.

[104] S. Saga and K. Deguchi, "Lateral-force-based 2.5-dimensional tactile display for touch screen," in *Proceedings of the Haptics Symposium (HAPTICS)*, 2012, pp. 15-22.

[105] G. Robles-De-La-Torre and V. Hayward, "Force can overcome object geometry in the perception of shape through active touch," *Natural*, vol. 412, pp. 445-448, 2001.

[106] P. Gallina, G. Rosati and A. Rossi, "3-d.o.f. wire driven planar haptic

interface," *Journal of Intelligent and Robotic Systems: Theory and Applications*, vol. 32, pp. 23-36, 2001.

[107] V. Richard, "Analysis of the Workspace of Tendon-based Stewart Platforms," Ph.D thesis, Universität Duisburg-Essen , 2004.

[108] S. Kawamura and K. Ito, "A new type of master robot for teleoperation using a radial wire drive system," in *Proceedings of the IEEE/RSJ International Conference on Intelligent Robots and Systems*, 1993, pp. 55-60 vol.1.

[109] R. L. Williams II, P. Gallina and J. Vadia, "Planar Translational Cable-Direct-Driven Robots ," in *Proceedings of the 2001 ASME Design Technical Conferences*, 2003

[110] Y. Rui, T. Xiaoqiang, W. Jinsong, and H. Peng, "Dimensional Optimization Design of the Four-Cable-Driven Parallel Manipulator in FAST," *IEEE/ASME Transactions on Mechatronics*, vol. 15, pp. 932-941, 2010.

[111] K. Tashiro, Y. Shiokawa, T. Aono, and T. Maeno, "A Virtual Button with Tactile Feedback Using Ultrasonic Vibration," in *Proceedings of the Virtual and Mixed Reality*, LNCS 5622, pp. 385–393, 2009.

[112] ISO, " Ergonomic requirements for office work with visual display terminals (VDTs), Part 9: Requirements for non-keyboard input devices," 2000.

[113] W. A. Rogers, A. D. Fisk, A. C. McLaughlin, and R. Pak, "Touch a Screen or Turn a Knob: Choosing the Best Device for the Job," *Human Factors: The Journal of the Human Factors and Ergonomics Society*, vol. 47, pp. 271 -288, 2005.

[114] "Touch Screen Technology With Knobs On,"

<http://www.podcomplex.com/blog/touch-screen-technology/>.

[115] C. Swindells, K. E. MacLean, K. S. Booth, and M. J. Meitner, "Exploring affective design for physical controls," in *Proceedings of the SIGCHI conference on Human factors in computing systems*, San Jose, California, USA, 2007, pp. 933-942.

[116] M. Amberg, Fr, D, R. Giraud, B. Semail, P. Olivo, G, R. Casiez, and N. Roussel, "STIMTAC: a tactile input device with programmable friction," in *Proceedings of the 24th annual ACM symposium adjunct on User interface*

software and technology, Santa Barbara, California, USA, 2011, pp. 7-8.

[117] N. D. Marchuk, J. E. Colgate and M. A. Peshkin, "Friction measurements on a Large Area TPAD," in *Proceedings of the Haptics Symposium, 2010 IEEE*, 2010, pp. 317-320.

[118] F. Giraud, M. Amberg, B. Lemaire-Semail, and G. Casiez, "Design of a transparent tactile stimulator," in *Proceedings of the Haptics Symposium (HAPTICS)*, 2012, pp. 485-489.

[119] "Tpad", <http://lims.mech.northwestern.edu/projects/TPAD/index.htm>

[120] M. Biet, G. Casiez, F. Giraud, and B. Lemaire-Semail, "Discrimination of Virtual Square Gratings by Dynamic Touch on Friction Based Tactile Displays," in *Proceedings of the Haptic symposium*, 2008, pp. 41-48.

[121] "http://store.apple.com/us/browse/home/shop_ipad/family/ipad/select?mco=MjE0OTI0MDI".

[122] "<http://www.samsung.com/global/microsite/galaxytab/2010/>".

[123] P. Sergeant, F. Giraud and B. Lemaire-Semail, "Geometrical optimization of an ultrasonic tactile plate," *Sensors and Actuators A: Physical*, vol. 161, pp. 91-100, 2010.

[124] F. Giraud, M. Amberg, R. Vanbelleghem, and B. Lemaire-Semail, "Power Consumption Reduction of a Controlled Friction Tactile Plate," in *Proceedings of the Eurohaptics 2010*, vol. 6192, pp. 44-49, 2010.

[125] M. Biet, F. Giraud and B. Lemaire-Semail, "Vibrating Tactile Interface," European Patent, EP1956466, 8-2008.

[126] S. B. Lang, H. L. W. Chan, K. Uchino, J. H. Zheng, Y. H. Chen, X. H. Du, J. Ryu, Y. Gao, S. Ural, S. Priya, and S. Hirose, "Loss mechanisms and high power piezoelectricsFrontiers of Ferroelectricity," *Journal of Materials Science*, pp. 217-228, 2007.

[127] "Noliac," <http://www.noliac.com/Specification-141.aspx>.

[128] S. Timoshenko, S. Woinowsky-Krieger, "Theory of Plates and Shells", McGraw-Hill, New York, 1959.

[129] E. Salbu, E. Salbu, "Compressible squeeze films and squeeze bearings,"

ASME Journal of Basic Engineering, vol. 86(3), pp. 355–364, 1964," 1964.

[130] V. Levesque, L. Oram and K. MacLean, "Exploring the design space of programmable friction for scrolling interactions," in *Proceedings of the Haptics Symposium*, 2012, pp. 23-30.

[131] H. Levitt, "Transformed Up-Down Methods in Psychoacoustics," *The Journal of the Acoustical Society of America*, vol. 49, pp. 467-477, 1971.

[132] M. Leek, "Adaptive procedures in psychophysical research," *Perception & Psychophysics*, vol. 63, pp. 1279-1292, 2001.

[133] D. R. Flatla, C. Gutwin, L. E. Nacke, S. Bateman, and R. L. Mandryk, "Calibration games: making calibration tasks enjoyable by adding motivating game elements," in *Proceedings of the 24th annual ACM symposium on User interface software and technology*, Santa Barbara, California, USA, 2011, pp. 403-412.

[134] E. Samur, J. E. Colgate and M. A. Peshkin, "Psychophysical evaluation of a variable friction tactile interface," in *Proc. of the SPIE-IS&T*, pp.1-7, 2009.

[135] W. Buxton, R. Hill and P. Rowley, "Issues and techniques in touch-sensitive tablet input," *SIGGRAPH Comput. Graph.*, vol. 19, pp. 215-224, 1985.

[136] A. Nashel and S. Razzaque, "Tactile virtual buttons for mobile devices," in *CHI '03 extended abstracts on Human factors in computing systems*, Ft. Lauderdale, Florida, USA, 2003, pp. 854-855.

[137] M. Hall, E. Hoggan and S. Brewster, "T-Bars: towards tactile user interfaces for mobile touchscreens," in *Proceedings of the 10th international conference on Human computer interaction with mobile devices and services*, Amsterdam, The Netherlands, 2008, pp. 411-414.

[138] B. Yi, X. Cao, M. Fjeld, and S. Zhao, "Exploring user motivations for eyes-free interaction on mobile devices," in *Proceedings of the 2012 ACM annual conference on Human Factors in Computing Systems*, Austin, Texas, USA, 2012, pp. 2789-2792.

[139] K. A. Siek, Y. Rogers and K. H. Connelly, "Fat finger worries: how older

and younger users physically interact with PDAs," in *Proceedings of the 2005 IFIP TC13 international conference on Human-Computer Interaction*, Rome, Italy, 2005, pp. 267-280.

[140] M. Pielot, A. Kazakova, T. Hesselmann, W. Heuten, and S. Boll, "PocketMenu: non-visual menus for touch screen devices," in *Proceedings of the 14th international conference on Human-computer interaction with mobile devices and services*, San Francisco, California, USA, 2012, pp. 327-330.

[141] Y. Yang, Y. Zhang, Z. Hou, Z. Chen, and B. Lemaire-Semail, "FingViewer: A new multi-touch force feedback touch screen," in *Proceedings of the 2011 IEEE International Conference on Consumer Electronics (ICCE)*, 2011, pp. 837-838.

[142] G. A. Gescheider, *Psychophysics: The Fundamentals*: L. Erlbaum Associates, 1997.

[143] R. H. LaMotte, "Softness Discrimination With a Tool," *Journal of Neurophysiology*, vol. 83, pp. 1777 -1786, 2000.

[144] E. Brodie and H. Ross, "Sensorimotor mechanisms in weight discrimination," *Perception & Psychophysics*, vol. 36, pp. 477-481, 1984.

[145] S. A. Cholewiak, H. Z. Tan and D. S. Ebert, "Haptic Identification of Stiffness and Force Magnitude," in *Proceedings of the 2008 Symposium on Haptic Interfaces for Virtual Environment and Teleoperator Systems*, 2008, pp. 87-91.

[146] X. D. Pang, H. Z. Tan and N. I. Durlach, "Manual discrimination of force using active finger motion," *Perception & Psychophysics*, vol. 49, pp. 531-540, 1991.

[147] P. Kammermeier, A. Kron, J. Hoogen, and G. Schmidt, "Display of Holistic Haptic Sensations by Combined Tactile and Kinesthetic Feedback.," *Presence: Teleoperators & Virtual Environments*, vol. 13, pp. 1-15, 2004-02-01 2004.

[148] A. Khatchatourov, J. Castet, J. Florens, A. Luciani, and C. Lenay, "Integrating tactile and force feedback for highly dynamic tasks: Technological, experimental and epistemological aspects," *Interacting with Computers*, vol. 21, pp. 26-37, 2009.

[149] H. Tan, N. Durlach, G. L. Beauregard, and M. Srinivasan, "Manual

discrimination of compliance using active pinch grasp: The roles of force and work cues," *Perception & Psychophysics*, vol. 57, pp. 495-510, 1995.